

FORMATION AND PATHOGENICITY OF CYTOTOXIC CURLI  
INTERMEDIATES

---

A Dissertation  
Submitted to  
the Temple University Graduate Board

---

In Partial Fulfillment  
of the Requirements for the Degree  
DOCTOR OF PHILOSOPHY

---

by  
Lauren Kathleen Nicastro  
August 2020

Examining Committee Members:

Çağla Tükel, Ph.D., Advisory Chair, Department of Microbiology and Immunology

Bettina A. Buttarò, Ph.D., Sol Sherry Thrombosis Research Center

Stefania Gallucci, M.D., Department of Microbiology and Immunology

Marc Monestier M.D., Ph.D., Department of Microbiology and Immunology

Gerard C. L. Wong, Ph.D., External Member, UCLA Department of Bioengineering, Chemistry, and Biochemistry

©  
Copyright  
2020

by

Lauren K. Nicastro  
All Rights Reserved

## ABSTRACT

The first observations of biofilms were made by the “father of microbiology” Antonie van Leeuwenhoek in the 17<sup>th</sup> century. The number of publications on biofilms has grown exponentially in the last 20 years, highlighting the medical relevance of the field. The complexity of the bacterial biofilm as well as its variability across species provides a continual channel for discovery. While all biofilms differ, there are some components that remain standard such as proteins, polysaccharides and DNA allowing for linkages between seemingly distinct biofilms. Biofilm-associated infections account for more than 65% of all infections implicating the need for understanding the stages of biofilm formation and development. Our lab focuses on the amyloid component of the biofilm and has identified that curli and extracellular DNA (eDNA) complex irreversibly within the biofilms of *Salmonella enterica* serovar Typhimurium and *Escherichia coli*. Here, we investigate the formation and pathogenicity of cytotoxic curli intermediates previously unidentified in the *in vitro* biofilm. The identification of multiple curli conformations within the biofilm biogenesis aides in the understanding of amyloid kinetics in the enteric biofilm. Together, these studies provide a link between biofilm-associated infections and autoimmune responses in the host.

In these studies, we planned to isolate curli from different stages in biofilm development to observe their differences both structurally and through their interactions. We identified turbulence has a significant impact on the formation of mature biofilm. We were able to isolate an intermediate form of curli through increased turbulence during biofilm growth. There has never been an intermediate form of curli isolated before our

studies due to the high efficiency of the nucleation-precipitation process of curli fiber formation. From this isolation, we characterized these intermediates in comparison to the mature curli complexes. We observed that higher turbulence leads to lesser biofilm formation by sedimentation assay and crystal violet staining. Additionally, we investigated the expression of the curli forming genes *csgBA* via flow cytometry analysis which indicated that *csgBA* was preferentially expressed under low turbulence conditions. When investigating the curli conformations isolated from the biofilm, we found that intermediate complexes incorporated less thioflavin T (ThT) indicating lesser amyloid content. We also differentiated the mature and intermediate curli aggregate populations using multiple microscopy techniques. Under confocal microscopy, intermediate fibers seldom measured larger than 100  $\mu\text{m}$ , while mature curli did. Electron dense regions were observed under transmission electron microscopy in the mature curli indicating high fibrillization and compact structure of these aggregates, not seen in the intermediates. Due to known interactions of curli with eDNA in the biofilm, next we investigated the DNA content of the complexes. We hypothesized that the mature structured complexes would have greater DNA content supporting the maturation of the fibrils and the structural compaction. Indeed, we found more DNA could be extracted from the mature curli fibers. Interestingly, we increased the fibrillization of intermediates upon addition of exogenous genomic DNA suggesting DNA incorporation was necessary for the formation of the mature fibrillar aggregates. Intermediates of amyloid  $\beta$  are found to be more cytotoxic than the mature form of the amyloid. For this reason, we hypothesized that curli intermediates could also be cytotoxic. After treating bone marrow-derived macrophages with mature and intermediate curli complexes, we observed that the intermediate aggregates were

significantly more cytotoxic to immune cells than mature aggregates. Together, this data implicates a role for the cytotoxic intermediate form of curli in the pathogenesis of *Salmonella* as well as other enteric bacteria.

Curli complexes have been previously described as a novel pathogen associated molecular pattern (PAMP) by their ability to activate numerous receptors in immune cells. The host immune response to curli complexes has been elucidated in our lab. First, binding to Toll-like receptor-2 (TLR2) begins with recognition of the conserved cross- $\beta$  sheet secondary structure. Mutations disrupting this structure are shown to abrogate immune cell recognition and signaling. For this reason, we next investigated the pathogenicity of the intermediates discovered and characterized above. As cytotoxic oligomers exist for human amyloids, we aimed isolate an earlier form of the intermediate curli and investigate the ability of these conformations to activate host immune responses. As mature curli has been reported to induce anti-dsDNA antibodies in murine models of systemic lupus erythematosus (SLE), we anticipated differences in the autoimmune response to these different curli aggregates as well. First, we isolated and characterized an early form of intermediates isolated at 24 hours which were smaller in size and incorporated less DNA within their complexes than the aforementioned intermediates. Further investigations into the structure of these early intermediates described altered secondary structure by circular dichroism. The lack of fully formed secondary structure in the early intermediates we hypothesized to decrease the ability of these complexes to interact with immune receptors as mature curli. Indeed, we saw decreased response in pro-inflammatory cytokine production as well as type I IFN production. This lack of type I IFN production, lead us to investigate the autoantibody response to the early intermediates. When treating both wild-

type and autoimmune-prone mice with curli complexes, early autoantibodies responses were dependent on the DNA content of the complex. However, after continual treatment for 10 weeks, intermediate complexes produced levels of anti-dsDNA similar to that of the mature curli treatment. In addition to anti-dsDNA antibodies, for the first time, other anti-nuclear antibodies, such as anti-C1q and anti-nucleosome, were produced in response to these treatments as well. Finally, chronic exposure to curli complexes led to significant histopathological changes including synovial proliferation and periosteal resorption, in the joints of mice autoimmune-prone mice. Together, this data identified that chronic exposure to curli induced autoimmune sequelae which is thought to be transient in genetically healthy individuals, but leads to joint inflammation in individuals whom are genetically predisposed to autoimmunity.

In summary, these data significantly broaden the knowledge of curli amyloid formation during biofilm biogenesis *in vitro* through the identification of previously unidentified cytotoxic intermediate conformations of curli. Additionally, our work forwards the fields of both autoimmunity and biofilm-associated infection research by providing evidence of the direct impact that chronic exposure to the biofilm has on the host, both transient and long-lasting in those whom are pre-disposed to autoimmunity.

I would like to dedicate this dissertation to my parents, Larry and Donna Nicastro.

## ACKNOWLEDGMENTS

The accomplishment of obtaining my doctoral degree is one that would not have been possible without immense support and friendship from all of those around me. My time at Temple has been life changing for numerous reasons: for shaping me as a person and scientist, for giving me confidence, for teaching me to learn from failures and keep on pushing for your goals, for showing me that I can do more than even I thought I could, and especially for all the amazing people who were there to get me through the bad times and celebrate the good times.

Firstly, the people who have been in it from the start and my biggest cheerleaders my whole life, my family. To my parents, Larry and Donna, who have also set an amazing example of how to work hard and setting me up for all my successes in life. For always being supportive, without judgement even if I made you mad. To my mom, thank you for always being my confidant and offering a listening ear and open heart. To my dad who I can always count on for a terrible dad joke even when I do not want to laugh, thanks for always providing the most obscure facts and comic relief. Daniel and Meredith, my brother and sister-in-law, thanks so much for sharing laughs and letting me complain about mom and dad and most of all for creating the little human that showed me how to love bigger than I ever knew, Joey. He has been an absolute light in my life since the day he was born and can always brighten a bad day. To my other siblings not by birth, but through life Bri and Britt. Regardless of how busy life becomes, I always know that I can count on you two to be there through it all. Next, my Pop, the man who sparked my sassiness from a young age. Thank you for teaching me to be a strong young woman with the confidence to stand up to all the boys (thanks to the Nicastro genetics). Lastly, to both of my grandmothers

passed who in their own ways have placed me and supported me on this journey. Grandmom Barb for making me want to do more for people with disease and igniting my interest in biomedical science. Finally, Grandmom Kay for being everything for all of us, there will never be enough words of thanks for you: your recipes, your love, your memory, and your support from beyond I am forever thankful.

I want to especially thank my advisor, Dr. Çağla Tükel for continually setting myself and the lab up for success. I truly believe that you are the best PI to work for at Temple as you always have a continual flow of interesting projects and ideas and know when to “drop it like a hot potato” to ensure we are always making progress in our work. Your mentorship has been unparalleled both in life and lab, especially when it comes to my wavering writing abilities. The source of comradery you build within the lab through collaboration and support is something I know I could not have succeeded in this program without.

My time in the Tükel lab was full of laughs and endless support. I am so happy that my co-workers have become like friends and even family. To Sarah Tursi and Amanda Miller, who were in it with me for long haul, thank you guys for always assisting when science made no sense or did not want to cooperate. Also, for building the greatest girl gang the micro and immuno department has ever seen and having my back through the successes and (lots of) tears. I appreciate, so much, your love and support through the years even when the sass was real. I also want to thank our lab techs during my time in the lab, Long, Jamie, and Amy. Thank you guys for always dropping what you were doing to help when needed and your stories, jokes, and laughs throughout the years. You really helped make a stressful process so much easier.

Not only was the Tükel lab important to my success, but the support of the department and my grad school friends was paramount. I want to thank my committee members, Dr. Bettina Buttarò, Dr. Stefania Gallucci, Dr. Marc Monestier, and Dr. Gerard Wong for sharing your endless knowledge and guidance. To the other department members, our department may be small but we are mighty and I appreciate the close-knit group that we have all become. To the other students of the department, thanks for making journal club so fun and always making for the best cookie swap every year. I will miss that treasure trove of treats each December. To my lunch besties, Ronald Lucarelli and Holly Fowle, I am so glad this program brought you both into my life. Our lunch adventures and conversations always brightened my day. I am so thankful for your friendship and for you listening to my every, single, complaint about life, you are the best hype squad. I owe my success in this program to the great support that the program and department has given me throughout the years, I could not have done this alone.

I also have to thank my Widener support system for getting me to this point and keeping me sane. Amanda Spurri and Matt McKain, thank you for supporting me in my decision not only to start this degree, but also for keeping me sane and your friendship throughout. I am so thankful to call you my friends and for you believing in me even when I did not believe in myself. Dr. David Coughlin I want to especially thank you for igniting my love for research science. Thank you for always making research fun and kickstarting my early career, I appreciate your continued support immensely.

This journey to my PhD has been long and winding with many bumps along the way. For all of you, and all of my other supporters, I am forever grateful.

# TABLE OF CONTENTS

	Page
ABSTRACT.....	iii
DEDICATION.....	vii
ACKNOWLEDGMENTS .....	viii
LIST OF TABLES.....	xvi
LIST OF FIGURES .....	xvii
LIST OF ABBREVIATIONS.....	xix
CHAPTER	
1. REVIEW OF THE LITERATURE .....	1
Biofilms in Research and Medicine.....	1
Enteric Biofilm Composition.....	3
Amyloid Curli.....	3
Identification of Amyloid Curli .....	4
Biogenesis of Curli Fibers .....	5
Functional Role of Curli Fibers in the Enteric Biofilm .....	8
<i>In Vivo</i> Expression of Curli fibers .....	9
Cellulose .....	11
Cellulose Biogenesis.....	11
Function of Cellulose in the Enteric Biofilm .....	11
Morphology of Curli and Cellulose Containing Biofilms .....	12
Extracellular DNA (eDNA).....	13

Secondary Biofilm Components .....	14
Curli and Other Bacterial Proteins Form Complexes with eDNA.....	15
Immunomodulatory Effects of Bacterial Amyloid Curli .....	16
Recognition of Curli by Immune Receptors .....	16
Immune Evasion and Virulence.....	18
Bacterial Infections and Human Diseases.....	19
Autoimmune Diseases .....	19
Reactive Arthritis .....	19
Systemic Lupus Erythematosus (SLE) .....	22
Biofilms on Implanted Devices and Autoimmune Disease .....	24
Autoimmune Sequelae and Amyloid-Expressing Bacteria.....	24
Neurodegenerative Diseases .....	26
Concluding Remarks.....	27
References Cited.....	30
2. CYTOTOXIC CURLI INTERMEDIATES FORM DURING <i>SALMONELLA</i>	
BIOFILM DEVELOPMENT.....	42
Abstract.....	43
Introduction.....	44
Results.....	46
High Turbulence Leads to Decreased Biofilm Development .....	46
Intermediate Forms of Curli Aggregates Are Detectable Under	
High-Turbulence Conditions .....	49
DNA Induces Formation of Mature Curli Fibrillar Aggregates .....	54

Curli Intermediates are More Cytotoxic to Macrophages than the Mature Fibrillar Aggregates.....	58
Discussion.....	61
Materials and Methods.....	66
Bacterial Strains and Growth Conditions .....	66
Purification of Curli .....	66
Sedimentation Assay.....	67
Crystal Violet Staining.....	68
Flow Cytometry .....	68
Thioflavin T Assay .....	69
Confocal Laser Scanning Microscopy .....	70
Transmission Electron Microscopy .....	70
DNA Extraction .....	70
Lactate Dehydrogenase Assay .....	71
Live/Dead Staining .....	72
Dot Blot.....	72
Statistical Analyses .....	73
Acknowledgements.....	74
References Cited.....	75
Supplemental Figures.....	81

3. STRUCTURAL ORGANIZATION OF DNA IN CURLI FIBRILS DURING BIOFILM FORMATION DICTATES THE TYPE I IFN SIGNATURE AND AUTOANTIBODY RESPONSE.....	85
Abstract.....	86
Introduction.....	87
Results.....	90
Curli and eDNA Interactions During the Biofilm Maturation.....	90
Association of DNA with Early Intermediate, Intermediate, and Mature Curli.....	93
Interactions of Early Intermediate, Intermediate and Mature Curli with Immune Cells.....	95
Structure and DNA Content of Curli Generated During Biofilm Formation Dictates the Autoimmune Response in Mice.....	99
Initiation of Joint Inflammation by Systemic Injection of Curli Complexes.....	102
Discussion.....	104
Future Directions.....	108
Materials and Methods.....	110
Bacterial Strains and Growth Conditions.....	110
Purification of Curli.....	110
Confocal Laser Scanning Microscopy.....	111
Ultraviolet Circular Dichroism.....	112
DNA Extraction.....	112

Single Angle X-Ray Scattering Analysis.....	113
Bone Marrow-Derived Macrophages (BMDMs).....	114
RNA Isolation and qPCR Quantification .....	114
Live/ Dead Staining .....	117
Animal Experiments .....	117
Anti-dsDNA Autoantibody ELISA.....	118
Luminex .....	119
Joint Inflammation Analysis.....	119
Statistical Analysis.....	119
References Cited .....	120
4. OVERALL DISCUSSION .....	124
References Cited .....	134
APPENDICES	
A. LIQUID CULTURE GROWTH CONDITIONS FOR EACH CURLI	
CONFORMATION .....	137
B. INCLUSION OF COPYRIGHTED MATERIAL FOR CHAPTER 2.....	144

## LIST OF TABLES

Table	Page
CHAPTER 3	
1. <b>Table 1.</b> Primers used for qPCR.....	117

## LIST OF FIGURES

Figure	Page
CHAPTER 1	
1. <b>Figure 1.1.</b> Human Infections Leading To Autoimmune Sequelae .....	21
CHAPTER 2	
2. <b>Figure 2.1.</b> Higher Turbulence Leads To Decreased Biofilm Formation.....	48
3. <b>Figure 2.2.</b> Curli Intermediates Are Detected Under High-Turbulence Growth Conditions.....	50
4. <b>Figure 2.3.</b> Transmission Electron Microscopy Of High- And Low-Turbulence Curli Aggregates Showing Electron Density Differences.....	53
5. <b>Figure 2.4.</b> DNA Is Necessary For Formation Of Mature Curli Fibrillar Aggregates.....	55
6. <b>Figure 2.5.</b> Curli Intermediates Are More Cytotoxic Than Mature Aggregates.....	59
7. <b>Figure 2.6.</b> Working Model.....	62
8. <b>Supplemental Figure 2.1.</b> Crystal Violet Staining Of Pellicle Associated Biofilm From Cultures Grown In Increasing Levels Of Turbulence .....	81
9. <b>Supplemental Figure 2.2.</b> Bacterial Growth As Measured By Optical Density Over 72 Hours Of Growth In Mixed And Unmixed Cultures.....	82
10. <b>Supplemental Figure 2.3.</b> Mature Aggregates Treated With Genomic DNA Display No Change In Amyloid Content.....	83
CHAPTER 3	
11. <b>Figure 3.1.</b> Unique Curli Conformations are Formed During The Biofilm Maturation .....	91
12. <b>Figure 3.2.</b> Association Of DNA With Early Intermediate, Intermediate, And Mature Curli .....	94

13. <b>Figure 3.3.</b> Interactions Of Early Intermediate, Intermediate, And Mature Curli With Immune Cells.....	97
14. <b>Figure 3.4.</b> Structure and DNA Content Of Curli Generated During Biofilm Development Dictates The Autoimmune Response In Mice.....	100
15. <b>Figure 3.5.</b> Initiation Of Joint Inflammation By Systemic Injection Of Curli/eDNA Complexes.....	103

CHAPTER 4

16. <b>Figure 4.1.</b> Working Model For The Role Of Curli Conformations Through Biofilm Development.....	129
17. <b>Figure 4.2.</b> Cytotoxicity By Intermediate Curli Complexes is Delayed.....	130

## LIST OF ABBREVIATIONS

Agf	Aggregative Fimbriae
AMP	Antimicrobial Peptide
ANA	Anti-nuclear Antibody
Autoab	Autoantibody
<i>B. subtilis</i>	<i>Bacillus subtilis</i>
BapA	Biofilm Associated Protein A
BBS	Borate Buffered Saline
BCA	Bicinchoninic Acid Assay
bcs	Bacterial Cellulose Synthesis
bdar	Brown Dry and Rough
BMDM	Bone Marrow-Derived Macrophages
C1q	Complement component 1q
CD14	Cluster of Differentiation 14
c-di-GMP	Cyclic Diguanylate
CF	Cystic Fibrosis
CLSM	Confocal Laser Scanning Microscopy
csg	Curli Specific Gene

DMSO	Dimethyl Sulfoxide
dsDNA	Double-stranded DNA
<i>E. coli</i>	<i>Escherichia coli</i>
ECM	Extracellular Matrix
eDNA	Extracellular Deoxyribonucleic Acid
ELISA	Enzyme-linked Immunosorbent Assay
FACS	Fluorescence-Activated Cell Sorting
FITC	Fluorescein Isothiocyanate
gDNA	Genomic DNA
GFP	Green Fluorescent Protein
GI	Gastrointestinal
H2A	Histone 2A
HLA-	Human Leukocyte Antigen
IFN	Interferon
Ig_	Immunoglobulin_
IL-	Interleukin-
KO	Knockout
LB	Luria-Bertani
LDH	Lactate Dehydrogenase

LPS	Lipopolysaccharide
MgCl <sub>2</sub>	Magnesium Chloride
MOI	Multiplicity of Infection
NLRP3	NOD-like Receptor Protein 3
NMR	Nuclear Magnetic Resonance
<i>P. aeruginosa</i>	<i>Pseudomonas aeruginosa</i>
PAMP	Pathogen Associated Molecular Pattern
PANDAS	Pediatric Autoimmune Neuropsychiatric Disorders Associated with Streptococci
PBMC	Peripheral Blood Mononuclear Cell
PBS	Phosphate Buffered Saline
pdar	Pink Dry and Rough
PSM	Phenol Soluble Modulins
PVDF	Polyvinylidene Difluoride
qPCR	Quantitative Polymerase Chain Reaction
rdar	Red Dry and Rough
ReA	Reactive Arthritis
RNA	Ribonucleic Acid
<i>S. aureus</i>	<i>Staphylococcus aureus</i>

<i>S. Typhimurium</i>	<i>Salmonella enterica</i> serovar Typhimurium
saw	Soft and White
SAXS	Small Angle X-ray Scattering
SDS	Sodium Dodecyl Sulfate
SEM	Standard Error of the Mean
SLE	Systemic Lupus Erythematosus
STM	<i>Salmonella</i> Typhimurium
TBS	Tris Buffered Saline
TE Buffer	Tris EDTA Buffer
TEM	Transmission Electron Microscopy
ThT	Thioflavin T
TLR-	Toll-like Receptor
TNF	Tumor Necrosis Factor
UTI	Urinary Tract Infection
UV CD	Ultra-violet Circular Dichroism
YESCA	Yeast Extract Supplemented with Casamino Acids

## **CHAPTER 1**

### **REVIEW OF THE LITERATURE**

#### **Biofilms in Research and Medicine**

The first bacterial biofilms were identified as early as the 17<sup>th</sup> century when Antonie van Leeuwenhoek described aggregates scraped from the surfaces of teeth as “animalcules” [1]. These aggregates from the dental plaques were later identified as multi-species biofilms. He was the first to discuss the protective nature of the biofilm noting that vinegar treatment only killed “animals which were on the outside of the scurf, but did not pass thro the whole substance” [1]. More than a century later, Louis Pasteur made his own observations and sketches of biofilms, he noted, as a potential causative agent for the acidification of wine [2]. In the 20<sup>th</sup> century, the term “film” was used for the first time in the marine microbiology field to distinguish the difference between free, planktonic bacteria from sessile, surface-adhering bacteria. Marine microbiology furthered the understanding of biofilms when Arthur Henrici observed that bacteria found in water were “not free-floating organisms, but grow attached upon submerged surfaces” [3]. Another scientist, Niels Hoiby, greatly expanded the study of biofilms into the medical field in the 1970s when he observed smears of the sputum from patients with cystic fibrosis (CF). He published some of the first data linking the chronic infection of the lung in CF patients to the presence of bacterial aggregates[4]. By the 1980s, J.W. Costerton coined the term “biofilm” after his microscopy work observed how bacteria adhere to surfaces [5, 6]. He is credited by many for being a pioneer of biofilm research who bridged disciplines to support the study of bacterial biofilms and their interactions with their environments.

Interactions between bacterial biofilms and the environment are complex. This is, in most part, due to the production of the extracellular matrix (ECM) during the formation of the biofilm, which assists bacteria with adherence and protection. Not only does the complexity and differences amongst species provoke great interest from the scientific community, but the medical relevance of understanding the biofilm is paramount. Though biofilm research began by investigating biofilms fouling biotic and abiotic surfaces in the marine biology setting, they are now at the forefront of medical research as up to 65% of all microbial infections are associated with biofilms [7]. With the advancements in medicine, an increase in the production and use of indwelling medical devices to improve quality of life such as joint replacements, stents, and catheters has occurred. Though these devices are beneficial and often necessary, bacteria frequently use the surfaces of these devices to adhere and form biofilms causing numerous problems within the body [8, 9]. As many components of the biofilm ECM have been independently identified as pathogen associated molecular patterns (PAMPs), studies understanding their interactions with the immune system, both as a whole and separately are not only important, but bring together numerous disciplines across medical research. Together with the recent increase in microbiome research, studies on the interactions of bacteria in the biofilm highlight the connection between bacterial biofilms and human disease pathogenesis. Most recently, studies have supported a connection between enteric bacterial biofilms and human diseases such as Systemic Lupus Erythematosus (SLE) and Parkinson's disease showing an impact on multiple body systems [10, 11]. Overall, this chapter discusses the aspects of the

bacterial biofilm, how they interact with the immune system, and the impact that they have on human disease states.

### **Enteric Biofilm Composition**

Biofilms are defined as a group of bacteria encapsulated in a self-produced ECM adhered to a surface [1, 12]. The bacteria in these biofilm communities can be single-species or multiple bacterial species working synchronously. Regardless of the species or bacterial composition, it has been shown that 90% of the biomass within a bacterial biofilm is composed of ECM while the remaining 10% of the biofilm mass is bacterial cells [13]. Also, the ECM, sometimes referred to as extra polymeric substance or “slime” layer that surrounds the bacterial cells, differs in its distinct components across bacterial species. However, most matrix components can be grouped into three main categories: proteins, polysaccharides, and DNA. The exact protein and polysaccharide portions of the biofilm are the main differences, varying greatly amongst species. Our lab focuses on the biofilms of enteric bacteria with an emphasis on the amyloid protein produced in most of their biofilms, curli. For the sake of this dissertation, I will reference the enteric bacterial biofilms as only those which produce curli, unless otherwise noted as it is the most abundant structural component of the enteric biofilm.

### **Amyloid Curli**

Amyloid proteins were first identified in the 1800s by German physician scientist Rudolf Ludwig Carl Virchow (Reviewed in [14]). He observed macroscopic abnormalities

in brains of post-mortem biopsies. In combination with findings from the 1630s of waxy livers and white stone containing spleens, he stained these deposits with iodine and determined them to starch-like [14]. In naming them amyloids, Virchow paid homage to the Latin for starch, “amylum” (Reviewed in [14]). It was not until 1859 that the protein content of amyloids was understood. Friedrich and Kekule identified both protein content and high nitrogen content, indicating a lack of carbohydrate within the amyloids [14-16]. This changed the classification of amyloids to proteins with a tendency to polymerize into fibers. The structure of these fibers was similar across both humans and animals, with an average 75-100Å width and 1,000-16,000Å length, which later became a distinguishing factor in fibril identification [14]. For many years after their discovery, amyloids were only associated with human disease states. However, it is now known that amyloids are not solely a human product as bacteria produce them as well. Amyloid proteins can be found in more than 40% of all bacterial biofilms [17]. The best and most well studied of the bacterial amyloids is amyloid curli found in the biofilms of enteric bacteria.

### ***Identification of Amyloid Curli***

Curli was first identified in *E. coli* strains that caused bovine mastitis in the 1980s by Chapman and colleagues [18]. When curli was later identified in *Salmonella*, it was termed thin, aggregative fimbriae [19]. Amyloid curli has a fibrillar structure with fibers of about 4-10nm in width [20, 21]. When polymerizing together, the 17 kD CsgA protein bind to repetitively to itself, attached to the cell surface by CsgB, the nucleator protein [22, 23]. The mature fibers then align into a  $\beta$  sheet secondary structure along the axis

perpendicular to the growth of the fibril [24]. Identifying the amyloid within a biofilm includes various dyes. One of the first identification techniques adopted for amyloid was Congo Red staining as well as apple green birefringence under polarized light [14]. Later, ThioflavinT (ThT) staining, originally used to monitor fibrillization of human amyloid  $\beta$ , was then adapted for use on bacterial amyloids like curli [25, 26]. Additionally, a spectroscopy technique circular dichroism can be employed to identify the  $\beta$  sheet secondary structure shared among amyloid proteins. Due to their size, amyloid fibers are best observed under electron microscopy. Investigation of curli on a nanomolecular scale has been done on curli both isolated through Small Angle X-ray Scattering (SAXS) analysis as well as whole extracellular matrix through solid-state nuclear magnetic resonance (NMR). NMR was used to identify interactions between curli and cellulose as making a honey comb or basket-like matrix structure [27-29].

### ***Biogenesis of Curli Fibers***

The genetic machinery behind the production of this major component of the biofilm, curli, is a bidirectional operon system [18]. Curli is produced through a type VIII secretion system with components produced by genes encoded by the *csgBAC* and *csgDEFG* operons [18, 30]. The *csg* name comes from curli specific genes, initially named for the genes in *E. coli* [18]. The gene homologs in *Salmonella* were named *agf* for aggregative fimbriae [31, 32]. These two nomenclatures are often used interchangeably as curli is produced by both bacteria. This dissertation uses the *csg* gene nomenclature throughout.

The complicated process of curli production is triggered under stress conditions *in vitro*. Under environmental stressors such as low temperature, lack of available of nutrients and oxygen, or osmolarity, enteric bacteria will make the switch from planktonic to sessile growth and begin biofilm formation [33-35]. To recapitulate this condition in the laboratory setting, all of these factors are combined to induce maximal biofilm production by the cells. Bacteria are grown at low temperature (28°C) in minimal broths, such as yeast extract supplemented with casamino acids (YESCA) or T-medium, or low to no salt added Luria-Bertani broth [36]. These stressful conditions initiate the production of biofilm and curli within the first 24-48 hours of growth [10].

Control of the switch between motile planktonic lifestyle and the sessile biofilm lifestyle of bacteria is under the control of *csgD*. The production of CsgD is the earliest sign of this transition and is the only protein of the curli machinery that has been observed during logarithmic phase of growth [37]. The production and accumulation of CsgD within the cell is a response to the aforementioned environmental stressors. In addition to stress, it has been shown that increased levels of the secondary messenger, cyclic-diguanosine monophosphate (c-di-GMP) are sensed by YcgR which then tightly binds to the flagellar proteins, FliG and FliM, to in turn inhibit flagellar activity [38]. Both of these pathways lead to the activation of the master regulator of curli production, *csgD* to begin the multifactorial process of curli formation. CsgD is the protein that bridges the two operons to begin amyloid production. As the master regulator of curli genes, the activation of *csgD* kick starts the production of all other curli genes when it binds to the *csg* promoter sequence. Alterations in *csgD* alone greatly affect the ability of bacteria to produce curli as

a single point mutation in the *Salmonella* Typhimurium gene can cause a 3-fold decrease in production [32].

The major structural proteins of the curli fibril are CsgA and CsgB. Upon binding of the master regulator CsgD, these proteins are produced under the control of the *csgBAC* operon responsible for the structural portion of the curli fiber. CsgA and CsgB are produced and trafficked to the outside of the cell. Once extracellular, CsgB acts as the nucleator protein tethering the curli fiber to the bacterial cell to which CsgA then binds and continues the nucleation and precipitation to form the final mature fibrils [18, 30]. An interesting capability of this system is that bacteria with mutations in *csgA* or *csgB* can be supplemented by the proteins of nearby bacterial cells in a process called interbacterial complementation [39]. This process allows a cell unable to produce functional CsgA or CsgB to use the excreted proteins of a nearby cell to form a fully functional curli fiber.

Lastly, the final gene of the operon *csgC* encodes the CsgC protein which halts CsgA-CsgA or CsgA-CsgB nucleation as the monomeric proteins pass through the periplasm of the cell [40]. This is an essential protein to protect the cell both from fibril formation within as well as any cytotoxicity associated with protein oligomers [41]. Although it does not directly form the curli fibril like its *csgBAC* counterparts, the importance of the role of CsgC in curli formation is supported by the discovery of a CsgC-like protein identified in systems lacking CsgC itself, CsgH in 2016. First identified in  $\alpha$ -Proteobacteria, CsgH shows little sequence similarity to the other curli gene with the closest sequence similarity to CsgC. CsgH also shares structural and genetic location

similarities with this homolog [40]. CsgH acts as an inhibitor of intercellular CsgA polymerization [40].

The other operon, *csgDEFG*, encodes the regulatory and accessory protein portion of the curli fiber formation process. The first important accessory protein is CsgG, the outer membrane pore-forming lipoprotein. This protein interacts with itself to form stable, ring-shaped pores through which CsgA and CsgB are excreted [42]. The excretion process is where the CsgE and CsgF proteins are important. Both produced in the periplasm, CsgE and CsgF are chaperone proteins that guide CsgA and CsgB, respectively, through the CsgG formed pore. Beyond its chaperoning activity, CsgE also protects CsgA from degradation by proteases in the periplasm [43]. CsgF is responsible for ensuring successful tethering of the nucleator protein CsgB to the outer membrane of the bacterial cell from which the mature fibril will form [44].

### ***Functional role of curli fibers in the enteric biofilm***

As the major proteinaceous component of the biofilm, curli is responsible for the majority of the structural features of the biofilm. In bacteria lacking the ability to produce curli, the three-dimensional structure of the biofilm architecture and its strength is greatly depleted [28, 45]. Using crystal violet staining, as well as confocal microscopy, the biofilm of curli mutant bacteria are lacking [28, 45]. In addition to physical support, curli also lends to the initial attachment of the biofilm. The resistant nature of amyloids provides protection to the bacterial cells throughout the life of the biofilm. The isolation of curli fibers from the biofilm involves multiple rounds of sodium dodecyl sulfate (SDS) treatment with curli

remaining unaffected [46]. In laboratory settings, strong chemicals such as 90% formic acid and hexafluoroisopropanol are required for the breakdown of curli into its monomeric form [47]. The resilience of these fibers to environmental insult is what allows for the stability and long-term survival of the biofilm.

### ***In vivo expression of curli fibers***

As low temperature has often been identified as an activator of *csgD*, and therefore curli production, the expression of curli *in vivo* is a hotly contested topic in the field. Recently, additional work has been done to prove the expression of curli at homeostatic conditions *in vivo*. Previous work on the presence of curli *in vivo* investigated the production of curli-specific antibodies. In animal models of *S. Typhimurium* infection as well as human sepsis patients infected with *E. coli*, antibodies against curli were isolated [48, 49]. However, the signaling responses identified in the *in vitro* studies of curli did not translate to the observations *in vivo* giving many scientists pause in confirming the expression and production of curli in the host.

The genetic mechanism of biofilm formation via *csgD* activation in humans provides evidence against the production of curli *in vivo*. There are multiple global regulatory proteins that influence the expression of curli-associated genes including H-NS, Crl, OmpR, and RpoS [33, 50]. Though generally RpoS sigma factor is used to transcribe *csgD*, a second protein, MlrA, is required for full efficiency of transcription [51]. In a study of O157:H7 strains of *E. coli*, the most common strains to be associated with human disease, more than 95% of the clinical isolates carried insertions in *mlrA*. This common

mutation caused restricted curli production identified by low level Congo Red staining [52] indicating clinical isolates would be prone to decreased or deficient curli production *in vivo*. An additional study by Uhlich and colleagues observed that curli expression in a group of O157:H7 clinical isolates was uncommon [53]. Across these studies of clinical isolates of *E. coli* capable of producing curli, the lack of curli production *in vivo* provides evidence that this production may not effectively occur within the host.

On the other hand, in a study of cystitis associated with urinary tract infections (UTI), all *E. coli* isolated carried the *csgA* gene [54-56]. As one of the major functions of curli in the biofilm is cell adhesion, these UTI strains were tested for their ability to adhere to different cell types. When the curli genes were intact, all strains adhered to all cell types. However, adhesion to human bladder carcinoma cells was diminished upon loss of *csgA* [54]. This implicates curli as a necessary factor in the adhesion of uropathogenic *E. coli* in order to induce cystitis and proof of *in vivo* curli production. Supplementary to this, the expression of curli genes has been identified to play a role in fitness during UTI [56].

Similar evidence of curli expression has been observed in *S. Typhimurium* infection as well. Oral infection with planktonic *S. Typhimurium* resulted in seroconversion of multiple fimbrial proteins including CsgA, which are undetectable before the infection [48]. This indicates the expression and production of curli occurred after infection within the host. More recently, the expression of curli was identified in the large intestine of mice using a reporter for the master regulator *csgD* during infection with *S. Typhimurium* grown under planktonic conditions [57]. Together with immunohistochemistry staining for *Salmonella* and curli in tissues from the gastrointestinal (GI) tract of mice, these data

support for the first time, the synthesis of curli *in vivo* under normal homeostatic conditions. This discovery provides a connection between persistence and virulence of curliated enteric bacteria and need for expression and production *in vivo*.

## **Cellulose**

### ***Cellulose Biogenesis***

Together with curli, the other major structural component of the enteric biofilm is cellulose. Appearing at a ratio of 6:1, curli and cellulose function together to form the major lattice structure that supports the biofilm structure [27]. Cellulose within the biofilm have been best studied in *Salmonella* and *E. coli*, however, other *Enterobacteriaceae* such as *Citrobacter*, *Klebsiella*, and *Enterobater* from the gut have also been examined [58]. The production of cellulose is closely coupled to curli production. Upon activation of *csgD*, the regulator of curli production, the *adrA* gene is transcribed. This gene encodes the production of AdrA which initiates the pathway for transcription of the cellulose genes [37]. The *bcs* (bacterial cellulose synthesis) operon controls the genes responsible for the production and secretion of cellulose. The necessary genes for cellulose production in the biofilm are *bcsA*, *bcsB*, *bcsC*, and *bcsD*. Similar to the activation of *csgD*, cellulose gene activation is responsive to c-di-GMP levels [59].

### ***Function of Cellulose in the Enteric Biofilm***

Cellulose is the most abundant natural polysaccharide on Earth. Though more often associated with plants, bacteria also produce cellulose. Due to the similarities to curli

activation, the individual functionality of cellulose within the biofilm is difficult to ascertain. Biofilms of *E. coli* produce a slightly altered form of cellulose from the traditional 1-4  $\beta$ -glycosydic linkage of glucan chains called phosphoethanolamine cellulose [60]. The chemical modification of the phosphoethanolamine cellulose causes it to form long, thick filaments as opposed to the short, thin curled standard cellulose [60]. This type of cellulose is known to strengthen the biofilm due to these structural changes. These cellulose filaments then interact with curli fibers to support the structure of the biofilm matrix. Together, the interwoven network of cellulose and curli are used functionally to stabilize the biofilm by resisting sheer stress and aiding in intercellular cohesion [60]. Additionally, the basket-like interlocking of curli and cellulose supports elasticity of the biofilm, adding an extra level of protection for the bacterial cells within the ECM [60].

### ***Morphology of Curli and Cellulose Containing Biofilms***

Genetic mutants of *E. coli* and *Salmonella* have been generated to analyze the morphological differences of the mutant biofilm. As reported numerous times in the literature, wild-type enteric biofilms grown on low-nutrient agar supplemented with Congo Red and Coomassie Blue show a rough, dry and red (rdar) morphology [61]. When bacteria are mutated to lack curli expression, they maintain their textured appearance, however, they are identified as pink, dry and rough (pdar) [62]. When the bacteria are cellulose mutants, but maintain curli production, the morphology once again changes to a brown, dry, and rough (bdar) colony [61]. Finally, the curli and cellulose mutant bacteria will form

a colony with a smooth and white (saw) morphology, losing both the rugosity in structure and the uptake of either of the two stains in the agar [61].

### **Extracellular DNA (eDNA)**

The third major component of enteric biofilms is extracellular DNA (eDNA). The presence of eDNA in biofilms can be seen using nucleic acid stains such as Hoescht, 4',6-diamidino-2-phenylindole (DAPI), or propidium iodide. Early studies of DNA within the biofilm believed that the source of DNA within the biofilm was solely a product of cellular lysis. Alternatively, work by Whitchurch and colleagues identified that not only could DNA export into the biofilm be purposeful, but that DNA was actually an important functional part of the biofilm ECM [63]. Treatment of *P. aeruginosa* with DNase I prevented biofilm formation supporting the need for DNA within the biofilm architecture [63]. Studies using recombinant human DNase I as a treatment for CF patients showed positive response in sputum thinning and, when used prophylactically, a decrease in biofilm formation highlighting the importance of eDNA within the biofilm as more than a cell death by-product [63].

While the mechanism by which enteric bacteria release DNA into the biofilm is not fully understood, there is evidence that the bacteria isolated from biofilms can be from either source. Autolysis processes have been understood for years, and the process of fratricide, where a portion of bacteria from a community release a factor that kills their siblings, is also well studied. While autolysis and fratricide are known sources of eDNA in the biofilm, there have also been examples of cell-lysis independent DNA release by *B.*

*subtilis* [64]. A sequence comparison of this extracellular DNA was identical to that of the intracellular DNA although they may differ chemically through distinct methylation patterns [64].

### **Secondary Biofilm Components**

BapA is a large protein component found on the surface of the enteric biofilm. Interestingly, in *Salmonella* Enteritidis, BapA is coordinated along with the other major components of curli and cellulose by CsgD [65]. Overexpression of a single copy of the *bapA* gene has been shown to increase biomass [65]. On the other hand, a lack of BapA can be complemented by extra curli production attesting to its role as a secondary support to the biofilm structure [65]. Analogous to curli and cellulose, *bapA* is controlled by the actions of CsgD [65].

Another secondary biofilm component partially controlled by CsgD is lipopolysaccharide (LPS), specifically its O-antigen [66]. First observed in *Vibrio cholerae*, mutations in O-antigen caused incomplete addition of sugars to the main core of LPS in *E. coli* decreasing and altering biofilm formation [67, 68]. Due to a pleotropic effect, the mutated LPS negatively influences the other ECM structures [68]. Furthermore, studies of gallstones after *Salmonella* infection implicated a role for O-antigen in biofilm formation induced by bile [69]. These studies, also linked O-antigen to biofilm formation on cholesterol coated surfaces [69].

A polysaccharide component secondary to cellulose is colanic acid. First identified in the 1960s, colanic acid is a polymer of sugars and glucuronic acid [70, 71]. Structured

similarly to *E. coli* group I capsules, colanic acid may be influenced by the *wca* gene cluster [72, 73]. Comparable to cues for *csgD* expression, variations in temperature and osmolarity lead to the activation of the *wca* genes (reviewed in [71], [74]). The functionality of colanic acid in *E. coli* biofilm mirrors functions of other components: support of the three-dimensional architecture [75]. While initially thought to assist in adherence and colonization of the biofilm, studies of curli-producing *E. coli* strains determined curli as the major component responsible for this attachment, however, that colanic acid was still essential to biofilm structure [76].

### **Curli and Other Bacterial Proteins Form Complexes with eDNA**

Curli and eDNA form strong bonds within the biofilm to further support the structure. When isolating curli from the biofilm, eDNA can be observed irreversibly bound to curli under confocal microscopy [10]. The insoluble curli serves to protect the DNA, as isolation using multiple treatments of DNase I, RNase, and boiling in sodium dodecyl sulfate does not destroy the existence of DNA in the complexes [46]. While the binding of eDNA to curli in the enteric biofilm is clear, this is not an enteric specific functionality as this protein to eDNA binding is seen in many systems. Another amyloid protein shown to bind with DNA is phenol soluble modulins (PSMs) in *Staphylococcus aureus*. Though mainly studied as toxins, the ability of PSMs from *S. aureus* to form amyloid fibers has been observed [77, 78]. The  $\beta$ -type PSMs also require eDNA for oligomerization as well [79]. The inclusion of eDNA in *S. aureus* biofilms provides structural support similar to enteric biofilms.

Amyloids are not the only proteins that form these protein/eDNA complexes. The extracellular cell wall protein, LytC, from *Streptococcus pneumoniae* binds to DNA to form complexes within the biofilm matrix [80]. The function of the nucleoprotein complexes formed in *Myxococcus xanthus* also parallels that of curli/eDNA complexes in enteric biofilms, adding mechanical strength and adherence [81]. The continual appearance of these complexes supports that they are a key component within the ECM and in turn provides a connection to compare function of ECM components in distinct bacterial biofilms. Additionally, polysaccharide components of *Pseudomonas* biofilms complex with DNA to support the structure of the biofilm [82].

## **Immunomodulatory Effects of Bacterial Amyloid Curli**

### ***Recognition of Curli by Immune Receptors***

The interactions of curli with the immune system have been well studied since the original observation that curli is recognized by Toll-like receptor (TLR)-2 in 2009 [83]. Follow-up studies found that TLR2 complexes with TLR1 and adaptor molecule CD14 to create a heterocomplex [84, 85]. This heterocomplex is the surface receptor responsible for the initial recognition of curli by immune cells via the  $\beta$  sheet secondary structure. A single point mutation in curli altering its secondary structure was observed to greatly reduce TLR2 recognition of curli [86]. The identification of beta amyloids by their secondary structure is not sequence specific as amyloid  $\beta$  from human, which shares no amino acid sequence homology to curli, activates TLR2 in the same way [83]. Upon binding to the

TLR2/TLR1/CD14 complex, the complex is internalized and pro-inflammatory cytokines are produced such as Interleukin (IL)-6 and Tumor Necrosis Factor (TNF)- $\alpha$  [83].

Once inside the immune cell, the curli complex is able to interact with multiple receptors. The endosome containing the curli can then fuse with an endosome containing TLR9. Once fused, the eDNA portion of the complex can interact with TLR9 leading to downstream activation of Type I Interferon (IFN) genes such as *ifn $\beta$* , *isg15*, and *irf7* [87]. While this interaction with curli remains contained within the endosomes, a cytosolic receptor, the NOD-like receptor protein 3 (NLRP3) inflammasome, has also been shown to interact with curli complexes. NLRP3 activation also occurs downstream of TLR2 activation and can lead to the production of pro-inflammatory cytokines IL-1 $\beta$  and IL-18 or induce cell death. In bone marrow-derived macrophages treated with curli complexes, NLRP3 activation induced the production of IL-1 $\beta$ , but no notable cell death was observed [85]. While the interaction of curli with the NLRP3 inflammasome has been described, the mechanism by which curli exits the endosome to meet the inflammasome in the cytosol remains unknown. Together, the ability to interact with multiple receptors both extra- and intra-cellularly in combination with the composition of the complex makes curli/eDNA a model PAMP.

Antimicrobial peptides (AMPs) are used by the innate immune system as a first line of defense. While working on opposite sides of host defense, they share properties with amyloids as described in the review by Lee and colleagues [88]. AMPs can organize DNA in a way similar to curli and other bacterial amyloids where their protofibrils function as

scaffolds for this binding to occur [88]. These complexes are a signature recognized, like curli, to induce a relevant immune response mainly through TLRs.

### ***Immune Evasion and Virulence***

The purpose of biofilm formation by bacteria is environmental survival and protection. The insoluble nature of the amyloid component within the ECM shields the bacterial community from enzymatic, proteolytic and chemical insults [19, 89]. However, the formation of biofilm provides a large mass of foreign matter that can be used to identify the bacteria and activate the immune response for its clearance. Bacteria have adapted techniques to confuse the immune response by decorating their ECM with molecules that resemble host material. In this way, the host might recognize the ECM as host material and induce a self-tolerance response instead. The use of molecules resembling host is called molecular mimicry. The structural and functional similarities between human and bacteria amyloids are well studied [18, 42, 89, 90]. Also, the conserved nature of curli machinery appears across four bacterial phyla [91]. This provides a link for molecular mimicry to assist in biofilm and bacterial survival across species, but also creates a pool of antigens capable of inducing autoimmune responses in the host as well.

As curli/eDNA complexes are recognized by multiple receptors both inside and outside of immune cells, the bacteria use different mechanisms to evade the immune response to maintain virulence. One notable technique is the binding of complement protein C1q. To protect from killing by the complement system, *E. coli* curli directly binds to C1q to block the complement cascade and protect itself from immune cell killing [92].

This direct binding to C1q has also been observed with human amyloid  $\beta$  implicating a this as a common mechanism among amyloids [93]. This blockage promotes the virulence of the bacteria allowing for its future spread in the host.

As a virulence mechanism, curli is important for adherence of the cells to each other and surfaces. In *E. coli*, the ability to produce curli fibers was found of importance to allow for bacterial entry into host cells [94]. Together, these abilities of curli constitute its contribution to virulence. Interestingly, this necessity of curli to aide in entry to host cells is not observed. Extracellular DNA has also been identified to enhance virulence in enteric bacteria. In *S. Typhimurium*, expression of the *pmr* antimicrobial resistance operon is induced by eDNA in the biofilm [95]. This operon protects the bacterial cells from environmental insults such as ciprofloxacin, aminoglycosides, and antimicrobial peptides. This protection mechanism is expressed significantly lower in planktonic cells supporting its importance as a part of the protective biofilm shield [95].

## **Bacterial Infections and Human Diseases**

### *Autoimmune Diseases*

#### *Reactive Arthritis*

There are many examples of diseases in which bacterial infections initiate or exacerbate autoimmune responses (Fig. 1.1) [96]. One of the well-described autoimmune conditions that develops in response to an infection is reactive arthritis (ReA), also known as postinfectious arthritis or ankylosing spondylitis. ReA is a painful form of inflammatory

arthritis caused after GI infections with enteric pathogens such as *Salmonella*, *Shigella*, *Yersinia*, or *Campylobacter* or after genital infection with *Chlamydia trachomatis* [97]. ReA usually starts 1–4 weeks post-infection. ReA affects the joints, and many patients also develop eye inflammation (conjunctivitis) and urinary problems (urethritis). ReA affects approximately 5% of patients following GI infections, and some patients remain symptomatic for 5 years or longer. ReA has traditionally been thought of as a 'sterile' arthritis because antibiotic treatment in individuals with ReA is ineffective [98, 99] and cultures of joint fluids yield no growth of organisms. Recent evidence suggests, however, that *Chlamydia* species can become persistent in joint and synovial tissue [100, 101] of patients with ReA, and immunocytochemical staining and mass spectrometry has demonstrated the presence of enteric bacterial products in the synovial fluid, further implicating microorganisms in the inflammatory process [102-104].

Genetic variations and differences in etiology make treatment of ReA difficult. For example, the histocompatibility leukocyte antigen (HLA)-B27 genotype is a risk factor for ReA, and over two-thirds of the patients with ReA carry the HLA-B27 genotype. Those patients negative for HLA-B27 are frequently positive for cross-reacting antigens such as HLA-B7, HLA-B22, HLA-B40, or HLA-B42 [105]. It has been suggested that the bacteria express antigens that react with HLA-B27, but it is still unclear why HLA-B27 predisposes individuals to ReA. Interestingly, there is recent evidence that the presence of curli complexes drive joint inflammation in mice [57].

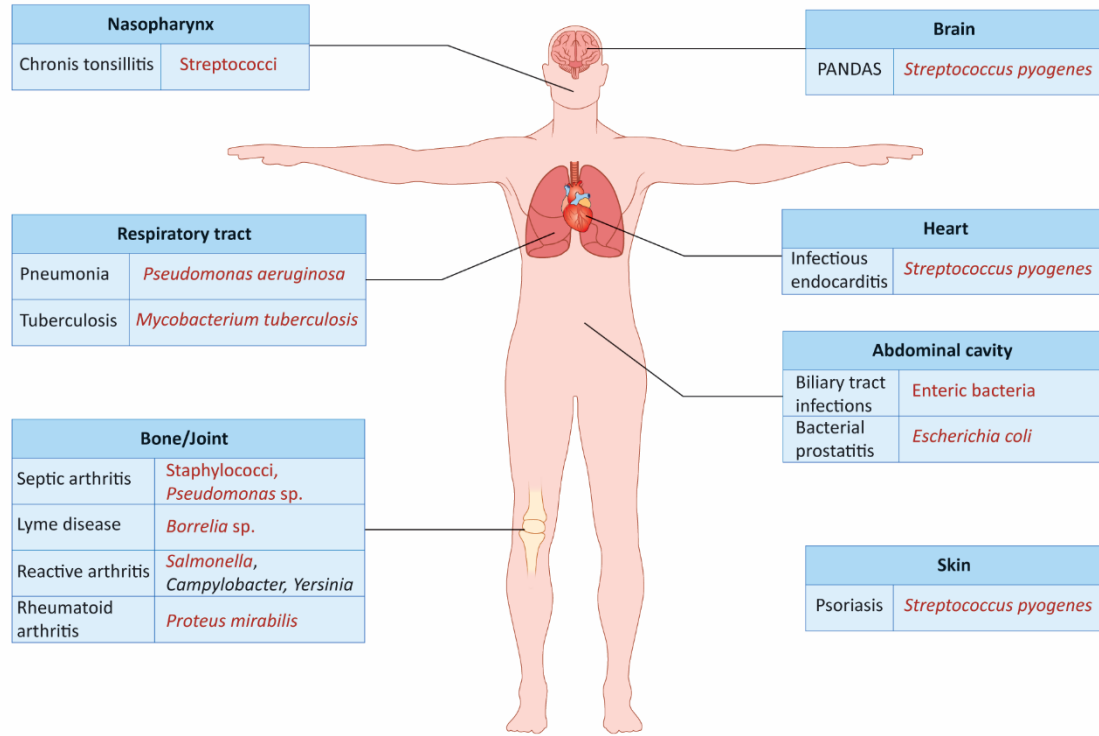


**Figure 1.1. Human Infections Leading to Autoimmune Sequelae.** Human infections and their causative bacteria. Each line links the infection type with the site location in the body. Bacteria colored red are amyloid-producing. PANDAS stands for pediatric autoimmune neuropsychiatric disorders associated with streptococci.

### *Systemic Lupus Erythematosus (SLE)*

Generation of autoantibodies, including anti-double-stranded DNA antibodies, and the type I IFN response, are hallmarks of the human autoimmune disease SLE [10]. SLE is considered a prototypical autoimmune disease; 80% of SLE patients develop joint and muscle pain, skin rashes, fatigue, and a general feeling of being unwell. SLE is often mistaken for other diseases. Anti-nuclear antibody (ANA) testing is used to confirm the presence of autoantibodies to aid in diagnosis [106]. Intriguingly, patients who eventually develop SLE show positivity for anti-double-stranded DNA and anti-chromatin years before their diagnosis [107].

Infections are the most common cause of hospitalization and mortality in SLE patients. The frequencies of infections in SLE patients, such as pneumonia, sepsis, skin infections, and UTIs, are similar to those of the general population and are caused by both Gram-positive and Gram-negative bacteria [108]. However, infections (both viral and bacterial) trigger flares in SLE patients. During a lupus flare, the most common complaints are of flu-like symptoms (with or without fever), fatigue, and muscle and joint pains. However, continual flare-ups negatively affect various organs including the kidneys and lungs, and can eventually lead to organ failure and death [109].

Genome-wide association studies suggest an involvement of TLRs in the pathogenesis of SLE [110]. It is well established that DNA triggers autoimmune responses and contributes to the pathogenesis of SLE via the activation of TLR9 [111]. Although polymorphisms of TLR2 have no correlation with predisposition to SLE, peripheral blood mononuclear cells (PBMCs) from lupus patients express higher levels of TLR2 than

PBMCs from healthy controls [110], suggesting that SLE patients may react more strongly to TLR2 ligands than do healthy individuals.

SLE patients have elevated levels of LPS in systemic circulation, suggesting that the immune systems of these patients are frequently exposed to bacterial products [112]. Consistent with this, infection with *S. Typhimurium* or *E. coli* causes bacteremia, sepsis, or soft-tissue infections in SLE patients instead of the gastroenteritis and urinary tract infections common in otherwise healthy individuals. This shows how the altered immune system of these patients can influence the location where bacteria establish an infection. The fact that curli/eDNA complexes from enteric biofilms, as well as several other infections by amyloid-producing bacteria, lead to positive ANA results suggests that there may be a link between the infections and autoimmunity. New reports have shown that lupus patients during flares have increased anti-curli/eDNA IgG antibodies compared to patients in remission. Additionally, mucosal anti-curli/eDNA IgA antibodies were found to be significantly increased in SLE patients compared to healthy controls. The source of interaction of these patients with curli-producing bacteria appeared to be UTI, as most SLE patients studied had bacteriuria at some point. Interestingly, the anti-curli/eDNA antibodies correlated with the amount of bacteria in the urine. This indicated curliated bacterial strains causing UTIs were indeed a potential source of the curli antigen and played a causative role in exacerbated flares [113].

### ***Biofilms on Implanted Devices and Autoimmune Disease***

Bacterial biofilms on implanted devices are difficult to treat, often requiring additional surgery or implant removal. Many bacteria that colonize implanted devices have the capacity to produce amyloids. There have been recent reports of patients who have undergone transvaginal mesh or hernia surgeries who have developed autoimmune diseases, including SLE, following surgery. It has been speculated that biofilms associated with the mesh break tolerance and trigger autoimmunity in these patients [114-117]. Consistent with this, recent work showed the presence of multiple species in biofilms on implanted mesh [118, 119]. The connection between implants colonized with biofilms and autoimmune disease remains controversial, as some studies have shown no direct correlation between infected mesh implants and autoimmune disease onset. More mechanistic studies, as well as epidemiological studies, are needed to determine the complex immune reactions to biofilms on implanted devices in the future.

### ***Autoimmune sequelae and amyloid-expressing bacteria***

In addition to ReA, there are other examples of arthritis likely induced by bacterial infection that are not associated with HLA-B27. Poststreptococcal arthritis is a poorly understood clinical syndrome; it is not clear whether it is a separate entity or a condition that presents with rheumatic fever. Group A streptococci colonize the throat or skin and are responsible for various infections and poststreptococcal immune sequelae. These bacteria are the most common cause of pharyngitis in school-aged children. Rheumatic fever or rheumatic heart disease is an important autoimmune sequela that follows

pharyngitis. Molecular mimicry by M-protein and the production of cross-reactive antibodies are important for the pathogenesis. Antibodies that recognize the M-protein and the N-acetyl-b-D-glucosamine of *Streptococcus pyogenes* cross-react with myosin, leading to heart damage [120, 121]. Some of the rheumatic heart disease patients also experience arthritis post-infection. However, the mechanisms that trigger arthritis are not known.

Recently, streptococcal carriage has been proposed to have a role in a human skin autoimmune disease, psoriasis. An interesting connection was discovered when researchers found that tonsillectomy provided relief of symptoms in psoriasis patients [122]. Streptococcal biofilms that cause chronic infections of the tonsils are thought to exacerbate psoriatic symptoms. This was supported by data showing that patients with moderate to severe chronic plaque psoriasis have shown improvement in skin lesions upon long-term penicillin treatment [122, 123]. Most interestingly, *Streptococcus* species have been reported to express amyloid proteins such as amyloidogenic P1, WapA and SMU\_63c [124]. As the amyloid complexes play a role in the autoimmune sequelae of SLE, we speculate that the amyloid proteins in *Streptococcus sp.* may have a similar influence.

Another example of autoimmunity induced by bacterial infections is Lyme disease. Lyme disease is a tick-borne disease caused mainly by the *Borrelia burgdorferi* bacterium, though other *Borrelia* species have been found to cause the disease in rare cases. If untreated, *Borrelia* species spread throughout the body and cause arthritis and nervous system problems as well as pain and fatigue. Although quite controversial, biofilms of *Borrelia* were detected in a recent study and proposed to be responsible for the persistent infection and continuation of disease symptoms [125]. Intriguingly, many Lyme disease

symptoms overlap with those of SLE. Furthermore, autoantibodies detected in sera from Lyme disease patients are the same as those observed in SLE patients. For example, Lyme patients, like SLE patients, test positive for ANAs [126, 127]. As we know that amyloids have a tendency to bind eDNA within the biofilm and form an immunogenic complex, the *Borrelia* amyloid, OspA has potential as a source of DNA for this ANA response. Published reports have also identified molecular mimicry of  $\gamma$ -enolase by *Borrelia* enolase has been suggested to drive the autoimmune response and more chronic symptoms [128].

The pediatric autoimmune neuropsychiatric disorders associated with streptococci, or PANDAS, are a neurological response seen in children after they have autoimmune reaction within the brain, most often thought of as an immune privileged area of the body. This provides evidence for an axis of interaction between the peripheral streptococcal infection and the neurological response.

### ***Neurodegenerative Diseases***

Amyloids are often associated with neurodegenerative disease, mostly Alzheimer's Disease and Parkinson's Disease. The main course of action in amyloid-associated neurodegenerative disease is the accumulation of amyloid inducing an inflammatory response at the sight of aggregation [90, 129, 130]. While amino acid sequences between human and bacterial amyloids differ greatly, the secondary structure and amyloid fibrillization process from monomeric subunits is shared [131, 132]. For this reason, cross-seeding of amyloids has been of interest to scientists of both amyloid and host response fields. Some of the first work proving this cross-seeding of amyloids involved curli

injection causing accelerated secondary amyloidosis disease progression [133]. Later, patient samples showing combinations of tau,  $\alpha$ -synuclein, prion protein and  $\beta$ -amyloid within deposits have supported this cross-seeding hypothesis [134]. Importantly, not only have human amyloid interactions been identified in human tissue, but curli protein CsgE has been reportedly observed bound to the non-amyloid region of  $\alpha$ -synuclein [11]. Seen in studies of  $\alpha$ -synuclein overexpressing mice, curled bacterial colonization in the gut exacerbated disease pathology associated with Parkinson's disease [135]. As curli is the product of a namely GI bacteria, the ability of the proteins to impact neuronal conditions provides evidence for an axis between the compromised gut and brain via the vagus nerve [136]. This coined "gut-brain axis" has become of great interest in the field as a link between the two spatial locations provides evidence for further potential interactions between bacterial and human amyloids and resulting disease state progressions.

### **Concluding Remarks**

The major components of the enteric biofilm, amyloid curli, eDNA and cellulose have been well studied. Each is a PAMP in its own right inducing a reaction from immune cells and various body systems. The interaction between the host and the biofilm is a continually growing field of research. Although much has been done to understand the interactions of biofilm components with the immune system, plenty is still unknown. Taking the example of enteric biofilms, while very recently there has been evidence of curli production *in vivo*, however this was only investigated for mature fibrils [57]. Our work here identifies a novel intermediate curli species which has yet to be investigated *in*

*vivo*. As we draw similarities to amyloid  $\beta$ , we hypothesize these intermediates have the potential to exist *in vivo* and have different immunomodulatory effects on their environment distinguishable from what is known about mature curli interactions. Also, our understanding of the biofilm continues to grow. As the immune system and biofilm continue to interact, new methods will evolve to better suit the success of one side or the other in a continual game of “tug of war”. Therefore, the continual exploration of the biofilm ECM components and the interplay with their environment is imperative.

Bacteria use biofilms as a refuge from the immune system to establish successful infections. Independent studies show that the resolution of many infections is complicated by autoimmune sequelae for unknown reasons. Recent evidence shows molecules used by bacteria to decorate the ECM of the biofilms, including amyloid/eDNA complexes, generate autoimmune responses during infections in animal models. It is thought that while biofilm-associated infections trigger a transient autoimmune response by bacterial amyloid/eDNA complexes in healthy individuals, this response may be sustained and detrimental in individuals genetically predisposed to an autoimmune disease. However, at this point, the role of biofilm-associated infections as a trigger and modulator for human autoimmune diseases remains to be formally proven. Epidemiological studies that delve into the clinical history of patients and consider biofilm-associated infections or possible exposure to bacterial amyloids as a risk factor to develop autoimmune diseases are needed. More importantly, new practices to ensure the eradication of biofilms are needed to prevent chronic exposure to biofilms. This will prevent long-term exposure of the immune system to the biofilm products such as amyloid/eDNA complexes that are capable of breaking

immune tolerance. Not only is autoimmune response important in the interactions of amyloids with host, but the cross-seeding influence that amyloids have demonstrated shows the strong influence they have on a multitude of body systems. With the information discussed here, it is clear that biofilms and their amyloids play an important role in many human disease states and their study and understanding are imperative in the advancement of medical research.

## References Cited

1. Costerton, J.W., *Introduction to biofilm*. Int J Antimicrob Agents, 1999. **11**(3-4): p. 217-21; discussion 237-9.
2. Pasteur, L., *Memoire sur la fermentation acetique*. Annales scientifiques de l' E.N.S., 1864. **1**: p. 113-158.
3. Henrici, A.T., *Studies of Freshwater Bacteria: I. A Direct Microscopic Technique*. J Bacteriol, 1933. **25**(3): p. 277-87.
4. Hoiby, N. and N.H. Axelsen, *Identification and quantitation of precipitins against Pseudomonas aeruginosa in patients with cystic fibrosis by means of crossed immunoelectrophoresis with intermediate gel*. Acta Pathol Microbiol Scand B Microbiol Immunol, 1973. **81**(3): p. 298-308.
5. McCoy, W.F., et al., *Observations of fouling biofilm formation*. Can J Microbiol, 1981. **27**(9): p. 910-7.
6. Costerton, J.W., G.G. Geesey, and K.J. Cheng, *How bacteria stick*. Sci Am, 1978. **238**(1): p. 86-95.
7. P., V.J., *Nature and Extent of Fouling of Ships' Bottoms*, B.o. Fisheries, Editor. 1927: Washington D.C.
8. Sunarintyas, S., *Bioadhesion of Biomaterials*, in *Biomaterials and Medical Devices*, F.a.H. Mahyudin, H., Editor. 2016, Springer: Switzerland.
9. Stoodley P., H.-S.L., Costerton B., DeMeo P., Shirtliff M., Gawalt E., Kathju S., *Biofilms, Biomaterials, and Device-Related Infections*, in *Handbook of Polymer Applications in Medicine and Medical Devices*. 2013. p. 77-101.
10. Gallo, P.M., et al., *Amyloid-DNA Composites of Bacterial Biofilms Stimulate Autoimmunity*. Immunity, 2015. **42**(6): p. 1171-84.
11. Chorell, E., et al., *Bacterial Chaperones CsgE and CsgC Differentially Modulate Human alpha-Synuclein Amyloid Formation via Transient Contacts*. PLoS One, 2015. **10**(10): p. e0140194.
12. Costerton, J.W., et al., *Microbial biofilms*. Annu Rev Microbiol, 1995. **49**: p. 711-45.
13. Flemming, H.C. and J. Wingender, *The biofilm matrix*. Nat Rev Microbiol, 2010. **8**(9): p. 623-33.

14. Sipe, J.D. and A.S. Cohen, *Review: history of the amyloid fibril*. J Struct Biol, 2000. **130**(2-3): p. 88-98.
15. Cohen, A.S. and E. Calkins, *Electron microscopic observations on a fibrous component in amyloid of diverse origins*. Nature, 1959. **183**(4669): p. 1202-3.
16. Eanes, E.D. and G.G. Glenner, *X-ray diffraction studies on amyloid filaments*. J Histochem Cytochem, 1968. **16**(11): p. 673-7.
17. Larsen, P., et al., *Amyloid adhesins are abundant in natural biofilms*. Environ Microbiol, 2007. **9**(12): p. 3077-90.
18. Chapman, M.R., et al., *Role of Escherichia coli curli operons in directing amyloid fiber formation*. Science, 2002. **295**(5556): p. 851-5.
19. Collinson, S.K., et al., *Purification and characterization of thin, aggregative fimbriae from Salmonella enteritidis*. J Bacteriol, 1991. **173**(15): p. 4773-81.
20. Schnabel, J., *Protein folding: The dark side of proteins*. Nature, 2010. **464**(7290): p. 828-9.
21. Chiti, F. and C.M. Dobson, *Protein misfolding, functional amyloid, and human disease*. Annu Rev Biochem, 2006. **75**: p. 333-66.
22. Wang, X., et al., *In vitro polymerization of a functional Escherichia coli amyloid protein*. J Biol Chem, 2007. **282**(6): p. 3713-9.
23. Hammer, N.D., et al., *The C-terminal repeating units of CsgB direct bacterial functional amyloid nucleation*. J Mol Biol, 2012. **422**(3): p. 376-89.
24. Sunde, M. and C. Blake, *The structure of amyloid fibrils by electron microscopy and X-ray diffraction*. Adv Protein Chem, 1997. **50**: p. 123-59.
25. Dueholm, M.S., et al., *Fibrillation of the major curli subunit CsgA under a wide range of conditions implies a robust design of aggregation*. Biochemistry, 2011. **50**(39): p. 8281-90.
26. Sleutel, M., et al., *Nucleation and growth of a bacterial functional amyloid at single-fiber resolution*. Nat Chem Biol, 2017. **13**(8): p. 902-908.

27. McCrate, O.A., et al., *Sum of the parts: composition and architecture of the bacterial extracellular matrix*. J Mol Biol, 2013. **425**(22): p. 4286-94.
28. Hung, C., et al., *Escherichia coli biofilms have an organized and complex extracellular matrix structure*. mBio, 2013. **4**(5): p. e00645-13.
29. Serra, D.O., A.M. Richter, and R. Hengge, *Cellulose as an architectural element in spatially structured Escherichia coli biofilms*. J Bacteriol, 2013. **195**(24): p. 5540-54.
30. Desvaux, M., et al., *Secretion and subcellular localizations of bacterial proteins: a semantic awareness issue*. Trends Microbiol, 2009. **17**(4): p. 139-45.
31. Hammar, M.R., et al., *Expression of two csg operons is required for production of fibronectin- and Congo red-binding curli polymers in Escherichia coli K-12*. Mol Microbiol, 1995. **18**(4): p. 661-670.
32. Romling, U., et al., *Curli fibers are highly conserved between Salmonella typhimurium and Escherichia coli with respect to operon structure and regulation*. J Bacteriol, 1998. **180**(3): p. 722-31.
33. Arnqvist, A., et al., *The Crl protein activates cryptic genes for curli formation and fibronectin binding in Escherichia coli HB101*. Mol Microbiol, 1992. **6**(17): p. 2443-52.
34. Gerstel, U. and U. Romling, *Oxygen tension and nutrient starvation are major signals that regulate agfD promoter activity and expression of the multicellular morphotype in Salmonella typhimurium*. Environ Microbiol, 2001. **3**(10): p. 638-48.
35. Maurer, J.J., et al., *The occurrence of ambient temperature-regulated adhesins, curli, and the temperature-sensitive hemagglutinin tsh among avian Escherichia coli*. Avian Dis, 1998. **42**(1): p. 106-18.
36. Olsen, A., et al., *Environmental regulation of curli production in Escherichia coli*. Infect Agents Dis, 1993. **2**(4): p. 272-4.
37. Romling, U., et al., *AgfD, the checkpoint of multicellular and aggregative behaviour in Salmonella typhimurium regulates at least two independent pathways*. Mol Microbiol, 2000. **36**(1): p. 10-23.
38. Paul, K., et al., *The c-di-GMP binding protein YcgR controls flagellar motor direction and speed to affect chemotaxis by a "backstop brake" mechanism*. Mol Cell, 2010. **38**(1): p. 128-39.

39. Hammar, M., Z. Bian, and S. Normark, *Nucleator-dependent intercellular assembly of adhesive curli organelles in Escherichia coli*. Proc Natl Acad Sci U S A, 1996. **93**(13): p. 6562-6.
40. Taylor, J.D., et al., *Electrostatically-guided inhibition of Curli amyloid nucleation by the CsgC-like family of chaperones*. Sci Rep, 2016. **6**: p. 24656.
41. Xue, W.F., et al., *Fibril fragmentation in amyloid assembly and cytotoxicity: when size matters*. Prion, 2010. **4**(1): p. 20-5.
42. Barnhart, M.M. and M.R. Chapman, *Curli biogenesis and function*. Annu Rev Microbiol, 2006. **60**: p. 131-47.
43. Nenninger, A.A., et al., *CsgE is a curli secretion specificity factor that prevents amyloid fibre aggregation*. Mol Microbiol, 2011. **81**(2): p. 486-99.
44. Nenninger, A.A., L.S. Robinson, and S.J. Hultgren, *Localized and efficient curli nucleation requires the chaperone-like amyloid assembly protein CsgF*. Proc Natl Acad Sci U S A, 2009. **106**(3): p. 900-5.
45. Kikuchi, T., et al., *Curli fibers are required for development of biofilm architecture in Escherichia coli K-12 and enhance bacterial adherence to human uroepithelial cells*. Microbiol Immunol, 2005. **49**(9): p. 875-84.
46. Collinson, S.K., et al., *Structural predictions of AgfA, the insoluble fimbrial subunit of Salmonella thin aggregative fimbriae*. J Mol Biol, 1999. **290**(3): p. 741-56.
47. Zhou, Y., et al., *Experimental manipulation of the microbial functional amyloid called curli*. Methods Mol Biol, 2013. **966**: p. 53-75.
48. Humphries, A., S. Deridder, and A.J. Baumler, *Salmonella enterica serotype Typhimurium fimbrial proteins serve as antigens during infection of mice*. Infect Immun, 2005. **73**(9): p. 5329-38.
49. Bian, Z., et al., *Expression of and cytokine activation by Escherichia coli curli fibers in human sepsis*. J Infect Dis, 2000. **181**(2): p. 602-12.
50. Gerstel, U., C. Park, and U. Romling, *Complex regulation of csgD promoter activity by global regulatory proteins*. Mol Microbiol, 2003. **49**(3): p. 639-54.

51. Brown, P.K., et al., *MlrA, a novel regulator of curli (AgF) and extracellular matrix synthesis by Escherichia coli and Salmonella enterica serovar Typhimurium*. Mol Microbiol, 2001. **41**(2): p. 349-63.
52. Chen, C.Y., et al., *Multiple mechanisms responsible for strong Congo-red-binding variants of Escherichia coli O157:H7 strains*. Pathog Dis, 2016. **74**(2).
53. Uhlich, G.A., J.E. Keen, and R.O. Elder, *Mutations in the csgD promoter associated with variations in curli expression in certain strains of Escherichia coli O157:H7*. Appl Environ Microbiol, 2001. **67**(5): p. 2367-70.
54. Cordeiro, M.A., et al., *Curli fimbria: an Escherichia coli adhesin associated with human cystitis*. Braz J Microbiol, 2016. **47**(2): p. 414-6.
55. Kai-Larsen, Y., et al., *Uropathogenic Escherichia coli modulates immune responses and its curli fimbriae interact with the antimicrobial peptide LL-37*. PLoS Pathog, 2010. **6**(7): p. e1001010.
56. Subashchandrabose, S., et al., *Host-specific induction of Escherichia coli fitness genes during human urinary tract infection*. Proc Natl Acad Sci U S A, 2014. **111**(51): p. 18327-32.
57. Miller, A.L., Pasternak, J.A., Medeiros N. J., Nicastro L. K., Tursi, S. A., Hansen E. G., Krochak, R., Sokaribo, A. S., MacKenzie, K. D., Palmer, M. B., Herman, D. J., Watson, N. L., Zhang, Y., Wilson, H. L., Wilson, R. P., White, A. P., Tukel, C. , *In vivo synthesis of bacterial amyloid curli contributes to joint inflammation during S. Typhimurium infection*. PLOS Pathog, 2020.
58. Zogaj, X., et al., *Production of cellulose and curli fimbriae by members of the family Enterobacteriaceae isolated from the human gastrointestinal tract*. Infect Immun, 2003. **71**(7): p. 4151-8.
59. Ross, P., et al., *Regulation of cellulose synthesis in Acetobacter xylinum by cyclic diguanylic acid*. Nature, 1987. **325**(6101): p. 279-81.
60. Thongsomboon, W., et al., *Phosphoethanolamine cellulose: A naturally produced chemically modified cellulose*. Science, 2018. **359**(6373): p. 334-338.
61. Bokranz, W., et al., *Expression of cellulose and curli fimbriae by Escherichia coli isolated from the gastrointestinal tract*. J Med Microbiol, 2005. **54**(Pt 12): p. 1171-1182.

62. Zogaj, X., et al., *The multicellular morphotypes of Salmonella typhimurium and Escherichia coli produce cellulose as the second component of the extracellular matrix*. Mol Microbiol, 2001. **39**(6): p. 1452-63.
63. Whitchurch, C.B., et al., *Extracellular DNA required for bacterial biofilm formation*. Science, 2002. **295**(5559): p. 1487.
64. Zafra, O., et al., *Extracellular DNA release by undomesticated Bacillus subtilis is regulated by early competence*. PLoS One, 2012. **7**(11): p. e48716.
65. Latasa, C., et al., *BapA, a large secreted protein required for biofilm formation and host colonization of Salmonella enterica serovar Enteritidis*. Mol Microbiol, 2005. **58**(5): p. 1322-39.
66. Gibson, D.L., et al., *Salmonella produces an O-antigen capsule regulated by AgfD and important for environmental persistence*. J Bacteriol, 2006. **188**(22): p. 7722-30.
67. Nesper, J., et al., *Characterization of Vibrio cholerae O1 El tor galU and galE mutants: influence on lipopolysaccharide structure, colonization, and biofilm formation*. Infect Immun, 2001. **69**(1): p. 435-45.
68. Genevaux, P., et al., *Identification of Tn10 insertions in the rfaG, rfaP, and galU genes involved in lipopolysaccharide core biosynthesis that affect Escherichia coli adhesion*. Arch Microbiol, 1999. **172**(1): p. 1-8.
69. Crawford, R.W., et al., *Identification of a bile-induced exopolysaccharide required for Salmonella biofilm formation on gallstone surfaces*. Infect Immun, 2008. **76**(11): p. 5341-9.
70. Goebel, W.F., *Colanic acid*. Proc Natl Acad Sci U S A, 1963. **49**: p. 464-71.
71. Beloin, C., A. Roux, and J.M. Ghigo, *Escherichia coli biofilms*. Curr Top Microbiol Immunol, 2008. **322**: p. 249-89.
72. Stevenson, G., et al., *Organization of the Escherichia coli K-12 gene cluster responsible for production of the extracellular polysaccharide colanic acid*. J Bacteriol, 1996. **178**(16): p. 4885-93.
73. Stout, V., *Identification of the promoter region for the colanic acid polysaccharide biosynthetic genes in Escherichia coli K-12*. J Bacteriol, 1996. **178**(14): p. 4273-80.

74. Sledjeski, D.D. and S. Gottesman, *Osmotic shock induction of capsule synthesis in Escherichia coli K-12*. J Bacteriol, 1996. **178**(4): p. 1204-6.
75. Danese, P.N., L.A. Pratt, and R. Kolter, *Exopolysaccharide production is required for development of Escherichia coli K-12 biofilm architecture*. J Bacteriol, 2000. **182**(12): p. 3593-6.
76. Prigent-Combaret, C., et al., *Developmental pathway for biofilm formation in curli-producing Escherichia coli strains: role of flagella, curli and colanic acid*. Environ Microbiol, 2000. **2**(4): p. 450-64.
77. Schwartz, K., et al., *Extracellular DNA facilitates the formation of functional amyloids in Staphylococcus aureus biofilms*. Mol Microbiol, 2016. **99**(1): p. 123-34.
78. Tayeb-Fligelman, E., et al., *The cytotoxic Staphylococcus aureus PSMalpha3 reveals a cross-alpha amyloid-like fibril*. Science, 2017. **355**(6327): p. 831-833.
79. Huseby, M.J., et al., *Beta toxin catalyzes formation of nucleoprotein matrix in staphylococcal biofilms*. Proc Natl Acad Sci U S A, 2010. **107**(32): p. 14407-12.
80. Domenech, M., et al., *Insight into the composition of the intercellular matrix of Streptococcus pneumoniae biofilms*. Environ Microbiol, 2013. **15**(2): p. 502-16.
81. Hu, W., et al., *Direct visualization of the interaction between pilin and exopolysaccharides of Myxococcus xanthus with eGFP-fused PilA protein*. FEMS Microbiol Lett, 2012. **326**(1): p. 23-30.
82. Jennings, L.K., et al., *Pel is a cationic exopolysaccharide that cross-links extracellular DNA in the Pseudomonas aeruginosa biofilm matrix*. Proc Natl Acad Sci U S A, 2015. **112**(36): p. 11353-8.
83. Tukel, C., et al., *Responses to amyloids of microbial and host origin are mediated through toll-like receptor 2*. Cell Host Microbe, 2009. **6**(1): p. 45-53.
84. Tukel, C., et al., *Toll-like receptors 1 and 2 cooperatively mediate immune responses to curli, a common amyloid from enterobacterial biofilms*. Cell Microbiol, 2010. **12**(10): p. 1495-505.

85. Rapsinski, G.J., et al., *CD14 protein acts as an adaptor molecule for the immune recognition of Salmonella curli fibers*. J Biol Chem, 2013. **288**(20): p. 14178-88.
86. Bian, Z., et al., *Activation of inducible nitric oxide synthase/nitric oxide by curli fibers leads to a fall in blood pressure during systemic Escherichia coli infection in mice*. J Infect Dis, 2001. **183**(4): p. 612-9.
87. Tursi, S.A., et al., *Bacterial amyloid curli acts as a carrier for DNA to elicit an autoimmune response via TLR2 and TLR9*. PLoS Pathog, 2017. **13**(4): p. e1006315.
88. Lee, E.Y., Srinivasan, Y., de Anda, J., Nicastro, L. K., Tukul, C., Wong, G. C. L., *Functional reciprocity of amyloids and antimicrobial peptide: Rethinking the role of supramolecular assembly in host defense, immune activation, and inflammation*. Front Immunol, 2020.
89. Hufnagel, D.A., C. Tukul, and M.R. Chapman, *Disease to dirt: the biology of microbial amyloids*. PLoS Pathog, 2013. **9**(11): p. e1003740.
90. Tursi, S.A. and C. Tukul, *Curli-Containing Enteric Biofilms Inside and Out: Matrix Composition, Immune Recognition, and Disease Implications*. Microbiol Mol Biol Rev, 2018. **82**(4).
91. Dueholm, M.S., et al., *Curli functional amyloid systems are phylogenetically widespread and display large diversity in operon and protein structure*. PLoS One, 2012. **7**(12): p. e51274.
92. Biesecker, S.G., et al., *The Functional Amyloid Curli Protects Escherichia coli against Complement-Mediated Bactericidal Activity*. Biomolecules, 2018. **8**(1).
93. Jiang, H., et al., *beta-Amyloid activates complement by binding to a specific region of the collagen-like domain of the C1q A chain*. J Immunol, 1994. **152**(10): p. 5050-9.
94. Gophna, U., et al., *Curli fibers mediate internalization of Escherichia coli by eukaryotic cells*. Infect Immun, 2001. **69**(4): p. 2659-65.
95. Johnson, L., et al., *Extracellular DNA-induced antimicrobial peptide resistance in Salmonella enterica serovar Typhimurium*. BMC Microbiol, 2013. **13**: p. 115.

96. Nicastro, L. and C. Tukel, *Bacterial Amyloids: The Link between Bacterial Infections and Autoimmunity*. Trends Microbiol, 2019. **27**(11): p. 954-963.
97. Carter, J.D. and A.P. Hudson, *Reactive arthritis: clinical aspects and medical management*. Rheum Dis Clin North Am, 2009. **35**(1): p. 21-44.
98. Carter, J.D. and A.P. Hudson, *The evolving story of Chlamydia-induced reactive arthritis*. Curr Opin Rheumatol, 2010. **22**(4): p. 424-30.
99. Kvien, T.K., et al., *Three month treatment of reactive arthritis with azithromycin: a EULAR double blind, placebo controlled study*. Ann Rheum Dis, 2004. **63**(9): p. 1113-9.
100. Carter, J.D., et al., *Combination antibiotics as a treatment for chronic Chlamydia-induced reactive arthritis: a double-blind, placebo-controlled, prospective trial*. Arthritis Rheum, 2010. **62**(5): p. 1298-307.
101. Gerard, H.C., et al., *Synovial Chlamydia trachomatis in patients with reactive arthritis/Reiter's syndrome are viable but show aberrant gene expression*. J Rheumatol, 1998. **25**(4): p. 734-42.
102. Nikkari, S., et al., *Salmonella-triggered reactive arthritis: use of polymerase chain reaction, immunocytochemical staining, and gas chromatography-mass spectrometry in the detection of bacterial components from synovial fluid*. Arthritis Rheum, 1999. **42**(1): p. 84-9.
103. Nikkari, S., et al., *Yersinia-triggered reactive arthritis. Use of polymerase chain reaction and immunocytochemical staining in the detection of bacterial components from synovial specimens*. Arthritis Rheum, 1992. **35**(6): p. 682-7.
104. Sibia, J. and F.X. Limbach, *Reactive arthritis or chronic infectious arthritis?* Ann Rheum Dis, 2002. **61**(7): p. 580-7.
105. Nasution, A.R., et al., *HLA-B27 subtypes positively and negatively associated with spondyloarthropathy*. J Rheumatol, 1997. **24**(6): p. 1111-4.
106. Petri, M., et al., *Derivation and validation of the Systemic Lupus International Collaborating Clinics classification criteria for systemic lupus erythematosus*. Arthritis Rheum, 2012. **64**(8): p. 2677-86.

107. Munroe, M.E., et al., *Altered type II interferon precedes autoantibody accrual and elevated type I interferon activity prior to systemic lupus erythematosus classification*. *Ann Rheum Dis*, 2016. **75**(11): p. 2014-2021.
108. Zandman-Goddard, G. and Y. Shoenfeld, *SLE and infections*. *Clin Rev Allergy Immunol*, 2003. **25**(1): p. 29-40.
109. Jung, J.Y. and C.H. Suh, *Infection in systemic lupus erythematosus, similarities, and differences with lupus flare*. *Korean J Intern Med*, 2017. **32**(3): p. 429-438.
110. Wu, Y.W., W. Tang, and J.P. Zuo, *Toll-like receptors: potential targets for lupus treatment*. *Acta Pharmacol Sin*, 2015. **36**(12): p. 1395-407.
111. Celhar, T., R. Magalhaes, and A.M. Fairhurst, *TLR7 and TLR9 in SLE: when sensing self goes wrong*. *Immunol Res*, 2012. **53**(1-3): p. 58-77.
112. Shi, L., et al., *The SLE transcriptome exhibits evidence of chronic endotoxin exposure and has widespread dysregulation of non-coding and coding RNAs*. *PLoS One*, 2014. **9**(5): p. e93846.
113. Pachucki, R., Corradetti, C., Kohler, L., Ghadiali, J., Gallo, P., Nicastro, L., Tursi, S., Gallucci, S., Tukel, C., Caricchio, R., *Persistent Bacteriuria and Antibodies recognizing Curli/eDNA complexes from E. Coli are Linked to Flares in Systemic Lupus Erythematosus*. *Arthritis Rheum*, 2020.
114. Chughtai, B., et al., *Hernia repair with polypropylene mesh is not associated with an increased risk of autoimmune disease in adult men*. *Hernia*, 2017. **21**(4): p. 637-642.
115. Chughtai, B., et al., *Is vaginal mesh a stimulus of autoimmune disease?* *Am J Obstet Gynecol*, 2017. **216**(5): p. 495 e1-495 e7.
116. Clancy, C., P. Jordan, and P.F. Ridgway, *Polypropylene mesh and systemic side effects in inguinal hernia repair: current evidence*. *Ir J Med Sci*, 2019. **188**(4): p. 1349-1356.
117. Strietzel, F.P., et al., *Implants in patients with oral manifestations of autoimmune or muco-cutaneous diseases - A systematic review*. *Med Oral Patol Oral Cir Bucal*, 2019. **24**(2): p. e217-e230.
118. Kathju, S., et al., *Direct demonstration of bacterial biofilms on prosthetic mesh after ventral herniorrhaphy*. *Surg Infect (Larchmt)*, 2015. **16**(1): p. 45-53.

119. Langbach, O., et al., *Oral, intestinal, and skin bacteria in ventral hernia mesh implants*. J Oral Microbiol, 2016. **8**: p. 31854.
120. Cunningham, M.W., et al., *Human and murine antibodies cross-reactive with streptococcal M protein and myosin recognize the sequence GLN-LYS-SER-LYS-GLN in M protein*. J Immunol, 1989. **143**(8): p. 2677-83.
121. Cunningham, M.W., *Streptococcus and rheumatic fever*. Curr Opin Rheumatol, 2012. **24**(4): p. 408-16.
122. Allen, H.B., et al., *Psoriasis, chronic tonsillitis, and biofilms: Tonsillar pathologic findings supporting a microbial hypothesis*. Ear Nose Throat J, 2018. **97**(3): p. 79-82.
123. Saxena, V.N. and J. Dogra, *Long-term use of penicillin for the treatment of chronic plaque psoriasis*. Eur J Dermatol, 2005. **15**(5): p. 359-62.
124. Besingi, R.N., et al., *Functional amyloids in Streptococcus mutans, their use as targets of biofilm inhibition and initial characterization of SMU\_63c*. Microbiology, 2017. **163**(4): p. 488-501.
125. Sapi, E., et al., *Evidence of In Vivo Existence of Borrelia Biofilm in Borrelial Lymphocytomas*. Eur J Microbiol Immunol (Bp), 2016. **6**(1): p. 9-24.
126. Federlin, K. and H. Becker, *[Borrelia infection and systemic lupus erythematosus]*. Immun Infekt, 1989. **17**(6): p. 195-8.
127. Singh, S.K. and H.J. Girschick, *Lyme borreliosis: from infection to autoimmunity*. Clin Microbiol Infect, 2004. **10**(7): p. 598-614.
128. Maccallini, P., S. Bonin, and G. Trevisan, *Autoimmunity against a glycolytic enzyme as a possible cause for persistent symptoms in Lyme disease*. Med Hypotheses, 2018. **110**: p. 1-8.
129. Meda, L., et al., *Activation of microglial cells by beta-amyloid protein and interferon-gamma*. Nature, 1995. **374**(6523): p. 647-50.
130. Guo, J.T., et al., *Inflammation-dependent cerebral deposition of serum amyloid a protein in a mouse model of amyloidosis*. J Neurosci, 2002. **22**(14): p. 5900-9.

131. Wang, X., N.D. Hammer, and M.R. Chapman, *The molecular basis of functional bacterial amyloid polymerization and nucleation*. J Biol Chem, 2008. **283**(31): p. 21530-9.
132. Tiiman, A., et al., *Effect of agitation on the peptide fibrillization: Alzheimer's amyloid-beta peptide 1-42 but not amylin and insulin fibrils can grow under quiescent conditions*. J Pept Sci, 2013. **19**(6): p. 386-91.
133. Lundmark, K., et al., *Protein fibrils in nature can enhance amyloid protein A amyloidosis in mice: Cross-seeding as a disease mechanism*. Proc Natl Acad Sci U S A, 2005. **102**(17): p. 6098-102.
134. Giasson, B.I., V.M. Lee, and J.Q. Trojanowski, *Interactions of amyloidogenic proteins*. Neuromolecular Med, 2003. **4**(1-2): p. 49-58.
135. Sampson, T.R., et al., *A gut bacterial amyloid promotes alpha-synuclein aggregation and motor impairment in mice*. Elife, 2020. **9**.
136. Holmqvist, S., et al., *Direct evidence of Parkinson pathology spread from the gastrointestinal tract to the brain in rats*. Acta Neuropathol, 2014. **128**(6): p. 805-20.

**CHAPTER 2**  
**CYTOTOXIC CURLI INTERMEDIATES FORM DURING *SALMONELLA***  
**BIOFILM DEVELOPMENT**

Lauren Nicaastro<sup>1</sup>, Sarah A. Tursi<sup>1</sup>, Long S. Le<sup>1</sup>, Amanda L. Miller<sup>1</sup>, Andrey Efimov<sup>2</sup>,  
Bettina Buttarò<sup>1</sup>, Vincent Tam<sup>1</sup>, and Çağla Tükel<sup>1</sup>.

<sup>1</sup> Department of Microbiology and Immunology, Lewis Katz School of Medicine,  
Temple University, Philadelphia, Pennsylvania, United States of America

<sup>2</sup> Fox Chase Cancer Center, Philadelphia, Pennsylvania, United States of America

Paper Published in Journal of Bacteriology

September 2019. Volume 201. Issue 18. eCollection 00095-19.

## Abstract

*Enterobacteriaceae* produce amyloid proteins called curli that are the major proteinaceous component of biofilms. Amyloids are also produced by humans and are associated with diseases such as Alzheimer's. During the multistep process of amyloid formation, monomeric subunits form oligomers, protofibrils, and finally mature fibrils. Amyloid  $\beta$  oligomers are more cytotoxic to cells than the mature amyloid fibrils. Oligomeric intermediates of curli had not been previously detected. We determined that turbulence inhibited biofilm formation and that, intriguingly, curli aggregates purified from cultures grown under high-turbulence conditions were structurally smaller and contained less DNA than curli preparations from cultures grown with less turbulence. Using flow cytometry analysis, we demonstrated that CsgA was expressed in cultures exposed to higher turbulence but that these cultures had lower levels of cell death than less-turbulent cultures. Our data suggest that the DNA released during cell death drives the formation of larger fibrillar structures. Consistent with this idea, addition of exogenous genomic DNA increased the size of the curli intermediates and led to binding to thioflavin T at levels observed with mature aggregates. Similar to the intermediate oligomers of amyloid  $\beta$ , intermediate curli aggregates were more cytotoxic than the mature curli fibrils when incubated with bone marrow-derived macrophages. The discovery of cytotoxic curli intermediates will enable research into the roles of amyloid intermediates in the pathogenesis of *Salmonella* and other bacteria that cause enteric infections.

## Introduction

Bacteria thrive in numerous, vastly different environments. Biofilms, which protect bacteria from environmental insults, immune defense mechanisms, and antimicrobial agents, are associated with up to 65% of human infections [1]. The extracellular matrix (ECM) of a biofilm is composed of proteins, DNA, and polysaccharides [2, 3] and is primarily responsible for the recalcitrance of bacterial infections to antimicrobial substances and the immune system [4].

Amyloid proteins are characterized by their conserved cross- $\beta$ -sheet quaternary structure [5]. It is estimated that amyloids decorate the biofilms of more than 40% of bacteria [6]. Amyloid curli, the best-characterized bacterial amyloids, are produced by members of the *Enterobacteriaceae* family. Curli are encoded by the *csgBAC* and *csgDEFG* operons and assembled via a nucleation precipitation pathway encoded by a type VIII secretion system [7, 8]. The *csgA* gene encodes the major subunit of the fibril, CsgA, and the *csgB* gene encodes a minor subunit, CsgB, a nucleator protein [9-12]. Together these proteins transport and assemble curli fibrils outside of the bacterial cell. Curli fibrils are critical for the structural integrity and stability of the biofilm. Previous work from our lab has described the inclusion of extracellular DNA (eDNA) into curli fibrils from *Salmonella enterica* serotype Typhimurium and *Escherichia coli* during biofilm formation. DNA incorporation increases the amyloid fibrillization rate of synthetic curli monomers [13]. Like curli, the bacterial amyloids produced by *Staphylococcus aureus*, phenol-soluble modulins (PSMs), also associate with eDNA [14, 15].

Amyloids not only are found in bacteria but also have been observed in humans. More than 60 amyloidogenic proteins are expressed under homeostatic conditions, but their physiological roles remain unclear. These amyloids can accumulate and form deposits that are associated with diseases such as Alzheimer's, type II diabetes, Huntington's, and secondary amyloidosis [16-18]. In each of these diseases, a unique amyloid accumulates in an organ associated with the disease. For instance, in Alzheimer's disease, amyloid  $\beta$  accumulates in the brain, forming plaques. The formation of fibrillar amyloid  $\beta$  has been extensively studied, and intermediate forms of amyloid  $\beta$  such as oligomers and protofibrils have been described. Briefly, the monomeric amyloid  $\beta$  first forms oligomeric units that have been shown to be cytotoxic to immune cells [19-21]. Oligomeric units then form protofibrils, which then form mature fibrillar amyloid  $\beta$ . Once the amyloid  $\beta$  fibrils have fully formed, they are less cytotoxic. Similar to bacterial amyloid curli and PSMs, amyloid  $\beta$  also binds to DNA [22]. Although bacterial and human amyloids do not have homology in their amino acid sequences, amyloids are characterized by their conserved  $\beta$ -sheet fibrillar structure and common functional properties [2, 7, 9, 23, 24]. This conserved structure is recognized by the innate immune receptors such as the Toll-like receptor 2 (TLR2)/TLR1 heterocomplex and Nod-like receptor protein 3 (NLRP3) inflammasome [25, 26]. It is thought that bacteria produce amyloids as part of their biofilm, introducing a common molecular pattern for host recognition [23]. Intriguingly, recent studies suggested a connection between bacterial amyloid curli and two complex human diseases, systemic lupus erythematosus and Parkinson's disease [13, 27]. However, the exact mechanism by which curli contribute to these human diseases *in vivo* remains unclear.

Curli assembly involves fibrillization, which has been monitored using approaches similar to those used to characterize fibrillization of amyloid  $\beta$  (e.g., binding to thioflavin T [ThT]), but structural intermediates in the curli fibrillization process had not been identified [28, 29]. We found that we could interfere with the formation of mature curli fibrils by increasing turbulence during the biofilm formation in liquid culture. For the first time, we were able to purify cytotoxic intermediate forms of curli that resemble protofibrillar structures formed by amyloid  $\beta$ .

## **Results**

### ***High Turbulence Leads To Decreased Biofilm Formation***

In the laboratory setting, curli expression is induced in *S. Typhimurium* cells grown under stress such as low temperature or low osmolarity [30-32]. If these conditions are applied to liquid static cultures, biofilm formation is observed at the air-liquid interface. Recently, it was also reported that the addition of dimethyl sulfoxide (DMSO) triggers curli expression and leads to the formation of biofilms even in shaken cultures [33]. We use DMSO to trigger curli expression in order to purify curli from *S. Typhimurium*. Briefly, cultures of *S. Typhimurium* are grown in yeast extract supplemented with Casamino Acids (YESCA) broth containing 4% DMSO. Cultures are shaken at 200 rpm for 72 h at 26°C. At this time point, biofilm (also termed the pellicle) is observed forming at the air-liquid-flask interface. Eight 150-ml cultures are pooled, and curli are purified as described previously [34]. In an attempt to increase production, we increased the culture volume from 150 ml to 500 ml and used a 1-liter flask. Although the starting inoculum ratio and all other variables were the same, we did not observe the production of a robust pellicle biofilm at

the air-liquid interface in the 1-liter flask. In addition, we observed a clear difference in turbulence in the 150-ml and 500-ml culture volumes. The larger volume culture was more turbulent than the smaller volume culture, and foamy bubbles were observed in the 500-ml culture. Finally, by decreasing the shaking speed of the 500-ml culture in the 1-liter flask, we were able to visibly decrease the turbulence and restore the biofilm formation (Fig. S2.1). Additionally, we examined the effect of different speeds that influence the turbulence seen in the batch culture flasks. In the 1-liter flask, decreasing turbulence was able to increase the biofilm pellicle formed on the air-liquid-flask interface. In contrast, increasing turbulence in the 150-ml flask disrupted pellicle formation, causing a decrease in pellicle size (Fig. S2.1).

We also observed that cultures with higher turbulence had less visible aggregation of bacteria. Visible aggregation and sedimentation were observed after only 2 min in an aliquot taken from the 150-ml culture (at 72 h of incubation), whereas there was no visible aggregation or sedimentation in the sample taken from the 500-ml culture after 10 min (Fig. 2.1A) or 72 h (Fig. S2.2). In the 150-ml culture, the biofilm pellicle was clearly visible and stained brightly with crystal violet (Fig. 2.1B). In the 500-ml culture, which had higher turbulence, the pellicle stained poorly with crystal violet (Fig. 2.1B). This difference in biofilm was not due to bacterial growth rate, as shown by optical density determination, but potentially was due to a difference in the ratios of planktonic and biofilm-forming bacteria (Fig. S2.2).

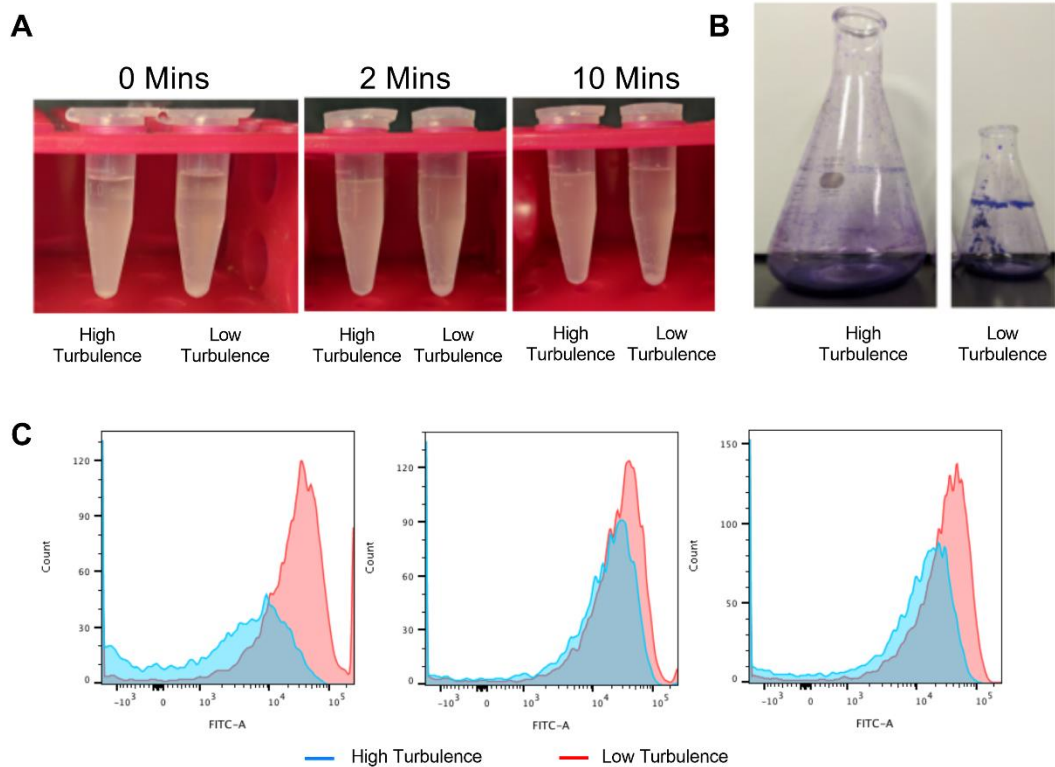


**Figure 2.1. Higher Turbulence Leads to Decreased Biofilm Formation.** (A) Sedimentation assay of aliquots of cultures from high-turbulence (500-ml) and low-turbulence (150-ml) cultures allowed to sediment for 0 min, 2 min, and 10 min. (B) Crystal violet staining of the pellicle-associated biofilm from high-turbulence and low-turbulence growth conditions. (C) Flow cytometry histograms of curli induction as measured by GFP expressed from a reporter plasmid conjugated to the *csgBA* promoter at 24 h (left), 48 h (middle), and 72 h (right) under high-turbulence and low-turbulence growth conditions.

As the major proteinaceous component of the enteric bacterial biofilm, curli fibrils are important for cell-to-cell interactions and surface attachment [35]. As the biofilm pellicle and aggregation differed depending on the turbulence of culture, we first investigated whether curli expression differed under the two conditions. To evaluate curli expression, we used a reporter strain of *S. Typhimurium* that contains the *P<sub>csgBA</sub>::gfp* reporter plasmid. When the *csgBA* gene is expressed, green fluorescent protein (GFP) is produced and can be detected by flow cytometry. GFP expression was detected in both cultures, although in the 500-ml high-turbulence cultures, expression was delayed and decreased relative to that in the 150-ml low-turbulence cultures (Fig. 2.1C). These data suggest that although the curli structural components are expressed, pellicle formation is not optimal under high turbulence.

#### ***Intermediate Forms Of Curli Aggregates Are Detectable Under High-Turbulence Conditions***

Although there was no pellicle in the 500-ml culture grown with shaking at 200 rpm, we were able to purify curli from both the 150-ml and the 500-ml culture conditions. When we performed a dot blot using anti-CsgA antibodies, CsgA was detected in both protein preparations, although the amount of curli recognized by the antibody was smaller in the sample from the 500-ml culture (Fig. 2.2A). We next stained samples with the amyloid-specific stain thioflavin T (ThT). Fluorescence due to ThT binding to curli increases as fibrillization increases [36]. The protein preparations from both conditions stained with ThT; however, the curli purified under high-turbulence conditions showed lower levels of ThT fluorescence compared to the curli purified from

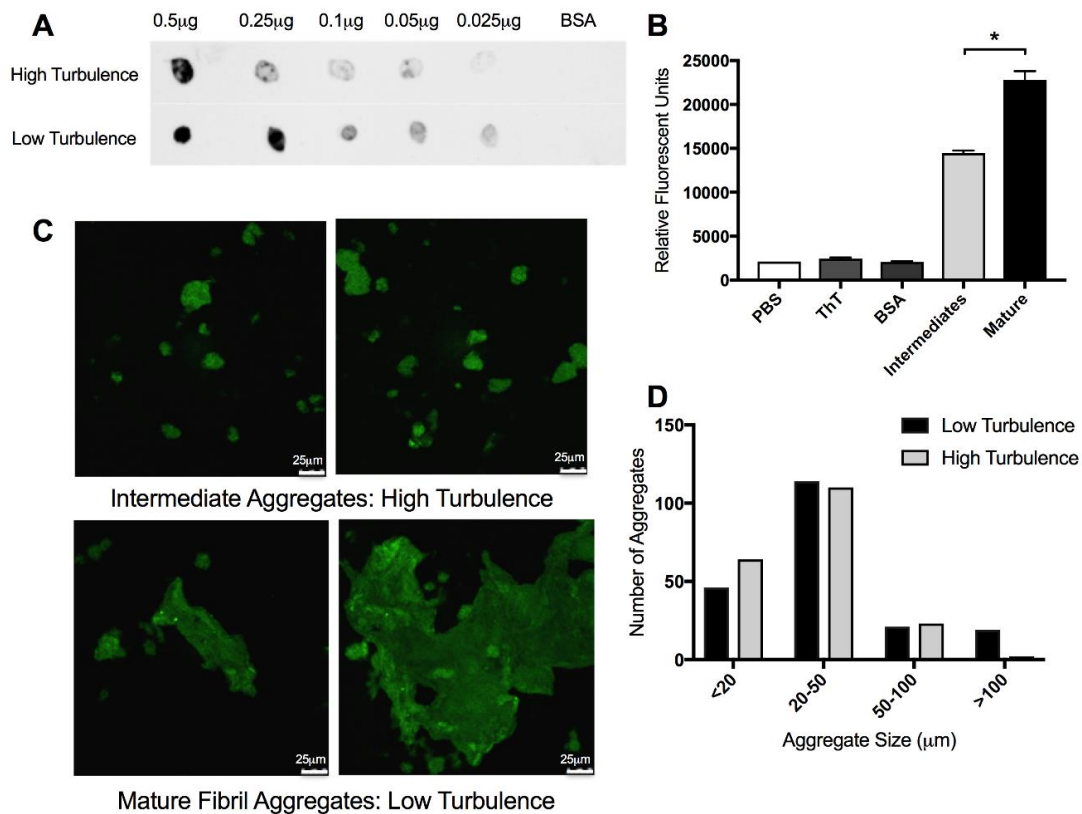


**Figure 2.2. Curli Intermediates are Detected under High-Turbulence Growth**

**Conditions.** (A) Dot blot analysis of decreasing concentrations of curli purified from high-turbulence and low-turbulence cultures was completed on PVDF membrane. BSA was used as a negative control. Blots were imaged on the Li-Cor Odyssey imaging system. (B) Aliquots of purified curli aggregates (400  $\mu$ g/ml) from high-turbulence and low-turbulence growth conditions were stained with 10  $\mu$ M ThT and quantified after a 10-min incubation at room temperature on a fluorescent plate reader at excitation 440 nm/emission 500 nm. Data are means ( $\pm$ standard error of the mean [SEM]) from three replicates. \*,  $P < 0.05$ . (C) Curli purified from high-turbulence (left panel) and low-turbulence (right panel) growth conditions stained with 10  $\mu$ M thioflavin T were imaged at  $\times 60$  magnification by confocal microscopy. Scale bars are 25  $\mu$ m. (D) Enumeration of

difference in size of aggregates calculated by confocal microscopy images. Aggregates were measured within the LAS AF confocal system and grouped into one of four groups. Two hundred aggregates were counted for each condition.

the low-turbulence conditions (Fig. 2.2B). Consistent with this, the curli purified under high-turbulence conditions displayed smaller curli aggregates under confocal microscopy compared to the curli purified from the low-turbulence conditions (Fig. 2.2C). Using the LAS AF software, we measured the size of the curli aggregates across multiple fields of view. After counting 200 aggregates from each condition, we found the average size of curli masses purified under high-turbulence conditions to be smaller than that of the mature aggregates purified from the low-turbulence conditions (Fig. 2.2D). Therefore, we termed these smaller curli masses curli intermediates. To confirm the physical differences in these aggregates, we also used transmission electron microscopy (TEM). Fibrillar structures were visible in both curli preparations purified from high-turbulence and low-turbulence conditions (Fig. 2.3). However, the curli purified from low-turbulence conditions displayed larger aggregates with spots showing greater electron density (Fig. 2.3, middle lower panel). Even small aggregates from the low-turbulence conditions showed electron-dense regions (Fig. 2.3, right lower panel), supporting the idea that these aggregates are highly fibrillized and aggregated into a compact structure compared to the intermediates that do not show this dense staining. Additionally, the density of the staining in the mature aggregates may be attributable to greater DNA incorporation and therefore structural support for these larger aggregations.

Overall, these experiments showed that although biofilm formation is inhibited by the increased turbulence in the bacterial culture, CsgA is expressed under both high- and low-turbulence conditions; however, larger mature fibrillar aggregates were observed only under lower turbulence, where the biofilm was visible at the air-liquid-flask interface.

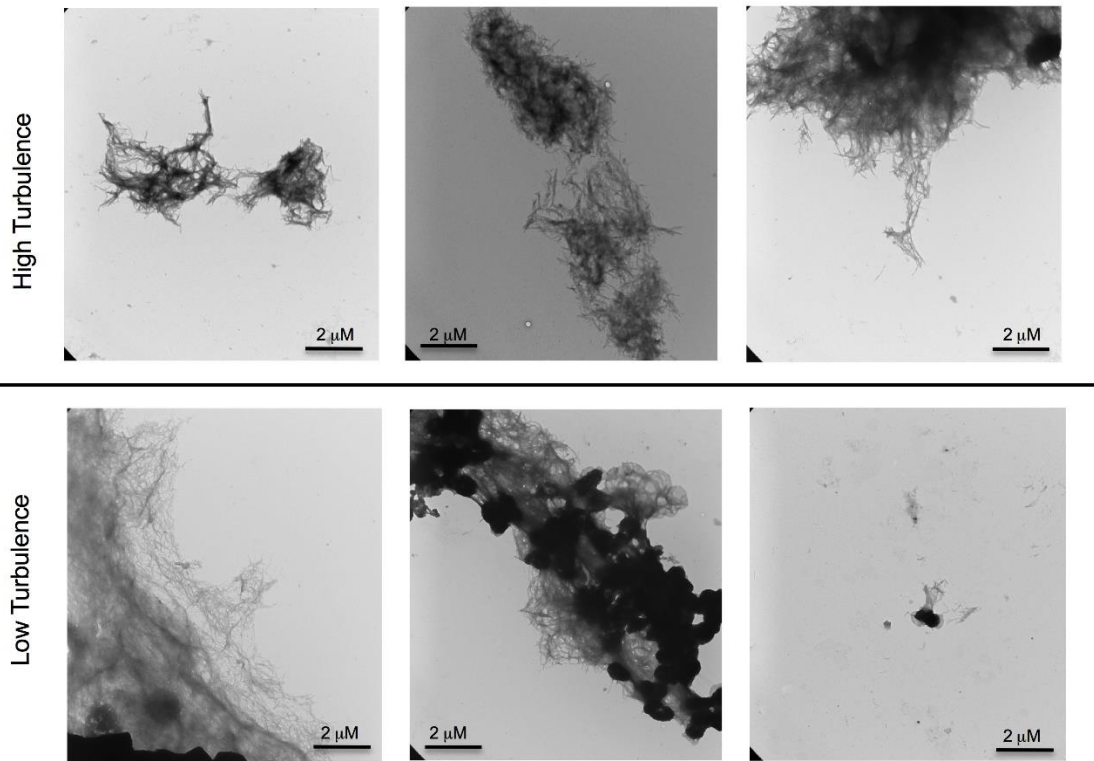


**Figure 2.3. Transmission Electron Microscopy of High- and Low-Turbulence Curli Aggregates Showing Electron Density Differences.** Purified curli from high-turbulence and low-turbulence conditions stained by negative staining were imaged at  $\times 16,500$  magnification by transmission electron microscopy, showing electron density differences.

### *DNA Induces Formation Of Mature Curli Fibrillar Aggregates*

Previous work from our lab has shown that eDNA associates with curli fibrils during the development of the mature biofilm and purified curli contains eDNA [13]. Moreover, eDNA accelerates the fibrillization of curli fibrils [13]. The reduced recognition of curli purified from 500-ml highly turbulent cultures by the anti-curli antibodies could be due to either a reduction of curli per  $\mu\text{g}$  of protein preparation or reduced binding to the curli intermediates by anti-curli antibodies. To investigate whether there are differences in the association of eDNA with curli under the two culture conditions, we first examined the DNA content in purified curli aggregates. We performed a phenol-chloroform DNA extraction from 500  $\mu\text{g}$  of the two curli preparations. We isolated more DNA from the curli purified under low-turbulence conditions than from those purified from the high-turbulence culture (Fig. 2.4A). This suggests that DNA contributes to the formation of the larger mature fibrillar aggregates observed in the low-turbulence preparation.

Cell death is a major source of eDNA during biofilm formation. We hypothesized that there is increased cell death under low-turbulence conditions where the mature fibrillar aggregates and biofilm are forming. To test this, we stained bacterial cells under both culture conditions with a live/dead stain and evaluated cell death via flow cytometry. At 24 h, few dead cells were observed. However, at 72 h, the time that we see a large amount of mature biofilm in low-turbulence cultures, there was clearly more cell death in the low-turbulence culture than in the high-turbulence culture (Fig. 2.4B). We reason that the low-turbulence cultures are poorly aerated due to the biofilm pellicle that forms on the air-liquid-flask interface, and this causes cell death and DNA release into culture media. It

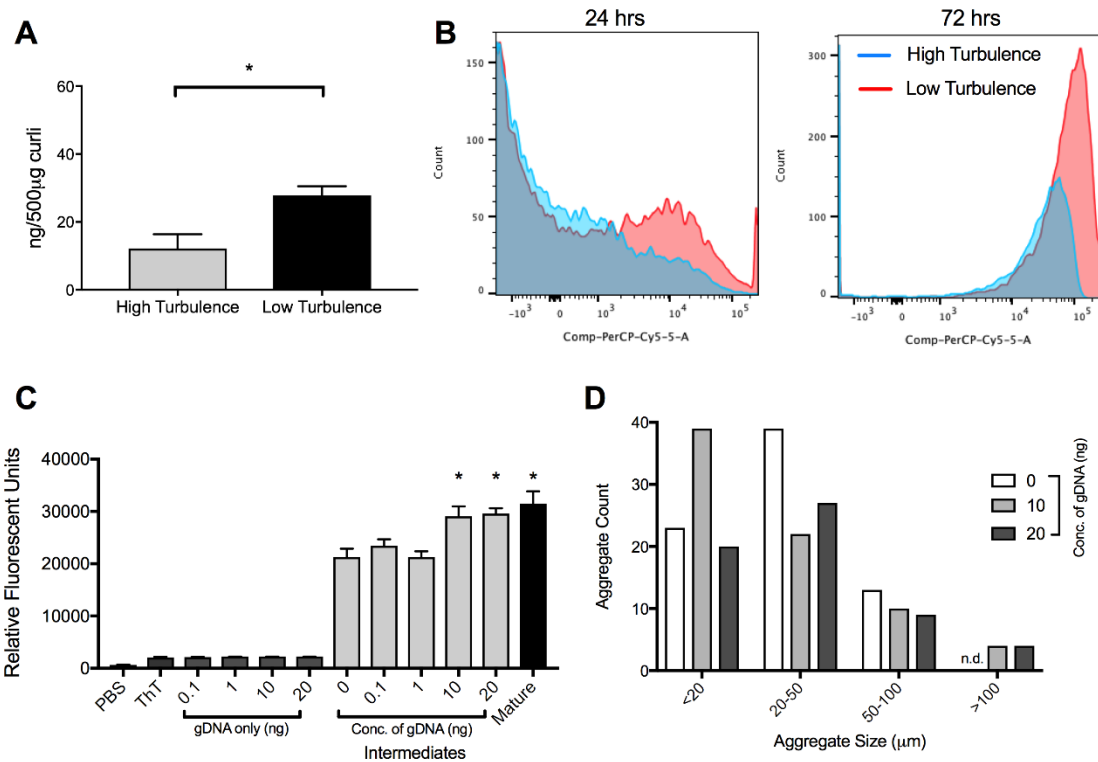


**Figure 2.4. DNA is necessary for formation of mature curli fibrillar aggregates.** (A) DNA content per 500 µg of curli preparations from high-turbulence and low-turbulence conditions. Plotted are means ( $\pm$ SEM) of data. One representative experiment of three independent experiments is shown. (B) Flow cytometry histograms of aliquots of cultures stained with propidium iodide after 24 h and 72 h in high-turbulence and low-turbulence cultures. (C) A purified curli preparation from a highly turbulent culture was treated with or without *S. Typhimurium* genomic DNA (gDNA) at the indicated concentrations. Fluorescence of samples incubated at 37°C for 24 h and stained with ThT was determined. Plotted are means ( $\pm$ SEM) from three replicates. The asterisks indicate significant increases ( $P < 0.05$ ) relative to intermediate aggregates without DNA. (D) Enumeration of

difference in size of aggregates calculated by confocal microscopy images. Aggregates were measured within the LAS AF confocal system and grouped into one of four groups. At least 60 aggregates were counted for each condition (0 to 75, 10 to 75, and 20 to 60 counts).

may be necessary for curli to complex with DNA to form the mature fibril aggregates necessary for biofilm formation.

As there is an association between DNA content and mature matrix formation, we sought to determine whether supplementing the smaller curli intermediates with DNA would lead to the formation of larger curli masses. To do this, we incubated the curli intermediates obtained from the high-turbulence culture with increasing concentration of genomic DNA (gDNA) purified from *S. Typhimurium* and then stained with ThT. As the amount of DNA increased, the relative fluorescence levels increased (Fig. 2.4C). This behavior was also observed with purified curli upon addition of exogenous DNA in a previous study [13]. When adding exogenous DNA to mature curli aggregates, we observed no increase in relative fluorescence intensity (Fig. S2.3A). Finally, using confocal microscopy, we observed that the addition of gDNA to intermediates increased the size of the aggregates. While there were no aggregates above 100  $\mu\text{m}$  observed in untreated intermediate, addition of genomic DNA resulted in aggregates above 100  $\mu\text{m}$ . There were no differences in the number of aggregates smaller than 20  $\mu\text{m}$  or 20 to 100  $\mu\text{m}$  (Fig. 2.4D). The addition of gDNA to the mature aggregates also did not show an increase in aggregate size, similar to the ThT results (Fig. S2.3B). Interestingly, when we isolated curli intermediates at earlier time points, we observed an increase in the number of fibril aggregates smaller than 20  $\mu\text{m}$  (Fig. S2.3C).

***Curli Intermediates Are More Cytotoxic To Macrophages Than The Mature Fibrillar  
Aggregates***

The early intermediate forms of human amyloid  $\beta$  are more cytotoxic to immune cells than mature amyloid  $\beta$  fibrils [19-21]. As curli fibrils are structurally similar to amyloid  $\beta$ , we evaluated the toxicities of curli prepared from high- and low-turbulence culture conditions. We treated bone marrow-derived macrophages (BMDMs) with the two different curli preparations for 24 h and performed a lactose dehydrogenase (LDH) assay to evaluate cell death. The percentage of dead cells was higher in the BMDMs treated with the preparation from the turbulent culture, which contains curli intermediates, than in cell samples treated with the mature curli aggregates from the low-turbulence culture (Fig. 2.5A). To confirm these findings, BMDMs were treated with the two preparations, stained with the Ready Probe cell viability kit, and imaged on the EVOS FL Auto2 fluorescence microscope. *S. Typhimurium* was used as a positive control. More dead cells were detected in the BMDMs treated with the preparation from the high-turbulence culture containing the curli intermediates than the preparation from the low-turbulence culture (Fig. 2.5B). The dead and live cells were quantified, demonstrating that the ratio of dead to live cells was significantly higher in the wells treated with the curli intermediates than mature curli fibrillar aggregates (Fig. 2.5C). Furthermore, decreasing the concentration of curli intermediates decreased the cytotoxicity observed on BMDMs (Fig. 2.5D).

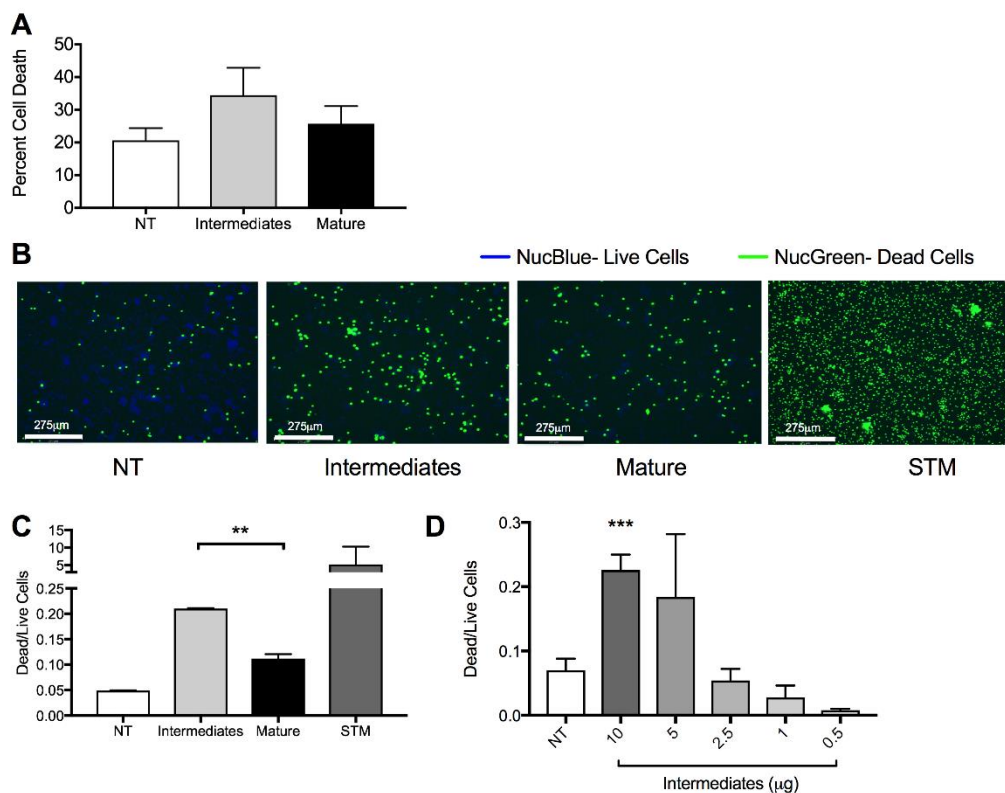


**Figure 2.5. Curli intermediates are more cytotoxic than mature aggregates.** (A) An LDH assay was used to determine the percentage of cytotoxicity in BMDMs treated with curli preparations from high-turbulence and low-turbulence cultures. Shown are means and a representative experiment from three independent experiments. (B) Images of BMDMs seeded at  $2.5 \times 10^5$  cells/well and not treated (NT) or treated with curli preparations from high-turbulence or low-turbulence cultures or with *S. Typhimurium* (STM). Cells were stained with NucBlue, which stains nuclei of live cells, and NucGreen, which stains nuclei of dead cells. Each image is a small portion of the full well. Representative images are shown for one of three independent experiments. (C) The ratios of dead to live cells obtained by analysis of multiple images accounting for the central 20% of well per condition in duplicate. Plotted are means ( $\pm$ SEM) from all images per condition. The

asterisks indicate significant difference between the effects of preparations from high- and low-turbulence cultures. (D) The ratios of dead to live cells obtained by analysis of multiple images accounting for the central 20% of the well per condition in duplicate. Plotted are means ( $\pm$ SEM) from all images per condition. \*\*,  $P < 0.01$ ; \*\*\*,  $P < 0.001$ .

## Discussion

Amyloid deposits appear to underlie symptoms of many debilitating human diseases, including Alzheimer's disease [5]. Studies on human amyloids have revealed that various intermediate structures form during amyloid polymerization. Soluble monomeric amyloid units first form oligomers, which then polymerize into protofibrillar structures. These protofibrils cross-assemble to form thicker mature fibrils [37]. Curli fibrillar assembly in *Enterobacteriaceae* is finely regulated via a type VIII secretion system, which results in a highly efficient nucleation precipitation process [7, 8]. The CsgA subunit efficiently fibrillizes in the presence of CsgB nucleator protein, which seeds the fibrillization process. At high concentrations without the CsgB protein, CsgA self-assembles into fibrils [9-12]. Intermediate oligomeric structures of curli, or any other bacterial amyloid, had not been isolated prior to this study. Here we describe for the first time intermediate protofibrillar structures of the bacterial amyloid curli. We observed that increasing the volume in our *S. Typhimurium* culture led to a more turbulent culture, which prevented biofilm formation at the air-liquid-flask interface. Curli intermediate structures purified from the highly turbulent culture were smaller and displayed decreased fibrillization kinetics and decreased density of aggregation. The bacteria in highly turbulent cultures produced curli accompanied by smaller amounts of dead cells and therefore eDNA. DNA stabilized the intermediate forms of curli into larger aggregates. Similar to amyloid  $\beta$ , curli intermediates were more cytotoxic to immune cells than its mature fibrillar aggregates (Fig. 2.6).

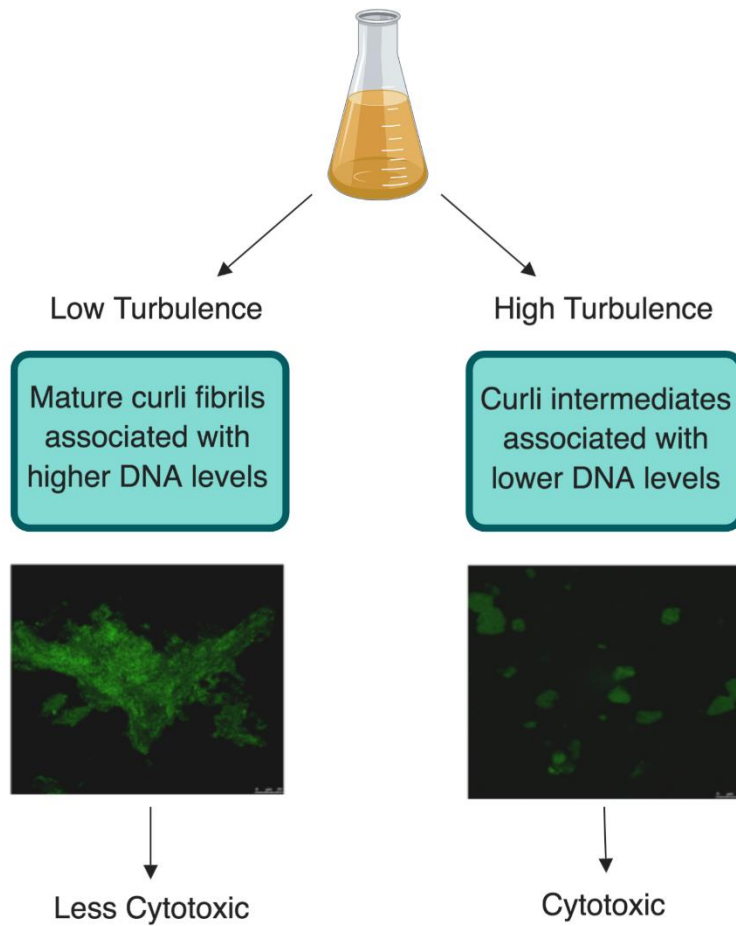


**Figure 2.6. Working Model.** This figure is a comparison of the two different curli preparations used throughout our experiments as well as the difference involved in their processing. High-turbulence growth conditions produced smaller curli intermediates, which incorporate less DNA and are cytotoxic to murine macrophages. Alternatively, low-turbulence growth conditions led to larger fibrillar aggregates, which incorporate more DNA and are not cytotoxic to murine macrophages.

Oxygen tension is a major signal that regulates the *csg* gene cluster expression in *S. Typhimurium* [30]. It was previously reported that oxygen-deprived biofilms produce larger amounts of extracellular polymers [38, 39]. Consistent with this, we observed more curli expression and increased aggregation under the low-turbulence culture conditions where the biofilm pellicle potentially limited oxygen penetration into the culture. In contrast, in high-turbulence cultures, the bubbles observed could be indicative of better oxygenation. In the high-turbulence cultures, decreased curli expression and mature fibril aggregate formation were observed compared to levels in low-turbulence cultures. Although we were not able to detect any differences in the growth using the two conditions, flow cytometry analysis revealed a higher percentage of dead cells in the low-turbulence culture. We reason that the formation of the biofilm pellicle may limit the oxygen penetration into the forming biofilm and increase the cell death. Similar observations were made for *Pseudomonas aeruginosa*, in which cell death and lysis occur during the development of biofilms [40].

It was previously demonstrated that curli associates with DNA during biofilm formation [13]. Both prokaryotic DNA and eukaryotic DNA accelerate the fibrillization of curli [13], although it is unclear whether DNA is needed for the formation of mature fibrillar structures. Here, we showed that reduced cell death was associated with smaller aggregate structures of curli, suggesting that the DNA released from dying cells is important for the assembly of larger, mature curli fibrillar aggregates. Consistent with this idea, addition of bacterial DNA to intermediates isolated from highly turbulent cultures was sufficient to trigger the assembly of larger curli masses. The turbulence may also

prevent formation of large fibril aggregates due to physical disruption. Previous work on  $\beta$ 2-macroglobulin, another human amyloid, showed that turbulent conditions resulted in intermediate forms of the fibrils [21]. Intriguingly, the TEM analysis revealed that curli fibrils purified from the low-turbulence culture that contains a pellicle biofilm displayed highly aggregated electron-dense spots in the images. This level of aggregation could be due to highly organized curli and DNA networks as several recent studies showed that amyloid and DNA form into highly ordered complexes, which also affect their immunomodulatory capacity [41-43].

Studies of amyloid  $\beta$  have shown that oligomeric structures and protofibrils are more cytotoxic and cause a greater degree of membrane disruption than their mature fibrillar counterparts [21]. This cytotoxicity was attributed to an enhanced ability of the oligomeric structures to permeabilize membranes, a mechanism shared by many amyloidogenic proteins [44, 45]. By permeabilizing the membrane, it is hypothesized that oligomers or protofibrils cause a chemical imbalance within the cell that leads to deregulated calcium-dependent signal transduction pathways. The immune system recognizes the mature fibrillar amyloids as a conserved molecular pattern via Toll-like receptor 2 (TLR2)/TLR1 heterocomplex [26, 43, 46-50] and the NLRP3 inflammasome [25, 51-54]. NLRP3 inflammasome activation leads to the activation of caspase 1 and has been associated with an inflammatory type of cell death. In the case of amyloid  $\beta$ , although NLRP3 is activated, which then leads to the activation of caspase 1, no cell death was observed [55], suggesting that this pathway is not associated with the cytotoxic events observed for the intermediate amyloid structures. Similarly, although curli activate the

NLRP3 inflammasome, this activation leads only to caspase-1 activation, not cell death [25]. Therefore, the cytotoxicity associated with the intermediate protofibrillar structures of curli may result from membrane disruption; however, this needs to be confirmed.

Amyloid proteins are produced by up to 40% of bacteria. Both commensal and pathogenic organisms produce amyloids that are secreted to the extracellular environment [2, 6, 23]. Our study provides insight into the fibrillization kinetics of curli as well as the role of mature curli fibrillar aggregates in the assembly of bacterial extracellular matrix and its stability as we showed that intermediate structures of bacterial amyloids form and that the presence of bacterial DNA accelerates mature fibrillar aggregate formation, limiting cytotoxic effects. Further work is needed to identify their role in host-microbe interactions and their immunological role within the host.

## Materials and Methods

### *Bacterial Strains and Growth Conditions*

*S. Typhimurium* strain IR715, a fully virulent, spontaneous nalidixic acid-resistant derivative of strain ATCC 14028, was grown in Luria-Bertani broth (LB) supplemented with 50 µg/ml nalidixic acid at 37°C [56]. The *S. Typhimurium msbB* mutant was previously described [57]. This strain was grown in 100 µg/ml kanamycin at 37°C.

### *Purification of Curli*

Curli aggregates were purified using a previously described protocol with some modifications and detailed in Appendix A [34]. Briefly, an overnight culture of *S. Typhimurium* IR715 *msbB* was grown in LB with appropriate antibiotic selection with shaking (200 rpm) at 37°C. Overnight cultures were then diluted 1:100 in yeast extract supplemented with Casamino Acids (YESCA) broth with 4% DMSO to enhance curli production [33]. Bacterial cultures were grown in either 150 ml liquid YESCA medium containing 4% DMSO in a 250-ml flask or in 500 ml liquid YESCA medium in a 1-liter flask. These cultures were grown at 26°C for 72 h with shaking (200 rpm). Bacterial pellets were collected by centrifugation, resuspended in 10 mM Tris-HCl at pH 8.0, and treated with a mixture of 0.1 mg/ml RNase A (Sigma, R5502) from bovine pancreas, 0.1 mg/ml DNase I (Sigma, DN25), and 1 mM MgCl<sub>2</sub> for 20 min at 37°C. Bacterial cells were then broken by sonication (30% amplification for 30 s twice). Next, lysozyme was added (1 mg/ml; Sigma, L6876), and samples were incubated at 37°C. After 40 min, 1% SDS was added, and the samples were incubated for 20 min at 37°C with shaking (200 rpm). After

this incubation, curli were pelleted by centrifugation (10,000 rpm in a J2-HS Beckman centrifuge with rotor JA-14 for 10 min at 4°C) and then resuspended in 10 ml Tris-HCl (pH 8.0) and boiled for 10 min. A second round of enzyme digestion was then performed as described above. Curli were then pelleted, washed in Tris-HCl at pH 8.0, and resuspended in 2× SDS-PAGE buffer and boiled for 10 min. The samples were then electrophoresed on a 12% separating/3 to 5% stacking gel run for 5 h at 20 mA (or overnight at 100 V). Fibrillar aggregates are too large to pass into the gel and therefore remain within the well of the gel and can be collected. Once collected, the curli aggregates were washed three times with sterile water and then extracted by being washed twice with 95% ethanol. Purified curli were then resuspended in sterile water. Concentrations of curli aggregates were determined using the bicinchoninic acid (BCA) assay according to the manufacturer's instructions (Novagen, 71285-3).

### *Sedimentation Assay*

To determine the differences in aggregation and planktonic cell populations between high-turbulence and low-turbulence conditions, 1 ml of culture was collected in a 1.5-ml tube at 72 h. These tubes were allowed to sit at room temperature to allow aggregates to precipitate over time. Images were taken at time zero and at multiple time points until no further sedimentation was observed (~30 min).

### *Crystal Violet Staining*

To image the pellicle-associated biofilm ring on the flask of shaken batch cultures, biofilms were stained with 1% crystal violet. Once the liquid culture was removed from the flasks—either for centrifugation or to be discarded—1% crystal violet was carefully added to the flask as to not displace the biofilm material. The staining solution was then gently rolled around the flask until the pellicle ring was fully stained, and the remaining crystal violet solution was removed. The crystal violet-stained pellicle-associated biofilm rings were then imaged using a Google Pixel 2.

### *Flow Cytometry*

All flow cytometry experiments were completed using the FACS Canto II fluorescence-activated cell sorter (FACS). Plasmid pDW6, which encodes a promoter-less green fluorescent protein (GFP), and pDW5, which contains GFP under the control of a tetracycline promoter, were kindly provided by Brad Cookson from the University of Washington (58). *S. Typhimurium* expressing GFP under the control of the curli promoter was obtained by cloning the *csgBA* promoter from *S. Typhimurium* IR715 using primer 5'-GGAATTCGAGACGTGGCATTAACTGGACAGCACAA-3' and reverse primer 5'-GGGATCCGCTGTCACCCTGGACCTGGTCGTACATAGC-3'. The resulting PCR product was cloned upstream of the gene encoding GFP on plasmid pDW6, yielding plasmid pCT125 (*PcsgBA::gfp*), which was then electroporated into *S. Typhimurium* IR715.

To investigate the expression of *csgBA* under different batch culture conditions, we used *S. Typhimurium* IR715, which contains pCT125 or pDW6 as a negative control. The cultures were examined once every 24 h for expression of *csgBA* via GFP expression. Briefly, 1 ml was sampled from shaken batch cultures and centrifuged at 10,000 rpm for 5 min. These pellets were then resuspended in 500  $\mu$ l phosphate-buffered saline (PBS), and GFP was detected in the fluorescein isothiocyanate (FITC) channel by FACS.

To investigate cell death in batch cultures, 1 ml was sampled from each of the growth conditions and pelleted. This pellet was washed once with PBS, resuspended in propidium iodide (2  $\mu$ l/ml), and incubated for 15 min at room temperature protected from light. These cells were then washed once with PBS and resuspended in 500  $\mu$ l PBS. Propidium iodide staining was evaluated in the peridinin chlorophyll protein (PerCP)-Cy5.5 channel by FACS.

### ***Thioflavin T assay***

A 1:1 mixture of 50  $\mu$ l of curli (400  $\mu$ g/ml) and 50  $\mu$ l 10  $\mu$ M thioflavin T was added to wells of a black 96-well plate and incubated for 10 min. After incubation, the relative fluorescence intensity was determined by a BMG Labtech POLARstar Omega plate reader using an excitation of 440 nm and an emission of 500 nm. In some experiments, genomic DNA (0.1, 1, 10, 20, 100, and 200 ng) extracted from *S. Typhimurium* cells and dissolved in PBS was added to curli preparations. These mixtures were then incubated at 37°C for 24 h.

### ***Confocal Laser Scanning Microscopy***

For confocal images of purified curli, preparations from each of the two conditions were stained with a 1:1 ratio of 10  $\mu$ M thioflavin T to curli (400  $\mu$ g/ml), and 5  $\mu$ l was spotted onto a microscopy slide. Spots were allowed to dry completely, and then images were analyzed on the Leica SP5 microscope with a TCS confocal system at magnifications as noted. For enumeration of aggregates by size, the LAS AF confocal system was used to draw scale bars on aggregates from multiple fields, and aggregates' sizes were recorded up to total numbers of 60 to 200 aggregates.

### ***Transmission Electron Microscopy***

Purified curli were prepared as described above, but were diluted to 1 mg/ml and frozen in 25% sucrose solution. Samples were absorbed to 200-mesh copper grids coated with Formvar/carbon (Electron Microscopy Sciences, Hatfield, PA) and stained with 2% uranyl acetate. Samples were visualized with an FEI Tecnai T12 transmission electron microscope equipped with 2K  $\times$  2K Megaplug camera model ES 4.0 (Roper Scientific MASD, San Diego, CA).

### ***DNA Extraction***

Beginning with 500  $\mu$ g of curli fibril complexes based on the BCA assay, complexes were centrifuged at 10,000 rpm for 3 min and resuspended in 550  $\mu$ l of TE buffer (10 mM Tris [pH 8.0], 1 mM EDTA), 30  $\mu$ l of 10% sodium dodecyl sulfate, and 20  $\mu$ l of 20 mg/ml proteinase K and mixed without vortexing. This mixture was incubated

at 37°C for 1 h. After incubation, 100 µl of 5 M NaCl and 80 µl of cetyltrimethylammonium bromide (CTAB) were mixed into the solution. After incubation at 37°C for 10 min, 300 to 400 µl of phenol-chloroform–isoamyl alcohol (Fisher BP1754-400) was added and mixed well without vortexing. The mixture was then centrifuged at 13,000 rpm for 5 min at 4°C. The supernatant was transferred to a 1.5-ml tube, and 700 µl of chloroform was added. The solution was mixed by pipetting and centrifuged again. Once again, the supernatant was transferred to a clean 1.5-ml tube, and an equal volume of isopropanol was added and shaken by hand to mix. This mixture was then incubated at –20°C for at least 30 min to precipitate DNA. The DNA was pelleted by centrifugation at 12,000 rpm for 5 min at 4°C. The pellet was then washed with 1 ml of 70% ethanol and spun down once more at 7,500 rpm for 5 min. The final DNA pellet was resuspended in 30 µl TE buffer, and DNA content was measured using a NanoDrop2000 spectrophotometer.

### *Lactate Dehydrogenase Assay*

Bone marrow-derived macrophages were generated from the leg bones of C57BL/6 wild-type mice. Macrophages were differentiated as previously described [49]. Cells were plated at  $5 \times 10^5$  cells/well and stimulated for 24 h with curli fibrillar aggregates (10 µg) prepared with or without shaking and a 1:20 multiplicity of infection with fully virulent *S. Typhimurium* IR715. *S. Typhimurium* IR715 was diluted 1:40 from an overnight culture in LB supplemented with 5 mM NaCl and grown statically at 37°C for 2 h. Supernatants and cell lysates were analyzed using the lactate dehydrogenase (LDH) assay. The LDH assay was performed using the Cytotox 96 nonradioactive cytotoxicity

assay (Promega, G1780) according to the manufacturer's protocol. Briefly, supernatants were collected from stimulated cells. The 10× lysis buffer supplied with the kit was diluted to 1× and added to cells in medium or PBS, and samples were incubated for 30 min at 37°C. Cell lysates were then collected for total LDH determination. One vial of substrate was resuspended in 12 ml of assay buffer, and 50 µl was added to each well of either supernatant or lysate (50 µl) in a 96-well plate. The plate was then incubated in the dark at room temperature for 15 min. Following incubation, 50 µl of stop solution supplied with the kit was added to each well. Absorbance was read on the BMG Labtech POLARstar Omega plate reader at 490 nm. Cell death was calculated as a ratio of LDH activity in supernatant to LDH activity of lysed cells.

### ***Live/Dead Staining***

Cells were stained using the ReadyProbes cell viability imaging kit (Thermo Fisher, R37609) following the manufacturer's instructions. Briefly, 2 drops of each color stain were added per 1 ml of medium, and stain was aliquoted into each well and incubated at room temperature for 15 min protected from light. Cells were then imaged on the EVOS FL Auto 2 microscope. Analysis of images to determine the percentage of dead cells to live cells was done using the HCS Studio software system.

### ***Dot Blot***

Dot blotting to detect curli within curli aggregates was completed by first carefully spotting 2 µl of serially diluted complexes beginning with a 500-µg/ml solution on a piece

of polyvinylidene difluoride (PVDF) membrane. The spots were given 1 to 2 h to fully dry. Next, the membrane was blocked in Tris-buffered saline (TBS [pH 7.5]) with 5% nonfat dry milk for 1 h at room temperature with rocking. The membrane was then incubated in 1:500 primary anti-CsgA antibody (generated in rabbit) diluted in TBS blocking buffer with 0.05% Tween 20 for 1 h with rocking. The membrane was then washed three times with TBS blocking buffer for 10 min each wash. Finally, the membrane was incubated in a 1:5,000 Li-Cor secondary antibody (anti-rabbit antibody) and blocking buffer with Tween for 1 h at room temperature with rocking. The membrane was then washed three times in TBS blocking buffer and then once with PBS and imaged on the Odyssey imaging system (Li-Cor).

### *Statistical Analyses*

Data were analyzed using Prism software (GraphPad, San Diego, CA). Student's *t* test was used as appropriate. Error was determined by standard error of the mean. *P* values of <0.05 were considered significant and are noted on the figures.

## **Acknowledgements**

We thank Joice Kanefsky for her useful discussions and Ronald Lucarelli for the generous donation of bone-marrow derived macrophages.

## References Cited

1. Jamal M, Ahmad W, Andleeb S, Jalil F, Imran M, Nawaz MA, Hussain T, Ali M, Rafiq M, Kamil MA. 2018. Bacterial biofilm and associated infections. *J Chin Med Assoc* 81:7–11. doi:10.1016/j.jcma.2017.07.012.
2. Hufnagel DA, Tukel C, Chapman MR. 2013. Disease to dirt: the biology of microbial amyloids. *PLoS Pathog* 9:e1003740. doi:10.1371/journal.ppat.1003740.
3. Costerton JW, Cheng KJ, Geesey GG, Ladd TI, Nickel JC, Dasgupta M, Marrie TJ. 1987. Bacterial biofilms in nature and disease. *Annu Rev Microbiol* 41:435–464. doi:10.1146/annurev.mi.41.100187.002251.
4. Hathroubi S, Mekni MA, Domenico P, Nguyen D, Jacques M. 2017. Biofilms: microbial shelters against antibiotics. *Microb Drug Resist* 23:147–156. doi:10.1089/mdr.2016.0087.
5. Chiti F, Dobson CM. 2006. Protein misfolding, functional amyloid, and human disease. *Annu Rev Biochem* 75:333–366. doi:10.1146/annurev.biochem.75.101304.123901.
6. Larsen P, Nielsen JL, Dueholm MS, Wetzel R, Otzen D, Nielsen PH. 2007. Amyloid adhesins are abundant in natural biofilms. *Environ Microbiol* 9:3077–3090. doi:10.1111/j.1462-2920.2007.01418.x.
7. Chapman MR, Robinson LS, Pinkner JS, Roth R, Heuser J, Hammar M, Normark S, Hultgren SJ. 2002. Role of *Escherichia coli* curli operons in directing amyloid fiber formation. *Science* 295:851–855. doi:10.1126/science.1067484.
8. Desvaux M, Hebraud M, Talon R, Henderson IR. 2009. Secretion and subcellular localizations of bacterial proteins: a semantic awareness issue. *Trends Microbiol* 17:139–145. doi:10.1016/j.tim.2009.01.004.
9. Barnhart M, Chapman M. 2006. Curli biogenesis and function. *Annu Rev Microbiol* 60:131–147. doi:10.1146/annurev.micro.60.080805.142106.
10. Taylor J, Zhou Y, Salgado P, Patwardhan A, McGuffie M, Pape T, Grabe G, Ashman E, Constable S, Simpson P, Lee W-C, Cota E, Chapman M, Matthews S. 2011. Atomic resolution insights into curli fiber biogenesis. *Structure* 19:1307–1316. doi:10.1016/j.str.2011.05.015.
11. Hammer ND, Schmidt JC, Chapman MR. 2007. The curli nucleator protein, CsgB, contains an amyloidogenic domain that directs CsgA polymerization. *Proc Natl Acad Sci U S A* 104:12494–12499. doi:10.1073/pnas.0703310104.

12. Wang X, Smith DR, Jones JW, Chapman MR. 2007. In vitro polymerization of a functional Escherichia coli amyloid protein. *J Biol Chem* 282:3713–3719. doi:10.1074/jbc.M609228200.
13. Gallo PM, Rapsinski GJ, Wilson RP, Oppong GO, Sriram U, Goulian M, Buttaro B, Caricchio R, Gallucci S, Tukul C. 2015. Amyloid-DNA composites of bacterial biofilms stimulate autoimmunity. *Immunity* 42:1171–1184. doi:10.1016/j.immuni.2015.06.002.
14. Schwartz K, Ganesan M, Payne DE, Solomon MJ, Boles BR. 2016. Extracellular DNA facilitates the formation of functional amyloids in Staphylococcus aureus biofilms. *Mol Microbiol* 99:123–134. doi:10.1111/mmi.13219.
15. Schwartz K, Syed AK, Stephenson RE, Rickard AH, Boles BR. 2012. Functional amyloids composed of phenol soluble modulins stabilize Staphylococcus aureus biofilms. *PLoS Pathog* 8:e1002744. doi:10.1371/journal.ppat.1002744.
16. Cherny I, Rockah L, Levy-Nissenbaum O, Gophna U, Ron EZ, Gazit E. 2005. The formation of Escherichia coli curli amyloid fibrils is mediated by prion-like peptide repeats. *J Mol Biol* 352:245–252. doi:10.1016/j.jmb.2005.07.028.
17. Hull RL, Westermark GT, Westermark P, Kahn SE. 2004. Islet amyloid: a critical entity in the pathogenesis of type 2 diabetes. *J Clin Endocrinol Metab* 89:3629–3643. doi:10.1210/jc.2004-0405.
18. Ross CA, Poirier MA. 2004. Protein aggregation and neurodegenerative disease. *Nat Med* 10(Suppl):S10–S17. doi:10.1038/nm1066.
19. Balducci C, Beeg M, Stravalaci M, Bastone A, Scip A, Biasini E, Tapella L, Colombo L, Manzoni C, Borsello T, Chiesa R, Gobbi M, Salmona M, Forloni G. 2010. Synthetic amyloid-beta oligomers impair long-term memory independently of cellular prion protein. *Proc Natl Acad Sci U S A* 107:2295–2300. doi:10.1073/pnas.0911829107.
20. Bucciantini M, Giannoni E, Chiti F, Baroni F, Formigli L, Zurdo J, Taddei N, Ramponi G, Dobson CM, Stefani M. 2002. Inherent toxicity of aggregates implies a common mechanism for protein misfolding diseases. *Nature* 416:507–511. doi:10.1038/416507a.
21. Xue WF, Hellewell AL, Hewitt EW, Radford SE. 2010. Fibril fragmentation in amyloid assembly and cytotoxicity: when size matters. *Prion* 4:20–25. doi:10.4161/pri.4.1.11378.

22. Maloney B, Lahiri DK. 2011. The Alzheimer's amyloid beta-peptide (A $\beta$ ) binds a specific DNA A $\beta$ -interacting domain (A $\beta$ IID) in the APP, BACE1, and APOE promoters in a sequence-specific manner: characterizing a new regulatory motif. *Gene* 488:1–12. doi:10.1016/j.gene.2011.06.004.
23. Tursi SA, Tükel C. 2018. Curli-containing enteric biofilms inside and out: matrix composition, immune recognition, and disease implications. *Microbiol Mol Biol Rev* 82:e00028-18. doi:10.1128/MMBR.00028-18.
24. Toyama BH, Weissman JS. 2011. Amyloid structure: conformational diversity and consequences. *Annu Rev Biochem* 80:557–585. doi:10.1146/annurev-biochem-090908-120656.
25. Rapsinski GJ, Wynosky-Dolfi MA, Oppong GO, Tursi SA, Wilson RP, Brodsky IE, Tükel Ç. 2015. Toll-like receptor 2 and NLRP3 cooperate to recognize a functional bacterial amyloid, curli. *Infect Immun* 83:693–701. doi:10.1128/IAI.02370-14.
26. Tükel C, Nishimori JH, Wilson RP, Winter MG, Keestra AM, van Putten JPM, Bäumlér AJ. 2010. Toll-like receptors 1 and 2 cooperatively mediate immune responses to curli, a common amyloid from enterobacterial biofilms. *Cell Microbiol* 12:1495–1505. doi:10.1111/j.1462-5822.2010.01485.x.
27. Chen SG, Stribinskis V, Rane MJ, Demuth DR, Gozal E, Roberts AM, Jagadapillai R, Liu R, Choe K, Shivakumar B, Son F, Jin S, Kerber R, Adame A, Masliah E, Friedland RP. 2016. Exposure to the functional bacterial amyloid protein curli enhances alpha-synuclein aggregation in aged Fischer 344 rats and *Caenorhabditis elegans*. *Sci Rep* 6:34477. doi:10.1038/srep34477.
28. Dueholm MS, Nielsen SB, Hein KL, Nissen P, Chapman M, Christiansen G, Nielsen PH, Otzen DE. 2011. Fibrillation of the major curli subunit CsgA under a wide range of conditions implies a robust design of aggregation. *Biochemistry* 50:8281–8290. doi:10.1021/bi200967c.
29. Sleutel M, Van den Broeck I, Van Gerven N, Feuillie C, Jonckheere W, Valotteau C, Dufrêne YF, Remaut H. 2017. Nucleation and growth of a bacterial functional amyloid at single-fiber resolution. *Nat Chem Biol* 13:902–908. doi:10.1038/nchembio.2413.
30. Gerstel U, Romling U. 2001. Oxygen tension and nutrient starvation are major signals that regulate agfD promoter activity and expression of the multicellular morphotype in *Salmonella typhimurium*. *Environ Microbiol* 3:638–648. doi:10.1046/j.1462-2920.2001.00235.x.

31. Olsen A, Arnqvist A, Hammar M, Normark S. 1993. Environmental regulation of curli production in *Escherichia coli*. *Infect Agents Dis* 2:272–274.
32. Romling U, Sierralta WD, Eriksson K, Normark S. 1998. Multicellular and aggregative behaviour of *Salmonella typhimurium* strains is controlled by mutations in the *agfD* promoter. *Mol Microbiol* 28:249–264. doi:10.1046/j.1365-2958.1998.00791.x.
33. Lim JY, May JM, Cegelski L. 2012. Dimethyl sulfoxide and ethanol elicit increased amyloid biogenesis and amyloid-integrated biofilm formation in *Escherichia coli*. *Appl Environ Microbiol* 78:3369–3378. doi:10.1128/AEM.07743-11.
34. Collinson SK, Emody L, Muller KH, Trust TJ, Kay WW. 1991. Purification and characterization of thin, aggregative fimbriae from *Salmonella enteritidis*. *J Bacteriol* 173:4773–4781. doi:10.1128/jb.173.15.4773-4781.1991.
35. Hung C, Zhou Y, Pinkner JS, Dodson KW, Crowley JR, Heuser J, Chapman MR, Hadjifrangiskou M, Henderson JP, Hultgren SJ. 2014. *Escherichia coli* biofilms have an organized and complex extracellular matrix structure. *mBio* 4:e00645-13. doi:10.1128/mBio.00645-13.
36. Xue C, Lin TY, Chang D, Guo Z. 2017. Thioflavin T as an amyloid dye: fibril quantification, optimal concentration and effect on aggregation. *R Soc Open Sci* 4:160696. doi:10.1098/rsos.160696.
37. Schnabel J. 2010. Protein folding: the dark side of proteins. *Nature* 464:828–829. doi:10.1038/464828a.
38. Applegate DH, Bryers JD. 1991. Effects of carbon and oxygen limitations and calcium concentrations on biofilm removal processes. *Biotechnol Bioeng* 37:17–25. doi:10.1002/bit.260370105.
39. Thormann KM, Saville RM, Shukla S, Spormann AM. 2005. Induction of rapid detachment in *Shewanella oneidensis* MR-1 biofilms. *J Bacteriol* 187:1014–1021. doi:10.1128/JB.187.3.1014-1021.2005.
40. Webb JS, Thompson LS, James S, Charlton T, Tolker-Nielsen T, Koch B, Givskov M, Kjelleberg S. 2003. Cell death in *Pseudomonas aeruginosa* biofilm development. *J Bacteriol* 185:4585–4592. doi:10.1128/jb.185.15.4585-4592.2003.
41. Lee EY, Zhang C, Di Domizio J, Jin F, Connell W, Hung M, Malkoff N, Veksler V, Gilliet M, Ren P, Wong G. 2019. Helical antimicrobial peptides assemble into protofibril scaffolds that present ordered dsDNA to TLR9. *Nat Commun* 10:1012. doi:10.1038/s41467-019-08868-w.

42. Schmidt NW, Jin F, Lande R, Curk T, Xian W, Lee C, Frasca L, Frenkel D, Dobnikar J, Gilliet M, Wong GC. 2015. Liquid-crystalline ordering of antimicrobial peptide-DNA complexes controls TLR9 activation. *Nat Mater* 14:696–700. doi:10.1038/nmat4298.
43. Tursi SA, Lee EY, Medeiros NJ, Lee MH, Nicastro LK, Buttaro B, Gallucci S, Wilson RP, Wong GCL, Tükel C. 2017. Bacterial amyloid curli acts as a carrier for DNA to elicit an autoimmune response via TLR2 and TLR9. *PLoS Pathog* 13:e1006315. doi:10.1371/journal.ppat.1006315.
44. Bucciantini M, Calloni G, Chiti F, Formigli L, Nosi D, Dobson CM, Stefani M. 2004. Prefibrillar amyloid protein aggregates share common features of cytotoxicity. *J Biol Chem* 279:31374–31382. doi:10.1074/jbc.M400348200.
45. Demuro A, Mina E, Kaye R, Milton SC, Parker I, Glabe CG. 2005. Calcium dysregulation and membrane disruption as a ubiquitous neurotoxic mechanism of soluble amyloid oligomers. *J Biol Chem* 280:17294–17300. doi:10.1074/jbc.M500997200.
46. Cheng N, He R, Tian J, Ye PP, Ye RD. 2008. Cutting edge: TLR2 is a functional receptor for acute-phase serum amyloid A. *J Immunol* 181:22–26. doi:10.4049/jimmunol.181.1.22.
47. Jana M, Palencia CA, Pahan K. 2008. Fibrillar amyloid-beta peptides activate microglia via TLR2: implications for Alzheimer's disease. *J Immunol* 181:7254–7262. doi:10.4049/jimmunol.181.10.7254.
48. Liu S, Liu Y, Hao W, Wolf L, Kiliaan AJ, Penke B, Rube CE, Walter J, Heneka MT, Hartmann T, Menger MD, Fassbender K. 2012. TLR2 is a primary receptor for Alzheimer's amyloid beta peptide to trigger neuroinflammatory activation. *J Immunol* 188:1098–1107. doi:10.4049/jimmunol.1101121.
49. Tükel C, Raffatellu M, Humphries AD, Wilson RP, Andrews-Polymenis HL, Gull T, Figueiredo JF, Wong MH, Michelsen KS, Akçelik M, Adams LG, Bäumlér AJ. 2005. CsgA is a pathogen-associated molecular pattern of *Salmonella enterica* serotype Typhimurium that is recognized by Toll-like receptor 2. *Mol Microbiol* 58:289–304. doi:10.1111/j.1365-2958.2005.04825.x.
50. Tükel C, Wilson RP, Nishimori JH, Pezeshki M, Chromy BA, Bäumlér AJ. 2009. Responses to amyloids of microbial and host origin are mediated through Toll-like receptor 2. *Cell Host Microbe* 6:45–53. doi:10.1016/j.chom.2009.05.020.

51. Ather JL, Ckless K, Martin R, Foley KL, Suratt BT, Boyson JE, Fitzgerald KA, Flavell RA, Eisenbarth SC, Poynter ME. 2011. Serum amyloid A activates the NLRP3 inflammasome and promotes Th17 allergic asthma in mice. *J Immunol* 187:64–73. doi:10.4049/jimmunol.1100500.
52. Heneka MT, Kummer MP, Stutz A, Delekate A, Schwartz S, Vieira-Saecker A, Griep A, Axt D, Remus A, Tzeng TC, Gelpi E, Halle A, Korte M, Latz E, Golenbock DT. 2013. NLRP3 is activated in Alzheimer's disease and contributes to pathology in APP/PS1 mice. *Nature* 493:674–678. doi:10.1038/nature11729.
53. Niemi K, Teirila L, Lappalainen J, Rajamaki K, Baumann MH, Oorni K, Wolff H, Kovanen PT, Matikainen S, Eklund KK. 2011. Serum amyloid A activates the NLRP3 inflammasome via P2X7 receptor and a cathepsin B-sensitive pathway. *J Immunol* 186:6119–6128. doi:10.4049/jimmunol.1002843.
54. Westwell-Roper C, Nackiewicz D, Dan M, Ehses JA. 2014. Toll-like receptors and NLRP3 as central regulators of pancreatic islet inflammation in type 2 diabetes. *Immunol Cell Biol* 92:314–323. doi:10.1038/icb.2014.4.
55. Halle A, Hornung V, Petzold GC, Stewart CR, Monks BG, Reinheckel T, Fitzgerald KA, Latz E, Moore KJ, Golenbock DT. 2008. The NALP3 inflammasome is involved in the innate immune response to amyloid-beta. *Nat Immunol* 9:857–865. doi:10.1038/ni.1636.
56. Stojiljkovic I, Baumler AJ, Heffron F. 1995. Ethanolamine utilization in *Salmonella typhimurium*: nucleotide sequence, protein expression, and mutational analysis of the *cchA cchB eutE eutJ eutG eutH* gene cluster. *J Bacteriol* 177:1357–1366. doi:10.1128/jb.177.5.1357-1366.1995.
57. Raffatellu M, Chessa D, Wilson RP, Dusold R, Rubino S, Baumler AJ. 2005. The Vi capsular antigen of *Salmonella enterica* serotype Typhi reduces Toll-like receptor-dependent interleukin-8 expression in the intestinal mucosa. *Infect Immun* 73:3367–3374. doi:10.1128/IAI.73.6.3367-3374.2005.
58. Cummings LA, Wilkerson WD, Bergsbaken T, Cookson BT. 2006. In vivo, *fliC* expression by *Salmonella enterica* serovar Typhimurium is heterogeneous, regulated by ClpX, and anatomically restricted. *Mol Microbiol* 61:795–809. doi:10.1111/j.1365-2958.2006.05271.x.

## Supplemental Figures

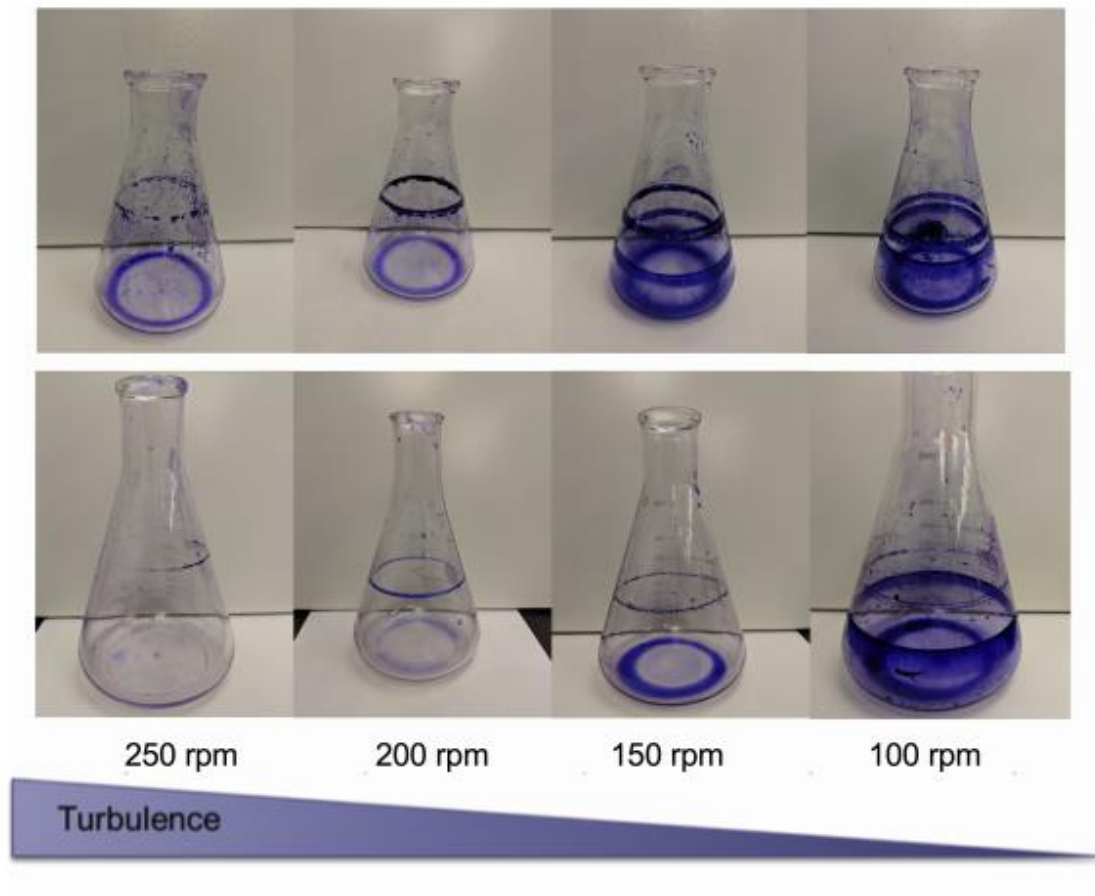


**Figure S2.1. Crystal Violet Staining of Pellicle Associated Biofilm from Cultures Grown in Increasing Levels of Turbulence.** The staining of 150-ml cultures (top) at 100 rpm and 50 rpm (lower turbulence) shows a dissociated surface biofilm on the bottom of the flasks. Decreasing turbulence results in better pellicle formation in 500-ml cultures (bottom) (compare to Fig. 2.1B).

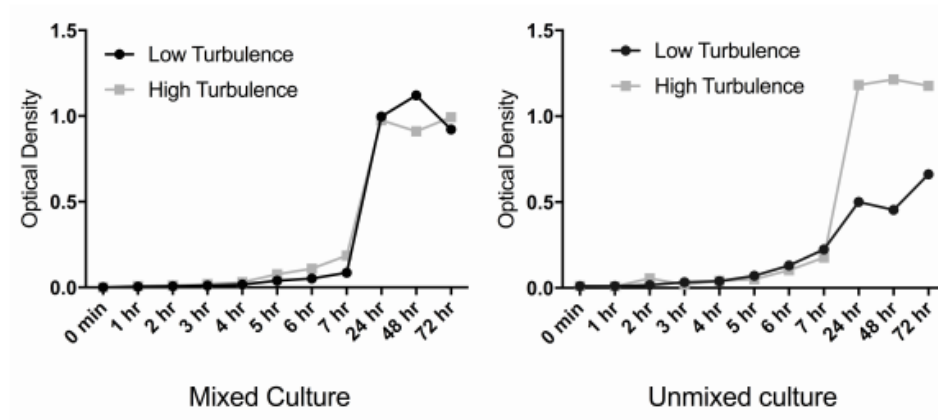


**Figure S2.2. Bacterial Growth As Measured By Optical Density Over 72 Hours Of Growth In Mixed And Unmixed Cultures.** (A) Optical density readings from well mixed (left) and umixed (right) aliquots of high-turbulence and low-turbulence cultures sampled at the time points shown on the x-axis. Lag phase growth of the two conditions was similar during the first 24 h of culture. Representative results of three independent experiments.

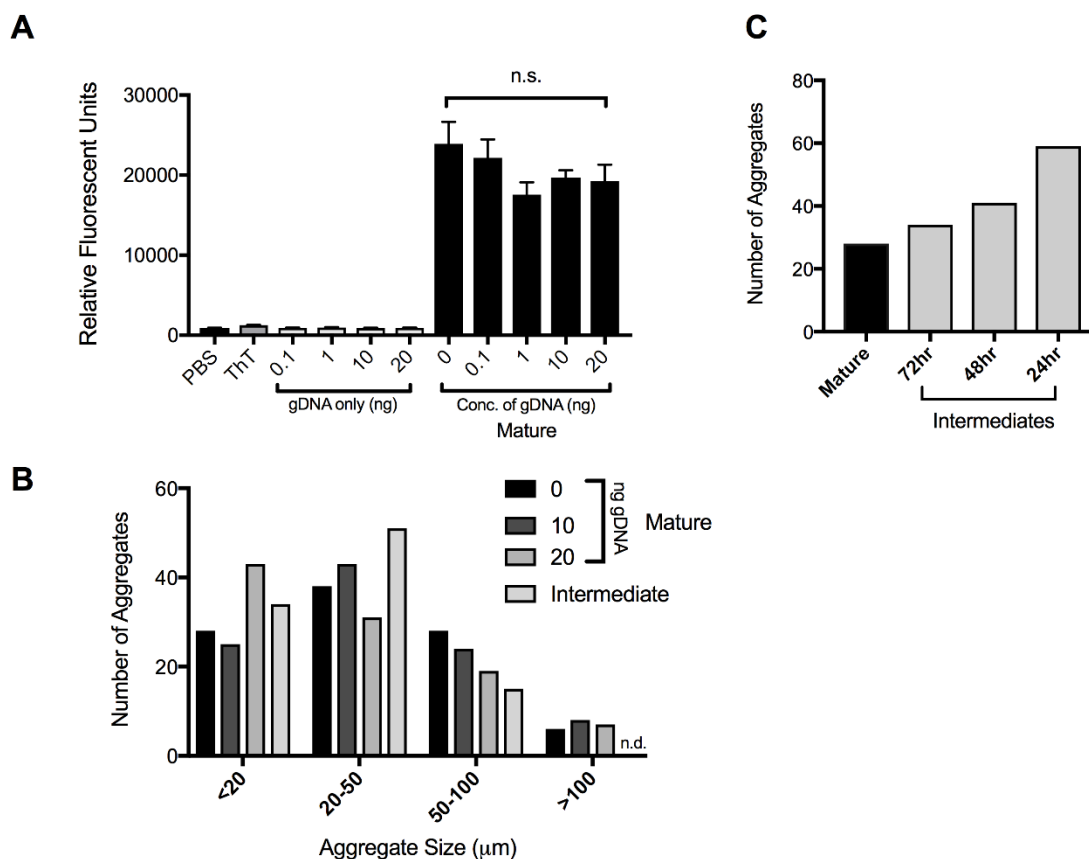


**Figure S2.3. Mature Aggregates Treated with Genomic DNA Display No Change in Amyloid Content.** (A) A purified curli preparation from a low turbulence culture was treated with or without STM genomic DNA (gDNA) at the indicated concentration. Fluorescence of samples incubated at 37 °C for 24 h and stained with ThT was determined. Plotted are mean relative fluorescent units ( $\pm$  SEM) of three replicates. No significant differences were observed (n.s.). (B) Enumeration of difference in size of aggregates calculated by confocal microscopy images. Aggregates were measured within the LAS AF confocal system and grouped into one of four groups. 100 aggregates were counted for each condition. n.d. stands for not determined. (C) Enumeration of 100 aggregates from mature aggregates and intermediates from three time points (72hrs, 48hrs, and 24hrs).

Shown are counts for aggregates less than 20  $\mu\text{m}$ . This graph shows increasing numbers of the smallest aggregates in earlier time point intermediates.

**CHAPTER 3**

**STRUCTURAL ORGANIZATION OF DNA IN CURLI FIBRILS DURING  
BIOFILM FORMATION DICTATES THE TYPE I INTERFERON SIGNATURE  
AND AUTOANTIBODY RESPONSE**

Lauren K. Nicaastro<sup>1</sup>, Jaime De Anda<sup>2</sup>, Neha Jain<sup>3</sup>, Sarah A. Tursi<sup>1</sup>, Long S. Le<sup>1</sup>, Amanda  
L. Miller<sup>1</sup>, Bettina A. Buttaro<sup>1,5</sup>, Gregg J. Silverman<sup>4</sup>, Stefania Gallucci<sup>1</sup>, Gerard C. L.  
Wong<sup>2</sup> and Çağla Tükel<sup>1\*</sup>.

<sup>1</sup>Department of Microbiology and Immunology, Lewis Katz School of Medicine, Temple  
University, Philadelphia, Pennsylvania, United States of America

<sup>2</sup>Department of Bioengineering, California Nano Systems Institute, University of  
California, Los Angeles, California, United States of America

<sup>3</sup>Department of Bioscience and Bioengineering, Indian Institute of Technology, Jodhpur,  
India

<sup>4</sup>Division of Rheumatology, Department of Medicine, New York University School of  
Medicine, New York, New York, United States of America

<sup>5</sup>Sol Sherry Center for Thrombosis, Lewis Katz School of Medicine, Temple University,  
Philadelphia, Pennsylvania, United States of America

## Abstract

Deposition of human amyloids is associated with complex human diseases such as Alzheimer's and Parkinson's disease. Bacteria also produce amyloid proteins that are often deposited in the extracellular matrix (ECM) of biofilms. Bacterial amyloid curli is found in the ECM of both commensal and pathogenic enteric bacterial biofilms. During biofilm formation, amyloid curli complexes with extracellular DNA (eDNA). We recently showed that curli/DNA complexes are recognized by the immune system as a conserved signature leading to the generation of an autoimmune response characterized by the production of anti-double stranded DNA (anti-dsDNA) autoantibodies and type I interferons. Here, we isolated different forms of curli during different stages of biofilm formation: early intermediate, intermediate and mature curli fibrils. Early intermediates were smaller in aggregate size compared to intermediate and mature curli fibrils. Circular dichroism analysis confirmed the highest beta-sheet secondary structure in mature curli fibrils. Furthermore, mature curli fibrils had the highest DNA association and small angle x-ray scattering analysis showed that DNA was organized as a lattice like structure. The early intermediate curli that had the lowest DNA content lead to the lowest levels of type I interferon responses in macrophages. Intriguingly, the anti-dsDNA autoantibody (autoab) levels in mice were also dependent on the DNA content but the levels were higher in autoimmune-prone mice compared to wild-type C57BL/6 mice. Besides, the anti-dsDNA antibodies, anti-nucleosome, anti-C1q and anti-H2A autoantibodies were present in the serum of mice injected with curli intermediates and mature curli fibrils. Finally, the chronic exposure to curli led to significant histopathological changes, synovial proliferation and

periosteal resorption, in the joints of mice autoimmune prone mice. In conclusion, we identified that the intermediate and mature forms of curli formed during biofilm formation leads to an increase in pathogenic immune responses due to its DNA content and that the chronic exposure to curli breaks tolerance in genetically predisposed individuals leading to joint inflammation.

### **Introduction**

Amyloids are proteins with a conserved cross beta-sheet structure. Amyloids form fibrils by a self-assembly process where the mature fibrils form beta-sheets which orient themselves perpendicular to the axis of fibril growth [1]. There are more than 60 amyloidogenic proteins expressed in humans. The physiological role of many of these proteins remains unclear. However, it is known that fibrillar deposits of human amyloids in various organs occur in patients with complex human diseases such as Alzheimer's Disease, Huntingdon's Disease, Parkinson's Disease, Type II diabetes, and secondary amyloidosis [2-4]. Often amyloid fibrils or deposits are referred as misfolded aggregates. However, amyloid fibrillization is a highly ordered process. Studies using amyloid  $\beta$ , found in senile plaques of Alzheimer's Disease patients, showed that in the earliest steps of amyloid fibrillization, amyloid  $\beta$  monomers form into oligomers. These oligomers then further fibrillize to form protofibrils and then mature fibrils. While the oligomeric forms of amyloids are cytotoxic to immune cells via membrane permeation, their fibrillar conformations interact with the human innate immune receptors inducing inflammation [5-7].

An estimated 40% of bacteria produce amyloid proteins within the extracellular matrix of their biofilms [8]. Curli, the most-well studied bacterial amyloid to date, is produced by enteric bacteria including *Escherichia coli* and *Salmonella enterica* serovar Typhimurium. Although the kinetics of curli fibrils are similar to those of amyloid  $\beta$  and others, unlike human amyloids, curli fibrils form through a nucleation precipitation process. The process of curli amyloid fibrillization is controlled by the *csg* gene cluster. The two divergent operons encoded by the gene cluster encode a Type VIII secretion system that controls the transport and assembly of the curli fibrils into the extracellular space. The major regulator CsgD protein also controls the regulation of other biofilm associated genes as well. The amyloid monomer CsgA, encoded by the *csgA* gene, can self-assemble into cross beta-sheet fibrils, while this process is augmented by the nucleator protein, CsgB. Due to the quick nature of amyloid fibrillization, no intermediate forms of curli fibrils were identified until recently. Our group was the first to isolate intermediate structures of curli from the biofilm of *Salmonella* Typhimurium. Intriguingly, the intermediate curli fibers were cytotoxic to immune cells similar to human amyloid  $\beta$  [9]. It is important to note that the fully formed mature curli fibrils are not cytotoxic to immune cells, although they elicit inflammation through their interactions with Toll-like receptor (TLR) 2-TLR1 heterocomplex. Overall, data from eukaryotic and prokaryotic amyloid proteins suggest that different structures that form during amyloid fibrillization lead to different pathological outcomes during their interactions with the immune cells.

Structure and stability of biofilms are attained by the incorporation of multiple molecules in the extracellular matrix. In enteric biofilms, amyloid curli, cellulose, BapA,

and extracellular DNA decorates the extracellular matrix. Although the individual molecules are well studied, the interactions between these molecules and how the immune system recognizes these molecules remains unknown. Recently, it was shown that extracellular DNA and curli fibrils form complexes during biofilm formation [10]. These amyloid/DNA complexes act as a conserved molecule to sense the presence of biofilms by the immune cells. Curli/DNA complexes induce immune responses stronger than curli or DNA alone [11]. Besides the activation of classical inflammatory cytokines such as IL-6, IL-10 and TNF $\alpha$ , curli/DNA complexes induce an autoimmune response characterized by the activation of the type I interferons and anti-dsDNA autoabs.

Here, using an interdisciplinary approach, we investigated how the various structural conformations of curli fibers formed during biofilm formation would interact with the immune system and which conformations would elicit autoimmune responses. We determined that the DNA content is important to elicit autoimmune responses and that the early intermediates and intermediates are not as efficient as the mature curli fibrils with higher DNA content in inducing such immune responses. During our studies we also identified novel autoabs and using mice that are prone to autoimmune disease, we established that the autoimmune outcome to cytotoxic intermediates of curli exceeds those of mature curli fibrils.

## Results

### *Curli and eDNA interactions during the biofilm maturation*

Amyloids including curli fibrillize through a self-polymerizing process starting from monomers, to oligomers, to intermediates and eventually mature fibril aggregates (Fig. 3.1A). Due to a nucleation event with CsgB, CsgA polymerizes at a high rate and gets incorporated into the biofilm matrix efficiently. Recently, we were able to purify intermediate forms of curli fibers during the establishment of biofilm formation [9]. These intermediates were enriched in smaller aggregates and lacked the larger aggregates observed in mature curli purified from an established biofilm (Fig 3.1B). To capture earlier structures and oligomeric units formed by CsgA, we grew *S. Typhimurium* for 24 hours utilizing the method to purify intermediate structures of curli. Curli intermediates were isolated at 72 hours under same conditions [9]. Curli conformations obtained by the 24-hour incubation are referred to as early intermediates from here on. We observed that this isolation resulted in an enrichment of smaller curli aggregates less than 20 $\mu$ m, an earlier stage in fibrillization than previously described or observed for curli. Additionally, when curli aggregates were stained with the fluorescent stain, ThioflavinT, and imaged by confocal microscopy, the early intermediate curli showed no aggregates larger than 100  $\mu$ m (Fig 3.1C). This lack of large aggregate formation implicates a lack of full fibrillization, different from the large aggregates previously described with mature fibrils [9]. As we see that the curli complexes we isolated had different aggregation phenotypes, we next investigated the secondary structure of the complexes. We used ultra-violet circular dichroism to investigate the beta-sheet secondary structure status of the early intermediates,

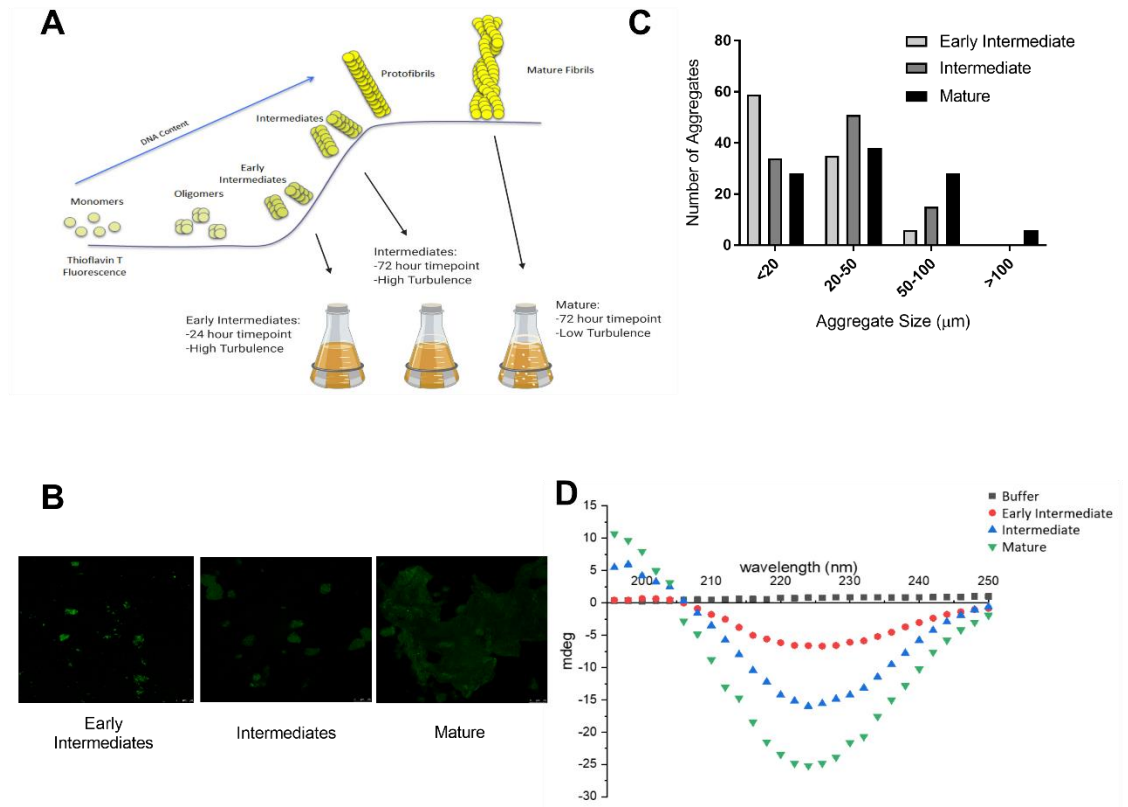


### Figure 3.1. Unique Curli Conformations are Formed During the Biofilm Maturation.

(A) Fibrillization curve showing the incorporation of ThioflavinT (ThT) stain through maturation of the amyloid fibril from monomer to intermediate to mature fibrils. The arrow at the top left of the image shows DNA content increases and assists in the maturation of the amyloid as well. The bottom left of the image gives information about growth and collection conditions used to isolate the early intermediate, intermediate, and mature curli complexes. Noted are the visual appearance of shaken cultures at the time of curli collection and isolation. (B) Early Intermediate (left), Intermediate (middle), and Mature (right) curli aggregates were isolated from conditions shown in the lower right section of 1A. 400  $\mu\text{g}/\text{mL}$  stocks of each form were stained with 100  $\mu\text{M}$  ThT and imaged at 60x

magnification by confocal microscopy. Scale bars are 25  $\mu\text{m}$ . (C) Enumeration of differences in size of aggregates calculated by confocal microscopy images. Aggregates were measured within the LAS AF confocal system and grouped into one of four groups. One hundred aggregates were counted for each condition. (D) Ultra-violet circular dichroism spectra of the different curli complexes. Each is 200  $\mu\text{L}$  of a 1mg/mL sample of curli. The curves of mature (green triangles) and intermediate (blue triangles) show a curve previously described for the beta-sheet secondary structure of curli amyloid. The early intermediate curve (red circles) shows a lack of the initial peak of the characteristic curve. The curve for buffer (black squares) is shown as a negative control.

intermediates and mature curli preparations. The beta-sheet secondary structure of curli is characterized by a peak at ~190nm and a trough at ~220nm as interpreted by circular dichroism [12]. The intermediate complexes are seen to share this same peak and trough pattern, however, the 24hr intermediate complexes are seen to lose the initial peak and the trough loses intensity (Fig 3.1D). This confirmed that through our purification protocol we were able to capture the formation of curli conformations that occur during the establishment of the biofilm. However, we were not able to catch oligomeric curli conformations.

#### *Association of DNA with early intermediate, intermediate and mature curli*

Curli and eDNA are two important determinants of the ECM of the enteric biofilm. Complexes formed between these two molecules have previously been shown. To identify the structural determinants and the association of eDNA with the different curli conformations, first we determined the DNA content in the three curli preparations. We utilized phenol chloroform extraction to estimate the amount of DNA within curli. 500ug of curli preparation was subjected to phenol chloroform extraction. Due to the nature of the curli complex, this extraction is not a perfect process as it estimates the DNA visible to immune cells and other interactions, but may not be an exact measurement of the full content. Increasing amounts of DNA were determined in early intermediates, intermediates and mature curli fibers suggesting that curli conformed into beta-sheets and incorporated DNA which corresponded to the maturation of the biofilm ECM (Fig 3.2A). To investigate the DNA organization in the various curli preparations and their macromolecular structure,

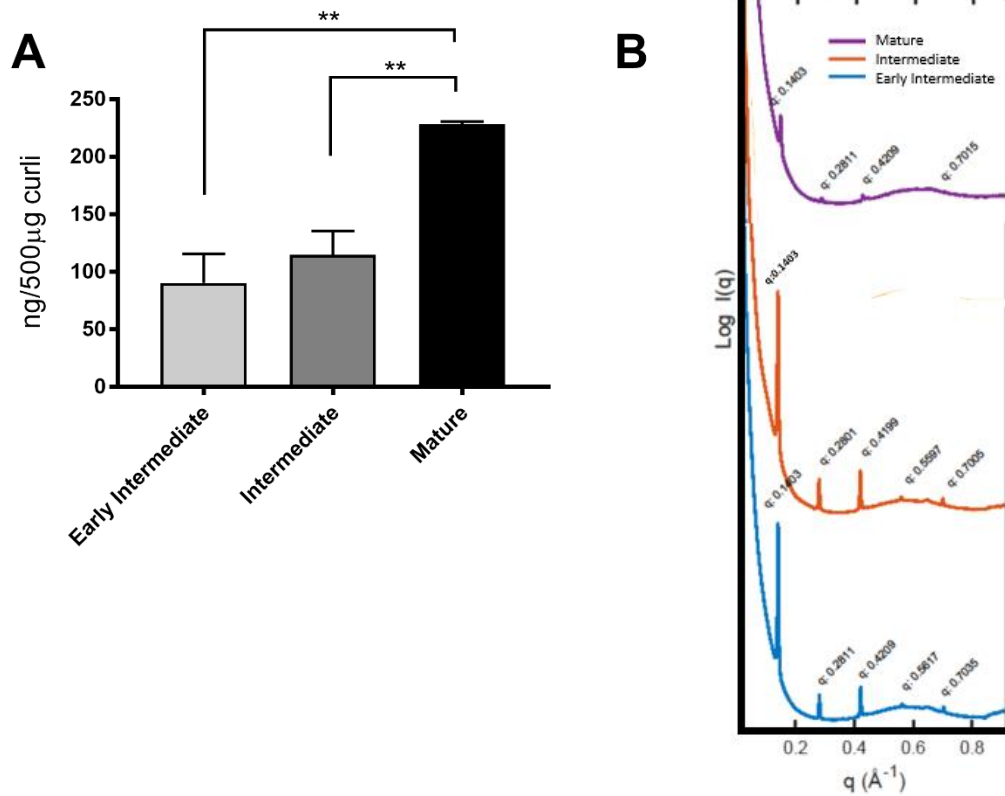


**Figure 3.2. Association of DNA with Early Intermediate, Intermediate, and Mature Curli.** (A) DNA content per 500µg of curli preparations. Plotted are means ( $\pm$ SEM) of data. One representative experiment of three independent experiments is shown. (B) SAXS diffraction profiles for three curli conformations. All conformations show a diffraction peak at  $qd = 0.1403 \text{ \AA}^{-1}$ . This indicates that the inter-DNA spacing is  $d = 2\pi/q_d = 4.47 \text{ nm}$  for all conformations indicating DNA incorporation occurs early in the biofilm development and curli synthesis process.

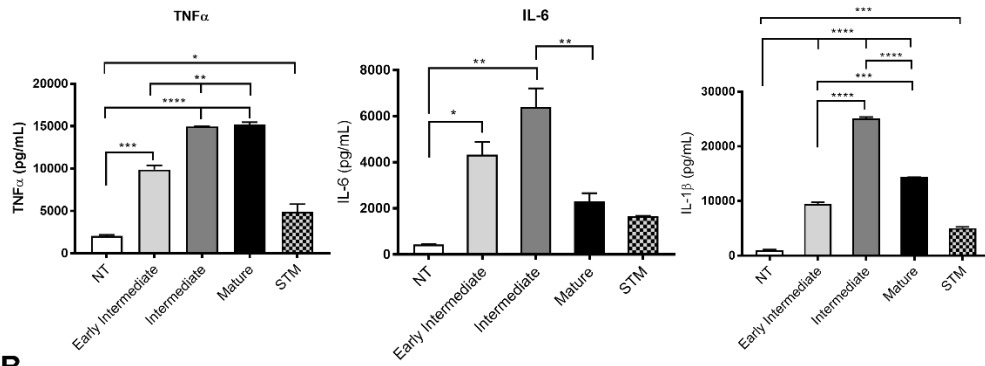
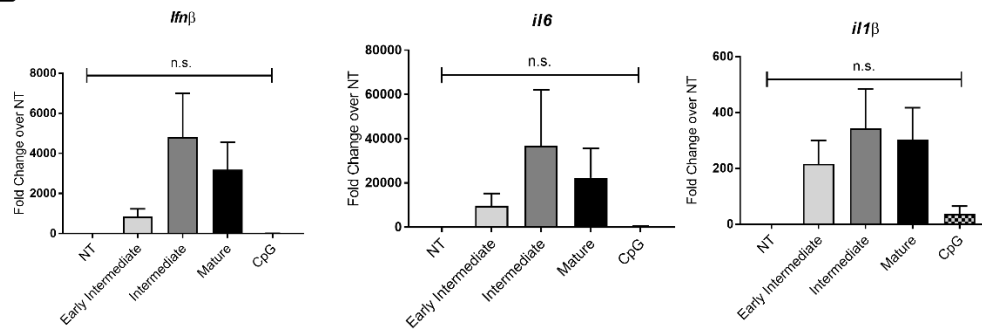
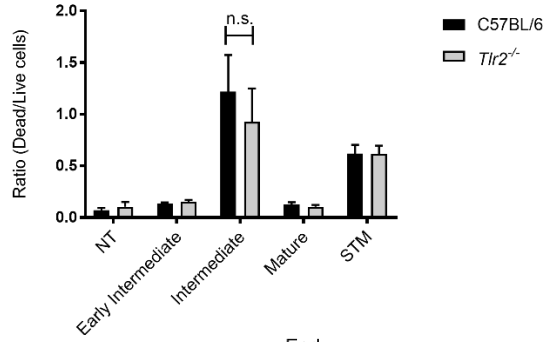
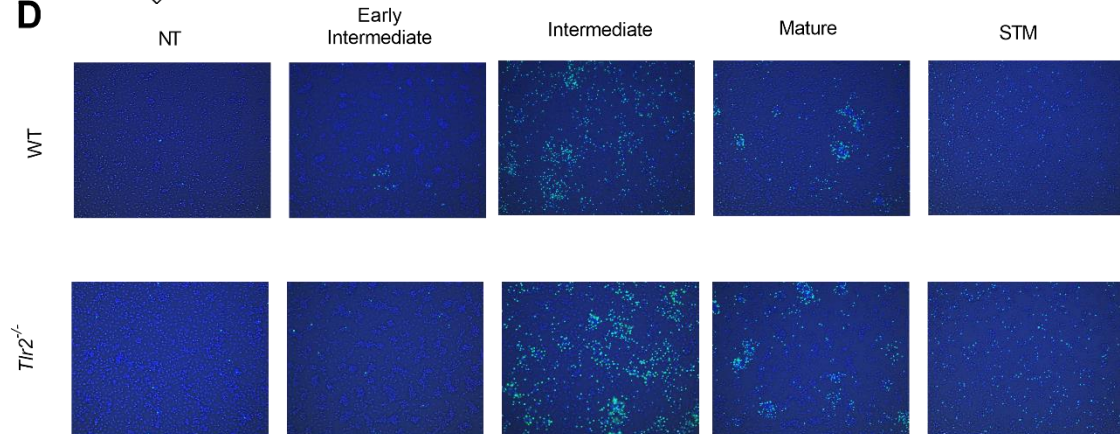
we used Small Angle X-ray Scattering (SAXS). Previously, our lab identified that a synthetic peptide of curli when fibrillized in the presence of DNA had inter DNA spacing of 4.16nm [10]. When we subjected the purified curli to SAXS analysis, we also observed the organization of DNA at 4.47nm in all conformations (Fig. 3.2B). This suggests that DNA is incorporated in early stages of biofilm development, concurrent with the synthesis of curli fibers.

### *Interactions of early intermediate, intermediate and mature curli with immune cells*

The beta-sheet structure of curli activates TLR2/TLR1 heterocomplex. We have shown previously that the bacterial DNA associated with curli activates TLR9. However, how the early structures formed by curli engage these receptors remains unknown. To identify the immune responses to the curli conformations that contain varying amounts of DNA isolated at different stages of the biofilm, we first treated bone marrow-derived macrophages with early intermediate, intermediate and mature curli complexes and collected supernatants after 4 and 24 hours. These supernatants were then used in an Enzyme-Linked Immunosorbent Assay (ELISA) to determine the production of the pro-inflammatory cytokines that are generated upon downstream activation of TLR2. We determined that macrophages treated with early intermediates produced significantly lower levels of TNF $\alpha$  compared to the macrophages treated with the intermediate and mature curli. The intermediate and mature curli treatments induced similar production of TNF $\alpha$  by macrophages (Fig. 3.3A). The macrophages treated with early intermediate and mature curli preparations showed similar production of IL-6 and IL-1 $\beta$ , while treatment with the

intermediates resulted in significantly higher levels of IL-6 and IL-1 $\beta$  (Fig. 3.3A). To identify the DNA related immune response induced by the treatment of macrophages with curli complexes, we determined the expression of IFN $\beta$ , a type I IFN related gene by qPCR. After 4-hour treatment of bone marrow-derived macrophages with 2.5  $\mu$ g/mL of curli preparations, IFN $\beta$  expression was measured. We observed an increase in type I IFNs in macrophages treated with mature and intermediate curli complexes as shown by IFN $\beta$  expression, while the early intermediate complexes induced the lowest expression of IFN $\beta$  (Fig. 3.3B). This result implicates decreased receptor engagement and signaling due to the lack of secondary structure of the early intermediates.

We previously reported an increase in the cytotoxic response of curli intermediates on macrophages. As amyloid  $\beta$  oligomers have been shown to be more cytotoxic to immune cells than their more mature counterparts [5-7], we tested whether the early intermediates, that display smaller aggregates compared to intermediate and mature forms of curli, would cause an increased cytotoxicity to macrophages compared to intermediate and mature curli conformations. Bone marrow-derived macrophages were treated with 10 $\mu$ g of each curli conformation for 24-hours. Next, cells were stained with a fluorescent live (NucBlue) and dead (NucGreen) cell stain and imaged using an EVOS2 fluorescent microscope. HCS analysis software was used to count the number of dead cells and live cells. Ratio of dead to live cells was determined. Consistent with our previous observations, intermediate curli showed again significant cytotoxicity to the macrophages. Intriguingly, no to low levels of cytotoxicity were determined in the cells treated with early intermediates similar to mature curli conformations (Fig. 3.3C). The cell death observed was comparable to that of the

**A****B****C****D**

**Figure 3.3. Interactions of Early Intermediates, Intermediates, and Mature Curli with Immune Cells.** (A) Wild-type and TLR2<sup>-/-</sup> bone marrow-derived macrophages (5x10<sup>5</sup> cells/well) were stimulated with 10ug of curli/DNA complexes purified from *S. Typhimurium* IR715 *msbB* mutant, LPS (50ng/mL) as a negative control, or left not treated (NT) for 4 or 24 hours. Cells were stimulated with STM grown in inflammasome inducing conditions at a MOI of 1:20 as a positive control for 1 hour and then treated with gentamycin (5mg/mL) to kill any extracellular bacteria. Production of TNF $\alpha$  (left), IL-6 (middle), and IL-1 $\beta$  (right) were quantified by ELISA in the supernatants. Means ( $\pm$ SEM) are shown. One representative experiment of three independent experiments is shown. (B) Wild-type bone marrow-derived macrophages (5x10<sup>5</sup> cells/well) were stimulated with 2.5 $\mu$ g/mL of curli complexes, 3  $\mu$ g/mL of CpG DNA, or left not treated (NT). Expression of IFN $\beta$  (left), IL-6 (middle), and IL-1 $\beta$  (right) were determined by qPCR. (C) Wild-type or TLR2<sup>-/-</sup> bone marrow-derived macrophages (2x10<sup>5</sup> cells/well) were stimulated with 10  $\mu$ g of each of the curli complexes, STM as described above, or left not treated (NT) for 24 hours. Cells were then stained with NucBlue (live nuclei) and NucGreen (dead nuclei) and imaged on the EVOS2 fluorescent microscope. The ratios of dead to live cells obtained by analysis of multiple images accounting for the central 20% of well per condition in duplicate. Means of at least three independent experiments are shown ( $\pm$ SEM). Result shows no significant (n.s.) difference between the cytotoxicity seen with intermediate stimulation of cells in wild-type and TLR2<sup>-/-</sup> cells. STM stands for *S. Typhimurium*. (D) Representative images of wells for each of the treatments used to obtain the data for C.

mature curli treated cells (Fig. 3.3C). Most interestingly, cytotoxicity of curli intermediates was not TLR2 dependent. No significant differences in cytotoxicity were detected when macrophages from wild-type or TLR2-KO mice were treated with the curli intermediates (Fig. 3.3C). To support the quantitative dead to live ratio data, representative raw images of the stained cells are shown as well (Fig. 3.3D). This data implicates an alternative interaction of the intermediate complexes with the macrophages in addition to the previously understood interaction with TLR2.

***Structure and DNA Content of Curli Generated during biofilm formation dictates the autoimmune response in mice***

We have established in our studies that the injection of mature curli fibrils elicited the generation of anti-dsDNA autoabs in mice in a TLR2 and TLR9 dependent manner. As we identified structural differences in early intermediate, intermediate and mature curli, we wanted to see whether these changes affected the autoab response through different stages of biofilm development. Additionally, we wanted to see if the DNA associated with curli was the main driver of anti-dsDNA autoabs or if the cytotoxicity of intermediates contributed to the generation of autoabs. We treated both C57BL/6 and autoimmune disease-prone NZBWxF/1 mice with 50 $\mu$ g of curli preparations twice weekly for up to 10 weeks and collected sera bi-weekly to analyze the autoab response. After 2 weeks of injections, both the wild-type and autoimmune-prone mice showed production of anti-dsDNA autoabs in their sera. The greatest response was observed with mature curli conformations (Fig. 3.4A) that carries the highest amount of DNA (Fig. 3.2A).

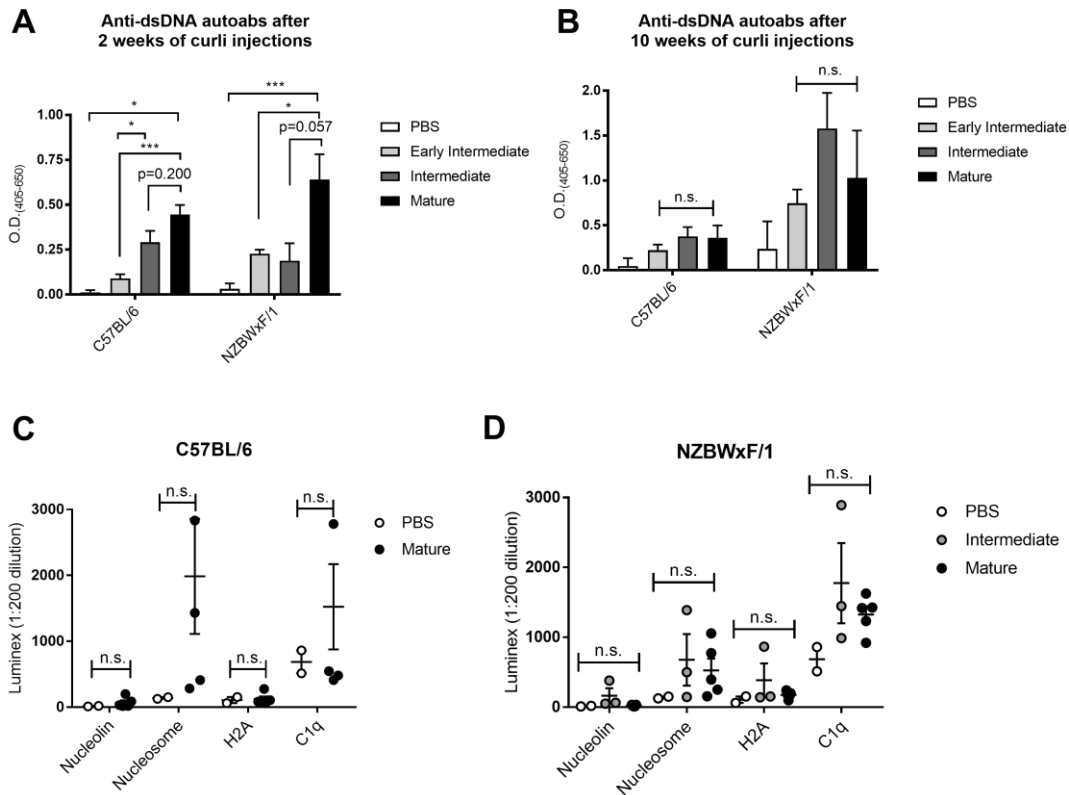


**Figure 3.4. Structure and DNA Content of Curli Generated during Biofilm Development Dictates the Autoimmune Response in Mice.** Anti-dsDNA autoantibody production by C57BL/6 and NZBWxF1 mice treated with curli complexes bi-weekly for 2 weeks (A) and 10 weeks (B). Experimental groups of 5 mice and 3 mice for each PBS control group were used in each experiment. One representative experiment of three independent experiments is shown. Significance is determined by one-way ANOVA with Tukey post-hoc secondary test. (C) Analysis of autoantibodies produced in sera of C57BL/6 treated with mature curli complexes and PBS twice weekly for 12 weeks by Luminex assay. (D) Analysis of autoantibodies produced in sera of NZBWxF1 treated with intermediate, mature curli complexes, and PBS twice weekly for 5 weeks by Luminex assay. \*,  $P < 0.05$ ; \*\*\*,  $P < 0.001$ ; n.s. not significant.

Interestingly, after 10 weeks of continual treatment of intermediate complexes, the anti-dsDNA autoab response is strengthened to levels not significantly different from that of the mature complexes (Fig. 3.4B). While the wild-type mice produce similar levels of antibodies at the early 2-week time point, the later 10-week data show similar trends in the data, but the lupus-prone NZBWxF/1 mice produce higher levels of autoabs overall.

To determine whether other autoabs were induced upon curli treatment, we used a Luminex based assay. An increase in anti-nucleosome and anti-C1q autoabs was observed in wild-type mouse sera upon treatment with mature curli preparations (Fig. 3.4C). Since we observed the highest levels of immune responses with intermediate and mature curli conformations, serum from mice treated with the latter preparations were tested. This result in combination with the strong anti-dsDNA response seen at later timepoints with the mature and intermediate complex treatments, we chose to focus on the differences between these two complexes alone. Additionally, we looked in NZBWxF/1 mice as sera from these mice showed higher antibody production than wild-type mice overall. We observe a strengthened anti-nucleosome and anti-C1q response to intermediate complexes compared to mature in the sera of treated NZBWxF/1 mice (Fig. 3.4D). There is also an increase in both anti-nucleolin and anti-H2A antibody production in the sera of mice repeatedly treated with curli intermediate complexes not seen in the wild-type sera (Fig. 3.4D). This late timepoint increased antibody response to the intermediate complexes, we hypothesize, to be associated with the cytotoxicity response observed in Figure 3.3D. The cell death response caused by these complexes may provide an increase nuclear material against

which the anti-nuclear antibodies are made providing the increased responses we have observed throughout this figure.

*Initiation of joint inflammation by systemic injection of curli complexes*

Recently, it has been shown that intraperitoneal treatment of wild-type mice with mature curli/eDNA complexes induced joint inflammation coupled with the anti-dsDNA autoab production reported [11, 13]. Here, we investigated the treatment of both wild-type and autoimmune-prone NZBWxF/1 mice with curli from the different stages of biofilm development. Mice were injected intraperitoneal twice weekly with 50  $\mu$ g of either mature, intermediate, or early intermediate complexes or PBS as a control. After 12 weeks of injections, knees were collected, fixed, and then decalcified. The, then paraffin-embedded, knees were blindly scored for pathology in the joints for each treatment condition. The pathology scoring indicated that autoimmune-prone mice experience greater synovial proliferation compared to wild-type mice indicating joint inflammation (Fig. 3.5A). Another pathological signature associated with the autoimmune condition, reactive arthritis, periosteal resorption was observed in both wild-type and lupus-prone mice (Fig. 3.5B). Additionally, mature curli/eDNA treatment induced the highest scoring of the knee pathology across all data. This data agrees with the previous reports on mature curli/eDNA and indicates that extended interaction with the mature and intermediate curli/eDNA complexes can induce autoimmune arthritis, especially in genetically pre-disposed mice.

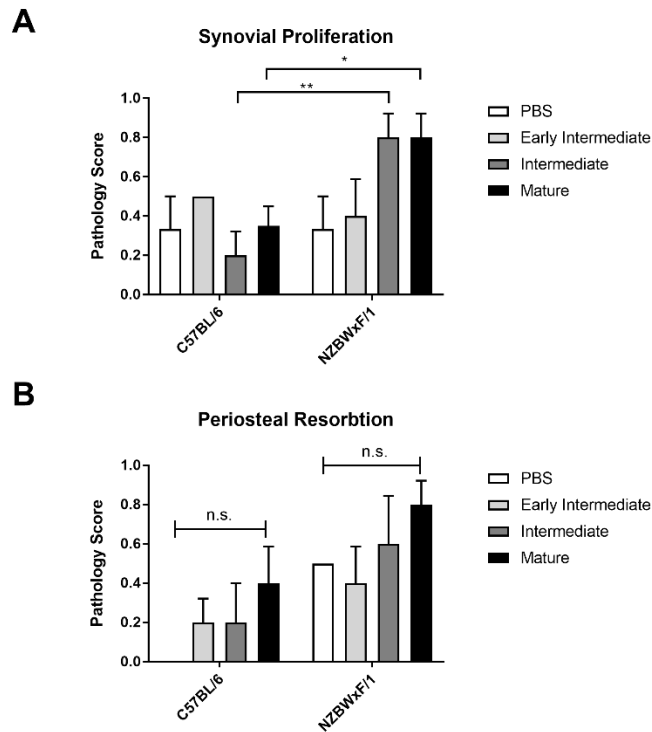


**Figure 3.5. Initiation of Joint Inflammation by Systemic Injection of Curli/eDNA Complexes.** C57BL/6 and NZBWF1 mice were injected with 50  $\mu$ g of either early intermediate, intermediate, or mature curli purified from the biofilms of *S. Typhimurium msbB* or PBS as a control twice weekly for 12 weeks. (A) The level of synovial infiltration in knee joints was blindly scored by a pathologist, following a scale based on histological parameters: 0, no changes; 1, slight thickening of synovial cell layer (< 3 layers of synoviocytes) accompanied by congestion and edema of the external membrane; 2, moderate thickening of synovial cell layer (3-5 layers of synoviocytes) accompanied by congestion and edema of the external membrane. The scoring was applied to tissue sections prepared from each infected mouse. (B) The level of periosteal resorption was scored by the pathologist as explained above for both C57BL/6 and NZBWF1.

## Discussion

Bacteria form biofilms in complex environments including the human gastrointestinal tract or tissues where they are exposed to stress conditions, including the immune system, antimicrobials, antibiotics etc. [14]. For bacteria, the biological purpose to establish a biofilm is to survive and thrive during environmental hazards such as sheer force, nutritional depletion, and oxidative stress. Therefore, biofilms have to be robust in order to protect the bacterial community. Bacteria achieve this by utilizing and incorporating multiple components into the extracellular matrix (ECM) that provide a strong and impenetrable shield [15]. The main protein component of enteric biofilm ECM, amyloid curli, provides structural support and impenetrable matrix properties by forming a beta-sheet structure [16, 17] DNA as well as cellulose can bind to curli to provide additional support, however the interactions between these molecules remain unknown [18, 19]. In this study, we investigated curli formation through multiple stages of biofilm development to better understand its interactions with other ECM components, mainly DNA, and how these structures are recognized by the immune system as conserved molecules triggering specific immunity. Here, we were able to use a multidisciplinary approach to show that the interaction of curli with DNA play numerous roles: from maturation of the curli fibrils, to structural support of the biofilm ECM, and increased immune responses. For the first time, we were able to isolate early intermediate, intermediate and mature forms of curli and determined their structural differences. We established that as curli matured, it established its characteristic beta-sheet fibrillar structure and displayed larger aggregates and incorporated more DNA. Mature curli

showed a crystal-like lattice structure through SAXS analysis. We observed that early intermediates, though lacking the beta-sheet secondary structure seen in more mature forms of curli, the DNA spacing within the complexes remained constant. Additional studies are needed to determine whether the identified peaks are a result of the repeating units of curli amyloid.

The oligomeric conformations that form during the initial steps of polymerization of amyloid  $\beta$  display cytotoxicity to immune cells. Curli and amyloid  $\beta$  follow similar kinetics for fibrillization as well as sharing functional and structural similarities [20]. The early intermediate conformations of curli did not show increased cytotoxicity. The most cytotoxic conformation was the intermediate form. Interestingly, the TLR2 receptor that recognizes the beta-sheet structure for both amyloids [21-23] was not involved in the cytotoxicity of these structures suggesting that alternative cytosolic cell death receptors such as inflammasomes or direct interactions with membranes could mediate the cell death. Consistent with this idea, earlier reports showed that both curli and amyloid  $\beta$  activated the NLRP3 inflammasome. Although no cell death was observed upon activation of NLRP3 with curli as well as amyloid  $\beta$ , both studies were investigating the mature fibrillar forms of both amyloids [24, 25].

Recently, it was reported that curli is expressed in the intestinal tract and displays pathogenic effects. It was observed that during *Salmonella* infection, production of curli was associated with an increase in anti-dsDNA autoabs and joint inflammation in infected mice. Additionally, colonization of mice with *E. coli* that produces curli was associated with increased alpha synuclein deposition in the brain possibly through the direct

interactions of curli with the enteric vagus nerve [26, 27]. However, the effects of the early intermediate or intermediate conformations of curli produced throughout the temporal development of an enteric biofilm on the immune system *in vivo* still remains unknown. Our results showed that the immune responses differed against the different conformations of curli. Anti-dsDNA autoab response was dependent on the DNA content of curli and the mature forms elicited the highest anti-dsDNA autoabs at the early 2-week timepoint. Treatment with intermediate curli complexes induced anti-dsDNA autoab production to levels similar to mature curli treatment suggesting that the production of antibodies by these different curli complexes work via different mechanisms. Mature forms of curli and the DNA associated with it stimulate the anti-dsDNA antibody production and type I IFN expression through TLR2 and TLR9 activation. We attribute the high levels of anti-dsDNA production induced by intermediate curli to the cytotoxicity associated with the fibers, as the death of cells caused by this effect may provide a pool of nuclear material against which the autoabs can be formed. At the later timepoints, however, the dependency of anti-dsDNA antibodies generated against curli conformations was no longer dependent on the DNA content of curli. We suspect that chronic injections of curli leads to immune tolerance breakdown leading to the loss of differences seen at earlier timepoints.

Importantly, in this study we have observed autoab production not previously identified in response to curli/eDNA complexes. In addition to the anti-dsDNA autoabs, we also detected the production of anti-C1q, anti-nucleolin, and anti-nucleosome and anti-H2A antibodies in both C57BL/6 mice as well as NZBWxF1 mice in response to mature and intermediate complex treatment. At this time, we do not know if these antibodies are

generated by mechanisms similar to anti-dsDNA autoabs. Since we previously reported that curli binds C1q [28], it is likely that curli acts as a carrier for C1q and leads to the amplification of immune responses upon chronic exposure to C1q. Overall, the observation that the repeated injections of curli over an extended time induces autoimmune responses in both healthy and genetically pre-disposed mice supports the idea that biofilms carrying amyloid and DNA complexes or other protein/DNA complexes may be stimulating autoimmune responses. Consistent with this idea, some pathogenic bacteria such as *Borrelia burgdorferi*, *Mycobacterium tuberculosis* and *Streptococci* produce curli-like amyloid proteins and that the infections with these pathogens lead to autoimmune sequelae [29-32]. Finally, these observations may not be specific to only bacterial amyloids. Recently, structural similarities between amyloid proteins and antimicrobial peptides (AMPs) were reported. The human AMP, LL-37, essential for normal immune function and protection against lethal infections [33], was reported to form insoluble complexes with DNA to activate TLR9 and promote type I IFN production [10, 34-37]. Most surprisingly, chronic exposure to LL-37/DNA complexes leads to autoimmunity in SLE patients similar to described for curli/eDNA complexes [11, 38].

One of the most common autoimmune sequelae observed following infections with Gram-positive and Gram-negative bacteria is post-infectious arthritis. After infections with invasive enteric bacteria such as *Salmonella* Typhimurium resolve, 5-10% of the patients develop an inflammatory form of arthritis termed Reactive Arthritis (ReA). ReA is strongly associated with the HLA-B27 genotype [39]. Our results showing that the increased joint inflammation in autoimmune prone mice upon injections of curli suggest that the

individuals that carry the HLA-B27 may also react stronger to bacterial curli. However, these findings need to be confirmed.

Amyloid/DNA complexes are found across numerous bacteria, both commensal and pathogenic. Though the proteins themselves may differ in primary amino acid sequence, amyloids self-assemble into a conserved beta-sheet structure and associate with DNA. As we have shown different immunological responses for each of the curli/eDNA conformations generated throughout the biofilm development and exaggerated immune responses in genetically predisposed animals, we believe our study provides a novel linchpin into the pathogenesis of ReA and possibly other infectious arthritis syndromes upon long-term systemic exposure to biofilms.

### **Future Directions**

In light of the work completed here, we conclude that as curli is synthesized, multiple unique molecular patterns, like the curli conformations we have identified in the experiments described here, are formed during the development of the biofilm. One unique conformation being the cytotoxic intermediate. The mechanism by which this complex is cytotoxic to mammalian cells remains undetermined. While amyloid  $\beta$  oligomers are cytotoxic to cells via membrane permeabilization, studies of the ability of curli intermediates to disrupt the cell membrane would be beneficial. Additionally, previous work has shown that mature curli complexes activate the NLRP3 inflammasome. Though mature curli is not cytotoxic, NLRP3-related cell death could be a potential mechanism of cytotoxicity by the curli intermediates. As the curli amyloid matures, it incorporates eDNA

changing the structure of the complex inducing an autoimmune response. We have additionally shown that chronic exposure to the cytotoxic intermediate form of the complex can also induce these autoimmune response, although delayed. Investigations into the mechanism by which these cytotoxic complexes induce autoimmune symptoms in both wild-type and autoimmune-prone mice are still needed. We anticipate an important role for the genetic pre-disposition in autoimmune symptom strength and severity. Future studies, using mice genetically predisposed to arthritis such as HLA-B27 mice or K/BxN mice will confirm and provide insight into how curli can contribute to disease pathogenesis and joint inflammation. These results would strengthen the connections of curli complexes as a unique molecular signature influencing autoimmunity across species.

## **Material and Methods**

### ***Bacterial Strains and Growth Conditions***

The *S. Typhimurium* IR715 *msbB* mutant was previously described [40]. This strain was grown in Luria-Bertani broth (LB) supplemented with 100 µg/ml kanamycin at 37°C. A *bscE*, cellulose mutant derived from the ATCC strain *Salmonella enterica* serovar Typhimurium 14028, a gift from Dr. John Gunn (Nationwide Children's Hospital, Columbus OH) was used for SAXS experiments.

### ***Purification of Curli***

Curli aggregates were purified using a previously described modified protocol detailed in Appendix A [9]. Briefly, an overnight culture of *S. Typhimurium* IR715 *msbB* was grown in LB with appropriate antibiotic selection with shaking (200 rpm) at 37°C. Overnight cultures were then diluted in yeast extract supplemented with Casamino Acids (YESCA) broth with 4% DMSO to enhance curli production [41]. Bacterial cultures were grown in either 150 ml liquid YESCA medium containing 4% DMSO in a 250-ml flask or in 500 ml liquid YESCA medium in a 1-liter flask. These cultures were grown at 26°C for 72 h with shaking (200 rpm). Bacterial pellets were collected by centrifugation, resuspended in 10 mM Tris-HCl at pH 8.0, and treated with a mixture of 0.1 mg/ml RNase A (Sigma, R5502) from bovine pancreas, 0.1 mg/ml DNase I (Sigma, DN25), and 1 mM MgCl<sub>2</sub> for 20 min at 37°C. Bacterial cells were then broken by sonication (30% amplification for 30 s twice). Next, lysozyme was added (1 mg/ml; Sigma, L6876), and samples were incubated at 37°C. After 40 min, 1% SDS was added, and the samples were

incubated for 20 min at 37°C with shaking (200 rpm). After this incubation, curli were pelleted by centrifugation (10,000 rpm in a J2-HS Beckman centrifuge with rotor JA-14 for 10 min at 4°C) and then resuspended in 10 ml Tris-HCl (pH 8.0) and boiled for 10 min. A second round of enzyme digestion was then performed as described above. Curli were then pelleted, washed in Tris-HCl at pH 8.0, and resuspended in 2× SDS-PAGE buffer and boiled for 10 min. The samples were then electrophoresed on a 12% separating/3 to 5% stacking gel run for 5 h at 20 mA (or overnight at 100 V). Fibrillar aggregates are too large to pass into the gel and therefore remain within the well of the gel and can be collected. Once collected, the curli aggregates were washed three times with sterile water and then extracted by being washed twice with 95% ethanol. Purified curli were then resuspended in sterile water. Concentrations of curli aggregates were determined using the bicinchoninic acid (BCA) assay according to the manufacturer's instructions (Novagen, 71285-3).

### ***Confocal laser scanning microscopy***

For confocal images of purified curli, preparations from each of three growth conditions were stained with a 1:1 ratio of Thioflavin T to curli (400ug/mL), and 5uL spotted onto a microscopy slide. Spots were allowed to dry completely and then were analyzed on the Leica SP5 microscope with a TCS confocal system at magnification as noted. For enumeration of aggregates by size, the LAS AF confocal system was used to draw scale bars on aggregates from multiple fields, and aggregate sizes were recorded up to a total number of 100 aggregates.

### ***Ultraviolet Circular Dichroism (UV CD)***

The UV CD spectra were recorded on a Chirascan CD spectrometer (Applied Photophysics, UK) at room temperature (25°C). The conformations of curli diluted in PBS were taken in 1 mm path length quartz cuvette. The secondary structural changes were recorded in the range of 195-260 nm and a scan rate of 1 nm/sec. All scans were taken at 1 mg/mL concentration. The final spectrum was averaged over three scans, was corrected with buffer baseline subtraction and plotted using Chirascan 'ProData viewer' software provided with the instrument.

### ***DNA extraction***

DNA was extracted using a previously described method [9]. Briefly, 500ug of curli fibril complexes based on the BCA assay, complexes were then centrifuged at 10,000 rpm for 3 mins to pellet. The pellets were then resuspended in 550 µl of TE buffer, 30 µl of 10% sodium dodecyl sulfate, and 20 µl of 20 mg/mL proteinase K and mixed by hand without vortexing. This mixture was incubated at 37°C for 1 hr. After incubation 100 µl of 5M NaCl and 80 µl of CTAB were added to the solution. After incubation at 37°C for 10 min, 300-400 µl of phenol-chloroform-isoamyl alcohol was added and mixed by pipetting up and down. This mixture was then centrifuged at 13,000 rpm for 5 mins at 4°C. The supernatant was transferred to a clean eppendorf tube and 700 µl of chloroform was added. The solution was mixed by hand and centrifuged again. Supernatant was then transferred to another new tube and equal volumes of isopropanol were added and mixed by hand. The

mixture was then incubated at  $-20^{\circ}\text{C}$  for at least 30 mins to precipitate the DNA. The DNA was pelleted at 12000rpm for 5 mins at  $4^{\circ}\text{C}$ . The pellet was washed with 70% ethanol and spun down again at 7500rpm for 5 mins. The supernatant was removed and pellet was resuspended in 30  $\mu\text{l}$  of TE buffer. The final DNA concentration was measured using the NanoDrop2000 spectrophotometer.

### *Small Angle X-ray Scattering Analysis*

Mature, intermediate, and 24hr intermediate curli complexes were isolated from biofilm pellicles of liquid cultures of the *bscE*, cellulose mutant *S. Typhimurium* as described above. Treatment for SAXS analysis was completed as previously described [10]. Briefly, complexes were pelleted in Eppendorf tubes for 20 minutes at 10,000 rpm. Supernatants were discarded except for the last 50  $\mu\text{L}$ . The complexes were resuspended in the remaining supernatant. These samples were then loaded and sealed in quartz capillaries (Mark-tubes, Hilgenberg, GmbH) and stored at  $4^{\circ}\text{C}$  until measurement. SAXS experiments were performed at the Stanford Synchrotron Radiation Lightsource (SSRL, Beamline 4-2) using 9 keV monochromatic X-rays. The scattered radiation was measured using a Rayonix MX-225-HE detector (pixel size 73.2  $\mu\text{m}$ ). 2D powder diffraction patterns were integrated using the Nika 1.74 [42] package for Igor Pro 6.37 and FIT2D [43]. SAXS data were analyzed by plotting integrated scattering intensity against the momentum transfer  $q$  using Mathematica. Peak positions were measured by fitting diffraction peaks to a Lorentzian. The inter-DNA spacing  $d$  was obtained from the first peak position  $qd$  by the formula  $a = 2\pi/qd$ .

### ***Bone Marrow-derived Macrophages (BMDMs)***

Bone marrow derived macrophages from C57BL/6 and TLR2<sup>-/-</sup> were differentiated as previously described [25]. Briefly, leg bones were flushed and a single cell suspension of the bone marrow was prepared in RPMI media. The cell suspension was then centrifuged at 1000 rpm for 10 mins to pellet the marrow cells. These cells were then resuspended in RPMI supplemented with L929 conditioned media and antibiotic/antimycotic. On day 4, 5mL of bone marrow differentiation media was added to dishes of cells. On day 7, cells were seeded into 24-well plates at a density of 500,000 cells/well.

To investigate cytokine response, BMDMs were stimulated with 2.5µg/mL of the appropriate curli complexes and incubated for 4 or 24 hours. After incubation the supernatant was collected and TNFα, IL-6 and IL-1β production was quantified by ELISA according to the manufacturer's protocol (eBiosciences). Additionally, to investigate type I IFN expression, cells lysates were collected using TriReagent for RNA extraction and analysis at 4 hours. For cytotoxicity experiments, cells were stimulated with 10µg of curli complexes for 24 hours. Live/Dead experiments were completed as described below. Cells treated with *Salmonella* Typhimurium as a positive control were treated with curli and *Salmonella* at time 0 and then treated with 5µg/mL of Gentamycin after 1 hour to kill any bacteria that had not been taken up by the macrophages.

### ***RNA Isolation and qPCR Quantification***

To determine type I IFNs and pro-inflammatory genes, RNA was isolated from bone marrow-derived macrophages using TriReagent according to the manufacturer's

instructions. Briefly, all surfaces were sprayed and cleaned with RNase Zap (AM97890). 500 $\mu$ L of TriReagent (Molecular Research Center TR-118) was added to a monolayer of  $0.5 \times 10^5$  cells. The homogenate was stored at room temperature for 5 minutes. Using RNase free- filtered tips, the TriReagent was moved to an RNase free Eppendorf tube. To the TriReagent homogenate, 100 $\mu$ L of chloroform was added to samples and mixed. Tubes were allowed to sit on the benchtop until phase separation occurs and then centrifuged for 15 mins at 4°C, 12000 rcf. During spin, new Eppendorf tubes were filled with 500 $\mu$ L of isopropanol and pre-chilled at -20°C. After centrifugation, the clear aqueous phase on top was carefully removed and added to the pre-chilled Eppendorf tubes of isopropanol. Tubes are then shaken by hand and incubated at -20°C for 30 mins. After incubation, samples were centrifuged at 12000 rcf for 8 mins at 4°C. The supernatant is removed carefully to avoid the pelleted RNA. The pellet was then washed with 1mL of 75% ethanol (100% ethanol diluted with molecular grade water) and then centrifuged at 7500 rcf for 5 mins at 4°C. The ethanol was carefully aspirated and pellets were allowed to air dry to allow for ethanol to evaporate or be re-aspirated if necessary. Dried pellets were then resuspended in 30 $\mu$ L of molecular grade water.

RNA was then treated with a DNase kit to remove any contaminating DNA according to the manufacturer's protocol (Ambion, AM1906). In short, 3 $\mu$ L of 10x buffer with 1 $\mu$ L of DNase I enzyme were added to each sample. Samples were incubated at 37°C for 30 mins. Next, 3 $\mu$ L of inactivation reagent was added to each sample, mixed, and incubated at room temperature for 5 mins. Samples are then centrifuged at 10,000g for 1 min. The clear supernatant is then moved to a fresh Eppendorf tube. The quality and

quantity of RNA is then calculated with a NanoDrop. The quantity as well as the quality in terms of 260/280 ratio were recorded.

The RNA was then reverse transcribed to cDNA using a TaqMan Reverse Transcription kit according to manufacturer's protocol (Invitrogen, N8080234). In brief, the RNA volume is adjusted to 1 $\mu$ g in a 19.25 $\mu$ L sample. A master mix of MgCl<sub>2</sub>, 10X reverse transcription buffer, RNase inhibitor, reverse transcriptase enzyme, and random hexamers. Adding to the 19.25 $\mu$ L, 30.75 $\mu$ L of master mix is added to each sample to make a 50 $\mu$ L final volume. The mix is then spun down shortly to move the entire sample to the bottom of the tube. The reverse transcriptase program is used on the BioRad S100 Thermo Cycler to create the cDNA (Step 1: 25°C for 10 mins, Step 2: 48°C for 30 mins, Step 3: 95°C for 5 mins, Step 4: 4°C hold).

To run the quantitative real-time PCR (qPCR), a master mix was made for each desired primer pair for target genes. Each master mix included: 0.75 $\mu$ L of both 100 $\mu$ M forward primer and reverse primer (Table 1), 12.5 $\mu$ L Power Up Sybr Green master mix (ThermoFisher A25742), and 6 $\mu$ L molecular grade water. In an 8-tube PCR strip, mix 20 $\mu$ L of master mix and 5 $\mu$ L of RNA and mix by pipetting. Spin down samples shortly to bring volume to bottom of the tube. Transfer 10 $\mu$ L of mixture to a MicroAmp qPCR plate in duplicate. Seal the plate using a Real Time PCR film plate sealer. Run the qPCR in the Applied Biosciences StepOne Plus Real Time PCR system. Transcript levels were determined using the  $\Delta$ CT approach.

Gene Target	Direction	Sequence	Source
<i>Ifn<math>\beta</math></i>	Forward	5' CAG CTC CAA GAA AGG ACG AAC 3'	Harvard Primer Bank ID: 6754304a1
	Reverse	5' GGC AGT GTA ACT CTT CTG CAT 3'	Harvard Primer Bank ID: 6754304a1
<i>Il6</i>	Forward	5' GGTGCCCTGCCAGTATTCTC 3'	Harvard Primer Bank ID: 7110655a1
	Reverse	5' GGCTCCCAACACAGGATGA 3'	Harvard Primer Bank ID: 7110655a1
<i>Il1<math>\beta</math></i>	Forward	5' GCA ACT GTT CCT GAA CTC AACT 3'	Harvard Primer Bank ID: NM_008361
	Reverse	5' ATC TTT TGG GGT CCG TCA ACT 3'	Harvard Primer Bank ID: NM_008361
<i>GAPDH</i>	Forward	5' CCA GGA AAT CAG CTT CAC AAA CT 3'	[44]
	Reverse	5' CCC ACT CCT CCA CCT TTG AC 3'	[44]

**Table 1. Primer sequences used for qPCR.**

### *Live/Dead Staining*

Cells were stained using the ReadyProbes cell viability imaging kit (Thermo Fisher, R37609) following the manufacturer's instructions. Briefly, 2 drops of each color stain were added per 1 ml of medium, and stain was aliquoted into each well and incubated at room temperature for 15 min protected from light. Cells were then imaged on the EVOS FL Auto 2 microscope. Analysis of images to determine the percentage of dead cells to live cells was done using the HCS Studio software system.

### *Animal Experiments*

To determine the autoantibody production by mice in response to systemic exposure to curli complexes of different maturity, female wild-type (C57BL/6) and lupus-prone (NZBWxF/1) mice were injected intraperitoneally with 50ug of curli complex in 100

µl of sterile PBS or 100 µl of sterile PBS twice a week for 12 weeks. Tail bleeds were used to collect sera before first injection and once every 2 weeks throughout the experimental timeline.

### ***Anti-dsDNA autoantibody ELISA***

ELISAs were performed according to previously published protocol [45]. Briefly, a 96-well plate (Costar, 07-200-33) was coated with 0.01% poly-L-lysine (Sigma, P8920) in PBS and incubated for 1 hour at room temperature. Plates were then washed 3 times with distilled water and dried. Plates were then coated with 2.5 µg/mL of calf thymus DNA (Invitrogen, 15633-019) in borate buffered saline (BBS) (17.5 g NaCl, 2.5 g H<sub>3</sub>BO<sub>3</sub>, 38.1 g sodium borate in 1 L H<sub>2</sub>O) and incubated at 4°C overnight. The next day, plates are washed 3 times with BBS and blocked with 200µL/well of BBT (BBS, 3% bovine serum albumin, 1% Tween20) for 2 hours at room temperature, gently rocking. After washing 5 times with BBS, serial dilutions of control serum and sample sera were incubated on the plate overnight at 4°C. Next, plates were washed 3-5 times with BBS and biotinylated goat anti-mouse IgG (Jackson ImmunoRes, 115-065-071) was added and incubated at room temperature for 2 hours gently rocking. Avidin-alkaline phosphate conjugate (Sigma, A7294) was added and incubated for 2 hours at room temperature. Finally, plates were washed 5 times with BBS and then 4-nitrophenyl phosphate disodium salt hexahydrate (Sigma-Aldrich, N2765) was added to the plate at 1mg/mL and incubated, protected from light. Optical densities were read using Molecular Devices Microplate reader at 650nm and 405nm. Positive control sera was taken from old B6.NZM Sle1/Sle2/Sle3 lupus-prone mice

(Sle1,2,3) which had previously tested for high levels of autoantibodies and used at a dilution of 1:250 in BBT. Results are shown by raw optical density (OD).

### ***Luminex***

IgG autoantibody anti-dsDNA, anti-nucleosome, anti-nucleolin, anti-nucleosome, anti-Histone 2A (H2A), anti-Complement component 1q (C1q), were analyzed by multiplexed bead technology (Luminex) using the BioPlex 2200 system (Bio-Rad, Hercules) according to the manufacturer's instructions.

### ***Joint Inflammation Analysis***

Murine knees were extracted and fixed in phosphate-buffered formalin. For decalcification, samples were incubated in formic acid for 3 days and then embedded in paraffin. 5  $\mu$ m sections of the tissue were stained with hematoxylin and eosin. The fixed and stained sections were blinded and evaluated by an experienced veterinary pathologist according to the criteria as described previously [46]. Images were taken at a magnification of 10x.

### ***Statistical Analysis***

Data were analyzed using Prism software (GraphPad, San Diego, CA). Student *t* test or one-way ANOVA were used when appropriate. Error was determined by standard error of the mean. *P* values of <0.05 were considered significant and were noted as such on figures.

## References Cited

1. Schnabel, J., *Protein folding: The dark side of proteins*. Nature, 2010. **464**(7290): p. 828-9.
2. Ross, C.A. and M.A. Poirier, *Protein aggregation and neurodegenerative disease*. Nat Med, 2004. **10 Suppl**: p. S10-7.
3. Hull, R.L., et al., *Islet amyloid: a critical entity in the pathogenesis of type 2 diabetes*. J Clin Endocrinol Metab, 2004. **89**(8): p. 3629-43.
4. Cherny, I., et al., *The formation of Escherichia coli curli amyloid fibrils is mediated by prion-like peptide repeats*. J Mol Biol, 2005. **352**(2): p. 245-52.
5. Xue, W.F., et al., *Fibril fragmentation in amyloid assembly and cytotoxicity: when size matters*. Prion, 2010. **4**(1): p. 20-5.
6. Bucciantini, M., et al., *Inherent toxicity of aggregates implies a common mechanism for protein misfolding diseases*. Nature, 2002. **416**(6880): p. 507-11.
7. Balducci, C., et al., *Synthetic amyloid-beta oligomers impair long-term memory independently of cellular prion protein*. Proc Natl Acad Sci U S A, 2010. **107**(5): p. 2295-300.
8. Barnhart, M.M. and M.R. Chapman, *Curli biogenesis and function*. Annu Rev Microbiol, 2006. **60**: p. 131-47.
9. Nicastro, L.K., et al., *Cytotoxic Curli Intermediates Form during Salmonella Biofilm Development*. J Bacteriol, 2019. **201**(18).
10. Tursi, S.A., et al., *Bacterial amyloid curli acts as a carrier for DNA to elicit an autoimmune response via TLR2 and TLR9*. PLoS Pathog, 2017. **13**(4): p. e1006315.
11. Gallo, P.M., et al., *Amyloid-DNA Composites of Bacterial Biofilms Stimulate Autoimmunity*. Immunity, 2015. **42**(6): p. 1171-84.
12. Tukel, C., et al., *Responses to amyloids of microbial and host origin are mediated through toll-like receptor 2*. Cell Host Microbe, 2009. **6**(1): p. 45-53.

13. Miller, A.L., Pasternak, J.A., Medeiros N. J., Nicastro L. K., Tursi, S. A., Hansen E. G., Krochak, R., Sokaribo, A. S., MacKenzie, K. D., Palmer, M. B., Herman, D. J., Watson, N. L., Zhang, Y., Wilson, H. L., Wilson, R. P., White, A. P., Tukel, C. , *In vivo synthesis of bacterial amyloid curli contributes to joint inflammation during S. Typhimurium infection*. PLOS Pathog, 2020.
14. Costerton, J.W., et al., *Microbial biofilms*. Annu Rev Microbiol, 1995. **49**: p. 711-45.
15. Hathroubi, S., et al., *Biofilms: Microbial Shelters Against Antibiotics*. Microb Drug Resist, 2017. **23**(2): p. 147-156.
16. Hung, C., et al., *Escherichia coli biofilms have an organized and complex extracellular matrix structure*. mBio, 2013. **4**(5): p. e00645-13.
17. Chapman, M.R., et al., *Role of Escherichia coli curli operons in directing amyloid fiber formation*. Science, 2002. **295**(5556): p. 851-5.
18. Zogaj, X., et al., *Production of cellulose and curli fimbriae by members of the family Enterobacteriaceae isolated from the human gastrointestinal tract*. Infect Immun, 2003. **71**(7): p. 4151-8.
19. McCrate, O.A., et al., *Sum of the parts: composition and architecture of the bacterial extracellular matrix*. J Mol Biol, 2013. **425**(22): p. 4286-94.
20. Fowler, D.M., et al., *Functional amyloid--from bacteria to humans*. Trends Biochem Sci, 2007. **32**(5): p. 217-24.
21. Tukel, C., et al., *Toll-like receptors 1 and 2 cooperatively mediate immune responses to curli, a common amyloid from enterobacterial biofilms*. Cell Microbiol, 2010. **12**(10): p. 1495-505.
22. Reed-Geaghan, E.G., et al., *CD14 and toll-like receptors 2 and 4 are required for fibrillar A{beta}-stimulated microglial activation*. J Neurosci, 2009. **29**(38): p. 11982-92.
23. Tahara, K., et al., *Role of toll-like receptor signalling in Abeta uptake and clearance*. Brain, 2006. **129**(Pt 11): p. 3006-19.
24. Halle, A., et al., *The NALP3 inflammasome is involved in the innate immune response to amyloid-beta*. Nat Immunol, 2008. **9**(8): p. 857-65.

25. Rapsinski, G.J., et al., *Toll-like receptor 2 and NLRP3 cooperate to recognize a functional bacterial amyloid, curli*. *Infect Immun*, 2015. **83**(2): p. 693-701.
26. Sampson, T.R., et al., *A gut bacterial amyloid promotes alpha-synuclein aggregation and motor impairment in mice*. *Elife*, 2020. **9**.
27. Holmqvist, S., et al., *Direct evidence of Parkinson pathology spread from the gastrointestinal tract to the brain in rats*. *Acta Neuropathol*, 2014. **128**(6): p. 805-20.
28. Biesecker, S.G., et al., *The Functional Amyloid Curli Protects Escherichia coli against Complement-Mediated Bactericidal Activity*. *Biomolecules*, 2018. **8**(1).
29. Nicastro, L. and C. Tukel, *Bacterial Amyloids: The Link between Bacterial Infections and Autoimmunity*. *Trends Microbiol*, 2019. **27**(11): p. 954-963.
30. Ohnishi, S., A. Koide, and S. Koide, *The roles of turn formation and cross-strand interactions in fibrillization of peptides derived from the OspA single-layer beta-sheet*. *Protein Sci*, 2001. **10**(10): p. 2083-92.
31. Alteri, C.J., et al., *Mycobacterium tuberculosis produces pili during human infection*. *Proc Natl Acad Sci U S A*, 2007. **104**(12): p. 5145-50.
32. Besingi, R.N., et al., *Functional amyloids in Streptococcus mutans, their use as targets of biofilm inhibition and initial characterization of SMU\_63c*. *Microbiology*, 2017. **163**(4): p. 488-501.
33. Putsep, K., et al., *Deficiency of antibacterial peptides in patients with morbus Kostmann: an observation study*. *Lancet*, 2002. **360**(9340): p. 1144-9.
34. Lande, R., et al., *Plasmacytoid dendritic cells sense self-DNA coupled with antimicrobial peptide*. *Nature*, 2007. **449**(7162): p. 564-9.
35. Lande, R., et al., *The antimicrobial peptide LL37 is a T-cell autoantigen in psoriasis*. *Nat Commun*, 2014. **5**: p. 5621.
36. Lande, R., et al., *Cationic antimicrobial peptides in psoriatic skin cooperate to break innate tolerance to self-DNA*. *Eur J Immunol*, 2015. **45**(1): p. 203-13.

37. Lande, R., et al., *Neutrophils activate plasmacytoid dendritic cells by releasing self-DNA-peptide complexes in systemic lupus erythematosus*. *Sci Transl Med*, 2011. **3**(73): p. 73ra19.
38. Pachucki, R., Corradetti, C., Kohler, L., Ghadiali, J., Gallo, P., Nicastro, L., Tursi, S., Gallucci, S., Tukul, C., Caricchio, R., *Persistent Bacteriuria and Antibodies recognizing Curli/eDNA complexes from E. Coli are Linked to Flares in Systemic Lupus Erythematosus*. *Arthritis Rheum*, 2020.
39. Nasution, A.R., et al., *HLA-B27 subtypes positively and negatively associated with spondyloarthritis*. *J Rheumatol*, 1997. **24**(6): p. 1111-4.
40. Larsen, P., et al., *Amyloid adhesins are abundant in natural biofilms*. *Environ Microbiol*, 2007. **9**(12): p. 3077-90.
41. Lim, J.Y., J.M. May, and L. Cegelski, *Dimethyl sulfoxide and ethanol elicit increased amyloid biogenesis and amyloid-integrated biofilm formation in Escherichia coli*. *Appl Environ Microbiol*, 2012. **78**(9): p. 3369-78.
42. Ilavsky, J., *Nika: software for two-dimensional data reduction*. *J Appl Crystallogr.*, 2012. **45**(2): p. 234-328.
43. *FIT2D: An Introduction and Overview*. [cited 2020 April 7]; Available from: [http://www.esrf.eu/computing/scientific/FIT2D/FIT2D\\_INTRO/fit2d.html](http://www.esrf.eu/computing/scientific/FIT2D/FIT2D_INTRO/fit2d.html).
44. Wilson, R.P., et al., *The Vi-capsule prevents Toll-like receptor 4 recognition of Salmonella*. *Cell Microbiol*, 2008. **10**(4): p. 876-90.
45. Sriram, U., et al., *Myeloid dendritic cells from B6.NZM Sle1/Sle2/Sle3 lupus-prone mice express an IFN signature that precedes disease onset*. *J Immunol*, 2012. **189**(1): p. 80-91.
46. Noto Llana, M., et al., *Salmonella enterica induces joint inflammation and expression of interleukin-17 in draining lymph nodes early after onset of enterocolitis in mice*. *Infect Immun*, 2012. **80**(6): p. 2231-9.

## CHAPTER 4

### OVERALL DISCUSSION

As biofilm-associated infections account for 65% of all infections, understanding the biogenesis of the biofilm and its interactions with the host immune system are paramount [1]. While not all biofilms are the same, they serve the same purpose, protection [2]. The protein, polysaccharide and DNA components that constitute the ECM may differ [3], but they work synchronously for the success of the bacterial community. Absence or alteration of any of these main components has been shown to decrease the overall strength and stability of the biofilm [4-6]. The major structural component of the enteric biofilm, curli amyloid, is the best studied bacterial amyloid. Curli supports the three-dimensional structure with assistance of other ECM components, like cellulose, that bind within the basket-like structure formed by the cross- $\beta$  sheet ordered fibrils [5, 7-9]. Under confocal microscopy, curli can be observed as ring structures surrounding the bacterial cells within the biofilm [10]. Curli is found irreversibly complexed to eDNA. These complexes are highly resistant, remaining intact even after DNase I treatment and highly denaturing conditions, like boiling in sodium dodecyl sulfate [11]. The encasement of bacteria by biofilm components such as curli and eDNA, act to protect the bacterial cells from environmental assaults such as antibiotics, complement, and enzymes, when isolated from the biofilm. Albeit studies of curli from enteric biofilms have been of interest for many years, there remains a significant gap of knowledge around the biogenesis of curli in the biofilm *in vivo*.

Previous work on curli illustrates a complicated picture of the *in vivo* expression and production of curli. The biogenesis machinery of curli is well studied *in vitro*. However, these studies mainly use synthetic peptides and the stages of fibrillization during real biofilm formation and *in vivo* is less well understood. In studies of human amyloid  $\beta$ , the intermediate oligomeric form of the amyloid protein is associated with cytotoxicity and pathogenicity [12-14]. Similarly, in Parkinson's disease, the aggregation process of the  $\alpha$ -synuclein amyloid moves through an oligomeric intermediate stage. These intermediates, though transient, are reportedly also cytotoxic to cells *in vivo* [15]. While these oligomeric intermediates have not been identified in the host, curli oligomers have only been observed *in vitro* through fibrillization of monomeric CsgA protein [16]. However, as amyloid proteins share a conserved structure and fibrillization procedure, we were interested to examine if we were able to identify intermediates of bacterial amyloid curli from the biofilm and if they shared this cytotoxic phenotype seen in the human amyloids.

It is reported that amyloids share a basic steric zipper structure and that the fundamental units that form amyloids may be the same but organized differently by the side-chains and interactions with other amyloids [17]. These small differences are thought to be the origin of the multiple human prion proteins known to exist. Together, this indicates a role for the environment and physiological conditions on formation of amyloids. Consistent with this idea, we determined that turbulence has a profound effect on the biofilm pellicle formation. As we noticed a lack of pellicle formation with increased turbulence, we further investigated the amyloid content isolated from these biofilms. Through a multi-factorial approach, we identified a distinct population of curli

intermediates in high turbulence conditions as described in Chapter 2. For the first time, we were able to isolate an intermediate of curli from a biofilm an important breakthrough in the understanding of curli during the development of the biofilm.

After identifying this intermediate curli conformation, we moved forward in characterizing them, keeping in mind what we know about other amyloids. The cytotoxic effect of oligomeric intermediates has been observed in other amyloids such as amyloid  $\beta$  and  $\alpha$ -synuclein, therefore we wanted to investigate the cytotoxicity of the curli intermediates. We treated bone marrow-derived macrophages from wild-type mice with mature curli and intermediate curli and stained for live and dead cells. The dead to live cell ratio was significantly increased in the intermediate treated cells indicating a cytotoxic effect similar to that reported for the other amyloid intermediates. This conclusion drew a connection between the human and bacterial amyloids not previously proven. Additionally, this indicated that the intermediate species we identified was not just smaller pieces of mature curli aggregate, but that there were distinct characteristics that could differentiate the two populations. It is important to note, however, that these intermediate conformations are not a homologous population of aggregates as amyloid fibrillization is a continual process.

While we successfully identified curli intermediates, we wanted to try to isolate an earlier oligomeric form of the curli aggregates. With the knowledge of increased cytotoxicity of oligomeric forms of other amyloids [12-15], we wanted to investigate the cytotoxic capacity of curli during its formation. We used the high turbulence conditions which provided the intermediate curli aggregates in our earlier studies, but isolated the

biofilm matrix earlier in growth at 24hrs. In this way, we anticipated isolating an oligomeric form of curli with an even greater potential for cytotoxicity. Although, we were indeed able to isolate preparations enriched for smaller aggregate forms, termed early intermediates, we found the absence of the cytotoxic response previously identified in the intermediated aggregates. Using UV CD, we observed that these new early intermediates had an altered curve indicating the incomplete formation of the secondary  $\beta$  sheet structure. This altered secondary structure, we anticipated to affect numerous interactions with the early intermediates including, decreased receptor recognition and eDNA incorporation.

It is well understood that curli and eDNA form complexes in the biofilm and add to the structural stability [6]. Earlier studies have shown that DNase treatment of a fully formed biofilm leaves the structure unaffected [10]. This suggests that the DNA complexes with the curli at earlier stages of biofilm development and our reports indicate that this is indeed the case as we are still able to isolate DNA even from the early intermediates. In addition to the importance of the eDNA content in structural support, the curli/eDNA complex is known to induce autoimmune responses strongly influenced by the presence of eDNA. Hallmarks of autoimmunity, both the production of type I IFNs and anti-nuclear autoantibodies (autoabs), are impacted by the presence of eDNA within the curli complex [18]. As we expect these cytotoxic intermediates as well as the other forms are produced during *in vivo* biofilm development, the implications of understanding the role of these curli aggregates from the different stages in the biofilm biogenesis is paramount in forwarding research on biofilm-associated infections and their effect on autoimmunity (Fig. 4.1).

With this in mind, we used our newly isolated early intermediate and intermediate curli complexes with the previously studied mature curli to investigate the autoimmune responses that can be initiated through biofilm development. Twice weekly intraperitoneal injection of mature curli/eDNA induces the production of anti-dsDNA autoabs in both wild-type and autoimmune-prone mice in as little as two weeks [10]. We also observed the production of anti-dsDNA autoabs with mature curli complex treatment in mice. At this early timepoint, we observed that anti-dsDNA autoabs were produced in a DNA content dependent manner in both wild-type and autoimmune-prone mice. Interestingly, though we expected this autoab response to increase proportionally over time, we observed a delayed spike in autoab production in both wild-type and autoimmune mice treated with intermediate complexes. As we know the DNA content of the intermediates is significantly less than that of the mature complexes, we hypothesize that the cytotoxicity of these intermediate complexes may play a role in the increase of autoabs generated. The cytotoxicity by these intermediates is a slower process as we did not observe significant differences in cell death until 24 hours post treatment indicating a receptor-mediated type of cell death that requires further investigation (Fig. 4.2). In addition to the anti-dsDNA production, the production of anti-nuclear antibodies (ANAs) are a hallmark of lupus as well as other autoimmune disorders. As we observed differential in induction of the anti-dsDNA autoantibodies, we collaborated with the Silverman lab (New York University, NY) to run a Luminex assay to determine the production of numerous ANAs in mice treated with curli complexes. Using sera collected from mice treated intraperitoneally with

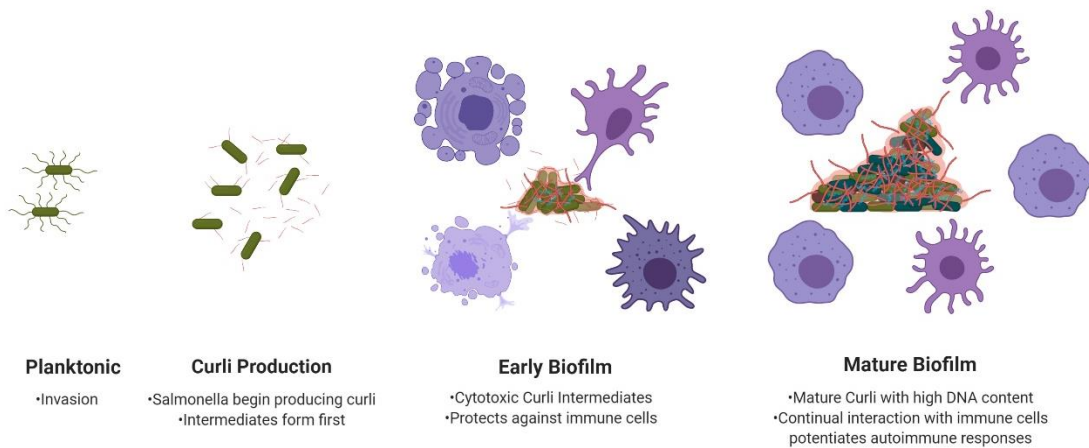


**Figure 4.1. Working Model for the Role of Curli Conformations through Biofilm Development.** Upon the switch from planktonic to curli production, early intermediates form first and begin incorporating DNA. Next, the cytotoxic intermediates can induce cell death during the early stages of development to help protect against immune cells. Cell death can allow for a larger DNA pool to incorporate into the mature fibrils. Additionally, we have shown that the continual interaction of curli with immune cells potentiates autoimmune responses in “healthy” and genetically pre-disposed individuals.

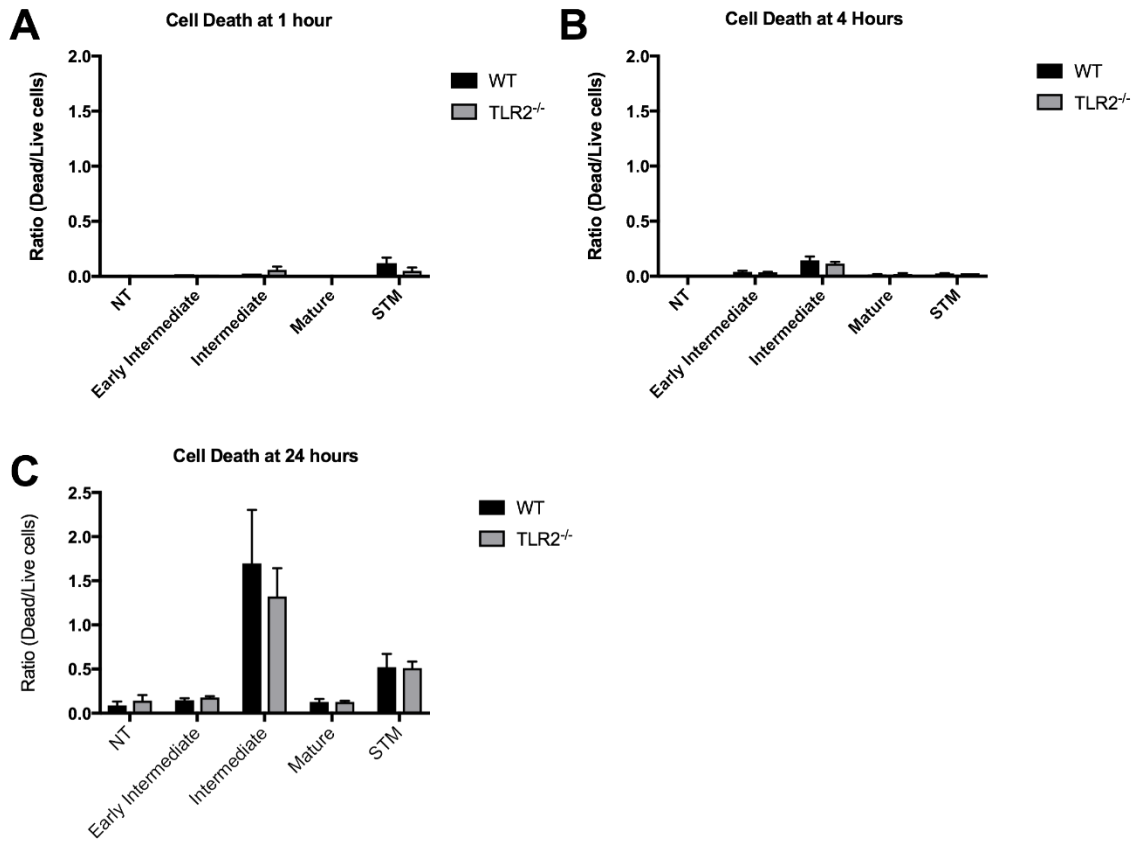


**Figure 4. 2. Cytotoxicity by Intermediate Curli Complexes is Delayed.** There is no notable cell death by intermediate curli complexes until later timepoints (24 hrs). This indicates a receptor-mediated functionality of this cell death.

mature or intermediate curli complexes for at least 5 weeks, the production of anti-nucleosome and anti-H2A antibodies were observed. The nucleosome is a structural unit of DNA packaging consisting of a DNA wrapped around a histone core. H2A is one of the five main histone proteins found within this core. The production of anti-nuclear antibodies in response to the intermediate curli/eDNA complex indicates a release of these, and related, nuclear material via an undetermined pathway, hypothesized to be cytotoxicity of the intermediate curli, allowing for the production of these antibodies. Additionally, production of anti-C1q antibodies was also observed in the sera of the curli treated mice as well. For the first time, we identified ANAs, aside from anti-dsDNA, produced in response to the treatment of curli/eDNA complexes in both wild-type and autoimmune-prone mice.

Curli has been shown to directly bind C1q of the complement pathway to protect *E. coli* against killing by the immune system [19]. This direct binding lends to the idea that curli/eDNA complexes act as a carrier for the C1q to induce the antibody production against it, similarly to the way that anti-dsDNA is produced from the complexes. Anti-C1q antibodies are often observed in SLE patients specifically those with lupus nephritis [20, 21]; however, they are also associated with multiple vascular conditions such as hypocomplementaemic urticarial vasculitis [22] and Behcet's disease [23]. Rheumatic syndromes involving immune complex mediated injury have been paired to the production of anti-C1q antibodies. Curli/eDNA can easily be an antigen source for the generation of the immune complex. As we have made several connections between the actions of multiple amyloid proteins and their interactions with eDNA, we can foresee the ability of

other amyloid/eDNA complexes to act similarly to carry antigen such as C1q to generate immune complexes implicating the greater impact of our results.

Aside from the immune complex associated conditions, infection associated autoimmune symptoms have been observed after numerous biofilm-associated infections. Notably for enteric infection, reactive arthritis is a syndrome that occurs after GI tract infections. Our group has published that systemic treatment with mature curli/eDNA complexes as well as infection with curli-positive bacteria induced joint inflammation in wild-type mice [24]. Complimenting this finding we also observed joint inflammation by intermediate curli/eDNA complexes in wild-type mice. Importantly, we saw increased pathological scoring in autoimmune-prone mice that were treated with mature and intermediate curli/eDNA complexes indicating an important role of the genetic predisposition in the outcome of the chronic exposure of the host to curli/eDNA complexes. While autoimmune diseases are multi-factorial and complex syndromes reportedly influenced by both genetic and environmental factors, our results implicate an exacerbation of symptoms upon infection with biofilm-producing bacterial species via a breaking of immune tolerance.

In summation, the data we have presented identified a previously unknown intermediate form of cytotoxic curli intermediates and broadened the understanding of the progression of curli development in the *in vitro* biofilm. We were also able to identify antibody production known to associate with autoimmune disorders, induced by both mature and intermediate curli complexes. Additionally, the impact of coupling our autoimmunity and immunogenicity findings with the understanding of amyloid/eDNA

complexes being a commonality among many biofilms, is bound to expand the knowledge for not only enteric bacteria, but other amyloid forming bacteria as well. The work presented here provides evidence that amyloid proteins are the potential link between bacterial infections and autoimmunity. It is also important to consider the localization of the complexes to be critical in their resulting responses as curli has the potential for anti-inflammatory effects and barrier support when localized to the GI tract [25, 26]. However, once these complexes reach systemic sites, with higher immune surveillance, immune interactions can induce the autoimmune sequelae. While, we show that tolerance can be broken to these curli complexes to induce autoimmune symptoms in the genetically “normal” host, it is thought that while biofilm-associated infections trigger a transient autoimmune response by bacterial amyloid/DNA complexes in healthy individuals, this response may be sustained and detrimental in individuals genetically predisposed to an autoimmune disease.

## References Cited

1. Jamal, M., et al., *Bacterial biofilm and associated infections*. J Chin Med Assoc, 2018. **81**(1): p. 7-11.
2. Costerton, J.W., et al., *Microbial biofilms*. Annu Rev Microbiol, 1995. **49**: p. 711-45.
3. Tolker-Nielsen, T. and S. Molin, *Spatial Organization of Microbial Biofilm Communities*. Microb Ecol, 2000. **40**(2): p. 75-84.
4. Kikuchi, T., et al., *Curli fibers are required for development of biofilm architecture in Escherichia coli K-12 and enhance bacterial adherence to human uroepithelial cells*. Microbiol Immunol, 2005. **49**(9): p. 875-84.
5. Hung, C., et al., *Escherichia coli biofilms have an organized and complex extracellular matrix structure*. mBio, 2013. **4**(5): p. e00645-13.
6. Whitchurch, C.B., et al., *Extracellular DNA required for bacterial biofilm formation*. Science, 2002. **295**(5559): p. 1487.
7. Serra, D.O., A.M. Richter, and R. Hengge, *Cellulose as an architectural element in spatially structured Escherichia coli biofilms*. J Bacteriol, 2013. **195**(24): p. 5540-54.
8. McCrate, O.A., et al., *Sum of the parts: composition and architecture of the bacterial extracellular matrix*. J Mol Biol, 2013. **425**(22): p. 4286-94.
9. Tursi, S.A. and C. Tukel, *Curli-Containing Enteric Biofilms Inside and Out: Matrix Composition, Immune Recognition, and Disease Implications*. Microbiol Mol Biol Rev, 2018. **82**(4).
10. Gallo, P.M., et al., *Amyloid-DNA Composites of Bacterial Biofilms Stimulate Autoimmunity*. Immunity, 2015. **42**(6): p. 1171-84.
11. Brodsky, I.E. and D. Monack, *NLR-mediated control of inflammasome assembly in the host response against bacterial pathogens*. Semin Immunol, 2009. **21**(4): p. 199-207.
12. Balducci, C., et al., *Synthetic amyloid-beta oligomers impair long-term memory independently of cellular prion protein*. Proc Natl Acad Sci U S A, 2010. **107**(5): p. 2295-300.

13. Bucciantini, M., et al., *Inherent toxicity of aggregates implies a common mechanism for protein misfolding diseases*. *Nature*, 2002. **416**(6880): p. 507-11.
14. Xue, W.F., et al., *Fibril fragmentation in amyloid assembly and cytotoxicity: when size matters*. *Prion*, 2010. **4**(1): p. 20-5.
15. Winner, B., et al., *In vivo demonstration that alpha-synuclein oligomers are toxic*. *Proc Natl Acad Sci U S A*, 2011. **108**(10): p. 4194-9.
16. Horvath, I., et al., *Mechanisms of protein oligomerization: inhibitor of functional amyloids templates alpha-synuclein fibrillation*. *J Am Chem Soc*, 2012. **134**(7): p. 3439-44.
17. Sawaya, M.R., et al., *Atomic structures of amyloid cross-beta spines reveal varied steric zippers*. *Nature*, 2007. **447**(7143): p. 453-7.
18. Tursi, S.A., et al., *Bacterial amyloid curli acts as a carrier for DNA to elicit an autoimmune response via TLR2 and TLR9*. *PLoS Pathog*, 2017. **13**(4): p. e1006315.
19. Biesecker, S.G., et al., *The Functional Amyloid Curli Protects Escherichia coli against Complement-Mediated Bactericidal Activity*. *Biomolecules*, 2018. **8**(1).
20. Potlukova, E. and P. Kralikova, *Complement component c1q and anti-c1q antibodies in theory and in clinical practice*. *Scand J Immunol*, 2008. **67**(5): p. 423-30.
21. Stojan, G. and M. Petri, *Anti-C1q in systemic lupus erythematosus*. *Lupus*, 2016. **25**(8): p. 873-7.
22. Wisnieski, J.J. and S.M. Jones, *IgG autoantibody to the collagen-like region of C1q in hypocomplementemic urticarial vasculitis syndrome, systemic lupus erythematosus, and 6 other musculoskeletal or rheumatic diseases*. *J Rheumatol*, 1992. **19**(6): p. 884-8.
23. Bassyouni, I.H., et al., *Autoantibodies against complement C1q in patients with Behcet's disease: association with vascular involvement*. *Mod Rheumatol*, 2014. **24**(2): p. 316-20.

24. Miller, A.L., Pasternak, J.A., Medeiros N. J., Nicastro L. K., Tursi, S. A., Hansen E. G., Krochak, R., Sokaribo, A. S., MacKenzie, K. D., Palmer, M. B., Herman, D. J., Watson, N. L., Zhang, Y., Wilson, H. L., Wilson, R. P., White, A. P., Tukel, C. , *In vivo synthesis of bacterial amyloid curli contributes to joint inflammation during S. Typhimurium infection*. PLOS Pathog, 2020.
25. Oppong, G.O., et al., *Biofilm-associated bacterial amyloids dampen inflammation in the gut: oral treatment with curli fibres reduces the severity of hapten-induced colitis in mice*. NPJ Biofilms Microbiomes, 2015. **1**.
26. Oppong, G.O., et al., *Epithelial cells augment barrier function via activation of the Toll-like receptor 2/phosphatidylinositol 3-kinase pathway upon recognition of Salmonella enterica serovar Typhimurium curli fibrils in the gut*. Infect Immun, 2013. **81**(2): p. 478-86.

## APPENDIX A

### GROWTH CONDITIONS FOR EACH OF THE CURLI CONFORMATIONS

#### Mature DNA curli:

Day 0: O/N strain of choice (CT13 *msbB* mutant- Kan resistance)

Day 1: Make preps in 250mL autoclaved flasks:

150mL YESCA broth

500  $\mu$ l O/N culture

6mL DMSO (do not flame)

Place into shaker at 26°C shaking at 200rpm for 72 hours

Day 4: Spin down cultures to pellet in Beckman centrifuge at 10000rpm for 15mins

\*Can freeze to store and prep later\*

Resuspend pellet in 30mL 10mM Tris HCl pH 8.0 (Tris HCl)

Add 0.1mg/mL DNase I and RNase A (stored at -20°C)

100  $\mu$ l from 30mg/mL stock to 30mL resuspension

Break bacterial cells by sonication (2x for 30sec each)

Sonicator set to 4

Add MgCl<sub>2</sub> to a final concentration of 1mM

30  $\mu$ l from 1M stock

Incubate at 37°C for 20 mins

Add lysozyme up to 1mg/mL (stored at -20°C)

100  $\mu$ l from 30mg/mL stock

Incubate at 37°C for 40 mins shaking

Add 1% SDS (300 µl from 10% SDS stock)

Incubate at 37°C for 30 mins with shaking

\*Turn on Beckman centrifuge if not already on to cool down\*

Centrifuge at 10000rpm for 15mins

Discard supernatant in bleach

Resuspend pellet in 10mL Tris HCl

Boil for 10mins

Centrifuge at 10000rpm for 15mins

\*Can stop and freeze pellet for another day here\*

Perform second enzyme digestion with RNase A, DNase I, and lysozyme

100 µl of each from stocks

Incubate for 40mins at 37°C with shaking

Centrifuge 10000rpm for 15mins

Wash pellet 2x with Tris HCl

Resuspend in 10mL Tris HCl and centrifuge at 10000rpm for 15mins

Resuspend pellet in 1X SDS-PAGE buffer

Up to 4mL depending on pellet size

Boil for 15 mins

Load on large 12% running/5% stacking gel

Run at 20mA for 5hrs or 50V O/N

Collection: Recover curli from gel well with stretched plastic dropper into 50mL tube

Spin down curli in tube at 5000rpm for 10mins

Resuspend in dH<sub>2</sub>O and spin at 5000rpm for 10mins to wash 3x

Resuspend in 95% EtOH and spin at 5000rpm for 10mins to extract final sample

Intermediate curli:

Day 0: O/N strain of choice (CT13 *msbB* mutant- Kan resistance)

Day 1: Make preps in 250mL autoclaved flasks:

500mL YESCA broth

1.67mL O/N culture

20mL DMSO (do not flame)

Place into shaker at 26°C shaking at 200rpm for 72 hours

Day 4: Spin down cultures to pellet in Beckman centrifuge at 10000rpm for 15mins

\*Can freeze to store and prep later\*

Resuspend pellet in **15mL** 10mM Tris HCl pH 8.0 (Tris HCl)

Add 0.1mg/mL DNase I and RNase A (stored at -20°C)

**50** µl from 30mg/mL stock to 30mL resuspension

Break bacterial cells by sonication (2x for 30sec each)

Sonicator set to 4

Add MgCl<sub>2</sub> to a final concentration of 1mM

**15** µl from 1M stock

Incubate at 37°C for 20 mins

Add lysozyme up to 1mg/mL (stored at -20°C)

**50**  $\mu$ l from 30mg/mL stock

Incubate at 37°C for 40 mins shaking

Add 1% SDS (**150**  $\mu$ l from 10% SDS stock)

Incubate at 37°C for 30 mins with shaking

\*Turn on Beckman centrifuge if not already on to cool down\*

Centrifuge at 10000rpm for 15mins

Discard supernatant in bleach

Resuspend pellet in 10mL Tris HCl

Boil for 10mins

Centrifuge at 10000rpm for 15mins

\*Can stop and freeze pellet for another day here\*

Perform second enzyme digestion with RNase A, DNase I, and lysozyme

**50**uL of each from stocks

Incubate for 40mins at 37°C with shaking

Centrifuge 10000rpm for 15mins

Wash pellet 2x with Tris HCl

Resuspend in 10mL Tris HCl and centrifuge at 10000rpm for 15mins

Resuspend pellet in 1X SDS-PAGE buffer

Up to 4mL depending on pellet size

Boil for 15 mins

Load on large 12% running/5% stacking gel

Run at 20mA for 5hrs or 50V O/N

Collection: Recover curli from gel well with stretched plastic dropper into 50mL tube

Spin down curli in tube at 5000rpm for 10mins

Resuspend in dH<sub>2</sub>O and spin at 5000rpm for 10mins to wash 3x

Resuspend in 95% EtOH and spin at 5000rpm for 10mins to extract final sample

Early Intermediate curli:

Day 0: O/N strain of choice (CT13 *msbB* mutant- Kan resistance)

Day 1: Make preps in 250mL autoclaved flasks:

500mL YESCA broth

1.67mL O/N culture

20mL DMSO (do not flame)

Place into shaker at 26°C shaking at 200rpm for **24** hours

Day 2: Spin down cultures to pellet in Beckman centrifuge at 10000rpm for 15mins

\*Can freeze to store and prep later\*

Resuspend pellet in **15mL** 10mM Tris HCl pH 8.0 (Tris HCl)

Add 0.1mg/mL DNase I and RNase A (stored at -20°C)

**50**µl from 30mg/mL stock to 30mL resuspension

Break bacterial cells by sonication (2x for 30sec each)

Sonicator set to 4

Add MgCl<sub>2</sub> to a final concentration of 1mM

**15** µl from 1M stock

Incubate at 37°C for 20 mins

Add lysozyme up to 1mg/mL (stored at -20°C)

**50**µl from 30mg/mL stock

Incubate at 37°C for 40 mins shaking

Add 1% SDS (**150**µl from 10% SDS stock)

Incubate at 37°C for 30 mins with shaking

\*Turn on Beckman centrifuge if not already on to cool down\*

Centrifuge at 10000rpm for 15mins

Discard supernatant in bleach

Resuspend pellet in 10mL Tris HCl

Boil for 10mins

Centrifuge at 10000rpm for 15mins

\*Can stop and freeze pellet for another day here\*

Perform second enzyme digestion with RNase A, DNase I, and lysozyme

**50**µl of each from stocks

Incubate for 40mins at 37°C with shaking

Centrifuge 10000rpm for 15mins

Wash pellet 2x with Tris HCl

Resuspend in 10mL Tris HCl and centrifuge at 10000rpm for 15mins

Resuspend pellet in 1X SDS-PAGE buffer

Up to 4mL depending on pellet size

Boil for 15 mins

Load on large 12% running/5% stacking gel

Run at 20mA for 5hrs or 50V O/N

Collection: Recover curli from gel well with stretched plastic dropper into 50mL tube

Spin down curli in tube at 5000rpm for 10mins

Resuspend in dH<sub>2</sub>O and spin at 5000rpm for 10mins to wash 3x

Resuspend in 95% EtOH and spin at 5000rpm for 10mins to extract final sample

## APPENDIX B

### INCLUSION OF COPYRIGHTED MATERIAL FOR CHAPTER 2



[Home](#)   [Subscriptions](#)   [Authors](#)   [Reviewers](#)   [Ethics](#)   [About](#)

#### Open Access Policy

[ASM Author Center / Open Access](#)

Authors may opt to publish their research as open access in one of two ways: in an ASM open access journal or in an ASM Journal that supports open access (a "hybrid" journal). The ASM open access journals include: *mBio*<sup>®</sup>, *Microbiology Resource Announcements*<sup>®</sup>, *mSphere*<sup>®</sup>, and *mSystems*<sup>®</sup>.

Selecting open access in a hybrid ASM journal (*Antimicrobial Agents and Chemotherapy*<sup>®</sup>, *Applied and Environmental Microbiology*<sup>®</sup>, *Infection and Immunity*<sup>®</sup>, *Journal of Bacteriology*<sup>®</sup>, *Journal of Clinical Microbiology*<sup>®</sup>, *Journal of Virology*<sup>®</sup>, and *Molecular and Cellular Biology*<sup>®</sup>) permits immediate access to both the preliminary accepted manuscript version\* and the copyedited, typeset version of record published in the online journal. Authors whose papers have already been submitted and who did not have the opportunity to specify their wish for open access during the submission process may [contact the ASM production editor to arrange it](#).

Publishing your research as open access in any of these titles will be covered by [Creative Commons Attribution 4.0 license](#).

Please note that open access is not available for content published in *Clinical Microbiology Reviews*<sup>®</sup> or *Microbiology and Molecular Biology Reviews*<sup>®</sup>.

For information related to open access fees and more information about licensing, please review our [open access resources](#).

\* *Antimicrobial Agents and Chemotherapy*<sup>®</sup>, *Applied and Environmental Microbiology*<sup>®</sup>, *Infection and Immunity*<sup>®</sup>, *Journal of Bacteriology*<sup>®</sup>, *Journal of Clinical Microbiology*<sup>®</sup>, *Journal of Virology*<sup>®</sup>, *Molecular and Cellular Biology*<sup>®</sup> publish accepted manuscripts.